# Spectroscopic Ellipsometer for Non-destructive Characterization of Semiconductors

A Thesis Submitted
to
The Department of Electronic Engineering
of
The Chinese University of Hong Kong
in
Partial Fulfilment of the Requirements
for
the Degree of Master of Philosophy

By : Kwong-Hon LEE
Supervisor : Dr. S.P.WONG
June 1993

**ACKNOWLEDGEMENT**

I would like to express my sincere gratitude to my supervisor Dr. S.P. Wong for his invaluable advice, comments and suggestions given for my research work and I would also like to thank the technicians of semiconductor laboratory, Mr. C.K.Pun and Mr. W.C.Chu for their kindly help during the research work.

**ABSTRACT**

Ellipsometry is a non-destructive and non-contact method for the characterization of materials. The technique is based on the measurement of the change of the polarization state of a beam of polarized light upon reflection from a sample surface. In this work, a rotating-analyzer spectroscopic ellipsometer was designed and constructed for the non-destructive characterization of semiconductors. The photon energy range covered is from 1.5eV to 3eV. The operation of the system is automated with a personal-computer. The reflected light intensity is analyzed by means of on-line Fourier analysis and the result is digitized and transferred to computer for storage and further study. Moreover, a software has been developed to analyze the ellipsometric spectra obtained from systems of layered structures of homogeneous and isotropic media.

The system is then tested and applied to a number of semiconductor systems including low temperature MBE grown GaAs on GaAs substrate, amorphous carbon thin film on silicon, LPE $Al_xGa_{1-x}As$ films on GaAs and buried nitride silicon on insulator structure by nitrogen implantation into silicon. From the ellipsometry spectra of these samples, useful information about these systems have been obtained and discussed.

**TABLE OF CONTENTS**

## CHAPTER 1 INTRODUCTION

Ellipsometry is a non-contact and non-destructive technique for the characterization of material. This technique is based on the measurement of the change of the polarization state of a beam of polarized light upon reflection from a sample surface. As the change of the polarization state is very sensitive to the variation in the optical and structural properties of the samples, ellipsometry can provide useful information in non-destructive way. The connection between the change of polarization state of a light beam upon transmission through or reflection from a sample and the material properties was first recognised and reported by P.Drude a hundred years ago[1,2]. The early instruments were based on the null technique and could only be operated manually at a single wavelength. Due to these limitation, the applications of the ellipsometry has not been very popular until the late sixties.

One important development in the instrumentation of ellipsometry was done by Cahan and Spanier[3] in 1969. Cahan and Spanier constructed an automatic rotating-analyzer type ellipsometer which did not involve the operator during the data acquisition process. Since then, the automatic ellipsometry has become one of the simplest and most popular photometric instrument. The automatic ellipsometer is usually constructed with a rotating optical elements (either a polarizer, a compensator or an analyzer) such that the intensity of the light beam can be modulated.

Because of the rapid development of the micro-computer, the progress in ellipsometry automation was greatly enhanced[4-10]. In addition to being used in analyzing the ellipsometry data, the computer has also been used to help collect the data, signal-averaging and store the data in digital form for further processing[11,12]. The wide use of the micro-computers has in fact extended the applications of ellipsometry in both of the following domains : (1) Spectroscopic domain where a continuum light source is used instead of a monochromatic

light source to measure the optical functions of the samples in a certain range of frequencies. (2) Time domain where the time evolution of the ellipsometry parameters are measured to study the dynamic processes of film growth, etching and other variations of the surface properties.

The ellipsometry measurement procedure can basically mentioned as follows. A polarized light of known polarization was first generated by using some optical components such as polarizer and compensator and acted as an incident light. The incident wave interacts with the sample surface leading to a change in the polarization of the light beam which is then characterized by another polarizer. The polarization states of the incident and the reflected beams are related to the physical properties of the sample by means of fundamental optical equations. Therefore, from the change in the polarization states, the physical parameters of the samples such as refractive indices and complex dielectric functions can be obtained[13,14].

The use of spectroscopic ellipsometry (SE) to characterize the properties and structures of semiconductors has attracted much attention in recent years. Being a non-destructive optical techniques SE can provide useful information of the sample without making any damage on the specimen. Being a spectroscopic technique, the measurements in SE are made at a certain frequency range and this has greatly extended the scope of possible applications of ellipsometry. For examples, with the help of the effective-medium model and least-square analysis, the composition of thin films can be estimated[15]. It has been demonstrated that SE can be used to determine the thickness of thin films to an accuracy comparable to that achieved using other direct investigation techniques such as cross-sectional transmission electron microscopy (XTEM) and Rutheford backscattering (RBS)[16-19]. The distinct advantage of ellipsometry over other intensity related photometric measurements is

that it is very sensitive to the extremely thin overlayers. Variations in the thickness of thin films from a few tens of angstroms to a length scale of penetration depth of the incident light can be measured. Moveover, the complex refractive index $N=n+jk$ and the complex dielectric function $\epsilon=\epsilon_1+j\epsilon_2$ of materials can be measured directly as a function of wavelength without the need for the Kramers-Kronig transformations or the complication of reflectance and transmittance measurements at different polarization angles or at different angles of incidence[21]. In recent years, SE measurements have been also extended to cover the UV and IR regions so that more complicated materials can be characterized[20].

The objective of this project is to construct an automated rotating analyzer type spectroscopic ellipsometer using a personal computer as the controller. In chapter 2 and 3, we will first have a description on the fundamental principles of ellipsometry and the mathematical representation of the relationship between the change of polarization state of the reflected beam and the optical and structural properties of the samples. After a brief review on the configurations of two main types of ellipsometers, we then focus on the design and construction of our instrument in chapter 4. The alignment procedures and the calibration method will also presented in chapter 5. The discussion on the analysis of the experimental results to convert the ellipsometric parameters into physical quantities will be given in chapter 6. As examples of applications, the SE system has been used to study various material system and the experimental results are report in chapter 7. Finally, a summary of the results of the applications as well as a few suggestions for future work will be given in the last chapter.

## CHAPTER 2. PRINCIPLE OF ELLIPSOMETRY

The principle of ellipsometry is based on the fact that a monochromatic electromagnetic wave will change its state of polarization when it strike non-perpendicularly onto the interface between two dielectric media. In order to interpret those ellipsometric data that have been taken when polarized light is reflected from a bare or filmed substrate, electromagnetic theory of light is used to derive expression for the complex amplitude coefficients.

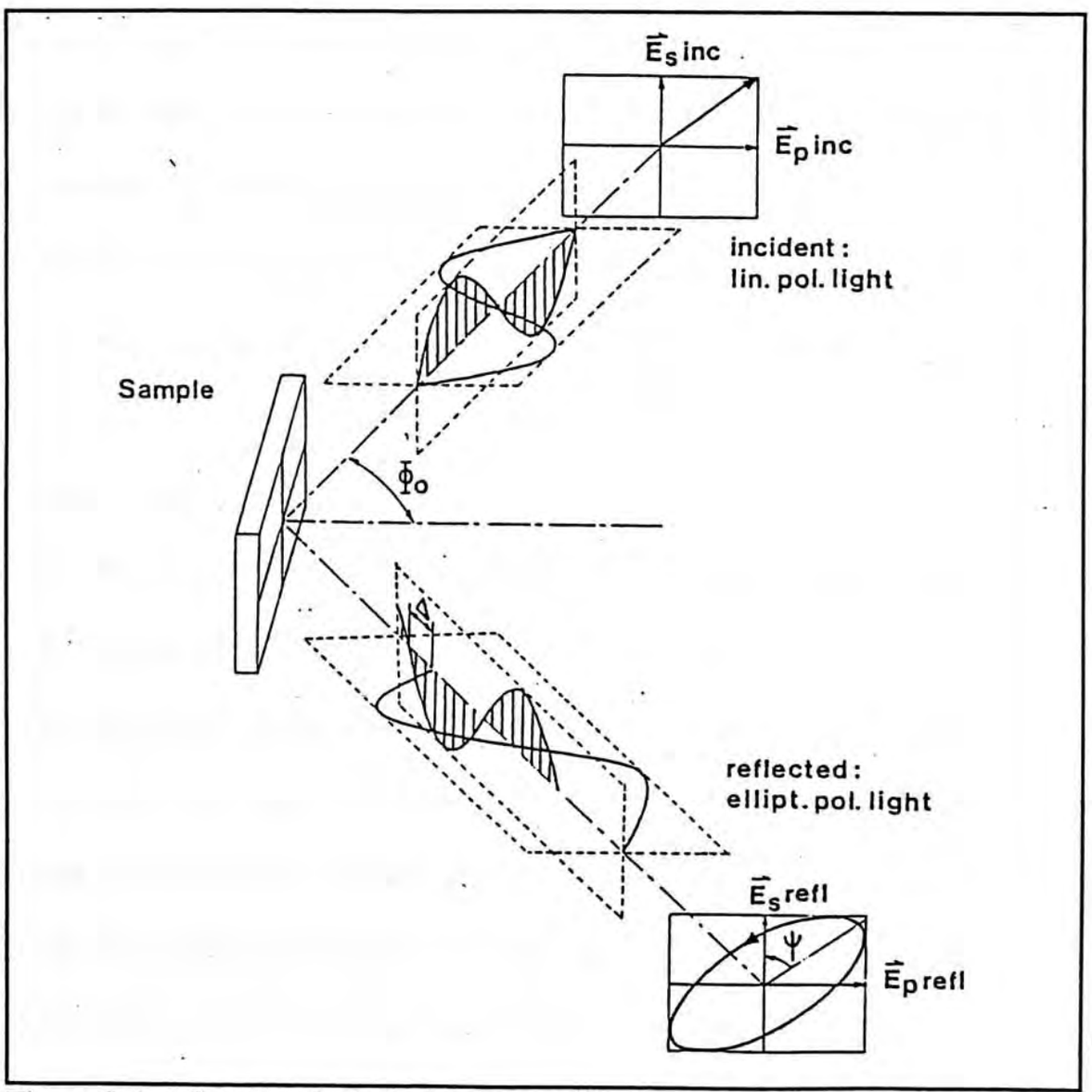


Figure 2.1 *A linear polarized electromagnetic wave perform a screw-like motion after reflected from a dielectric material (From ref.36)*

In general, an arbitrary monochromatic transversal wave are composed of two orthogonal coherent waves. ie. The field vector E can be resolved into $E_p$ and $E_s$ components. $E_p$ and $E_s$ lies in direction perpendicular and parallel to the plane of incident respectively. When monochromatic waves reflected from the sample are out of phase, field vector will perform a screw-like motion around the direction of its propagation (z-direction). If we projected the field vector onto a plane perpendicular to z-axis, in general, an ellipse will be obtained. The ellipse will degenerate to a line if phase different between $E_p$ and $E_s$ reflected is a multiple of $\pi$. If the amplitude of the two reflected components wave are equal, a circle will be obtained. It is obvious that the polarization ellipse and the elipticity can be used to describe the optical properties of the sample.

The surface properties of material is described by the reflectance $r_p$ and $r_s$. These complex coefficients describe the influence on sample by the electromagnetic field components parallel(p) and perpendicular(s) to the plane of incidence. In order to have a complete description of the system, there are totally eight parameters. Four of them are used to describe the amplitude and phase of incident and reflected wave. Others are used to describe the sample and ambient.

The polarization ellipse can be represented by two attributes that known as size and shape (elipticity). The size of ellipse $E = | E_p^2 + E_s^2 |^{1/2}$ is a scalar whose square is proportional to the intensity I. On the other hand, the sample which represented by $E_p/E_s$ is an intensity independent quantity that specified by minor/major axis ratio and the azimuth angle of the major axis of the ellipse. The absolute reflectance $R_p$ and $R_s$ are an important parameters used in reflectometry and they are defined as the square of respective complex reflectance coefficient $R_p = | r_p |^2$, $R_s = | r_s |^2$. In ellipsometry, we have to consider both the amplitude and phase of reflected field. Thus, the ratio of polarization state is written as

$r_p/r_s = \rho = \tan \psi \, e^{j\Delta}$ [13]. The complex reflectance ratio $\rho$ is expressed as an amplitude $\tan \psi$ and phase difference $\Delta$ p and s components.

The ellipsometry method can be described as the measurement of two complex reflectance $r_p$ and $r_s$. It is in fact the combination of the photometric technique and polarimetric technique. Photometric technique involved the measurement of reflectance of linearly polarized light at a number of different angle of incidence. The optical constants of materials were calculated by a graphical process. Avery in 1950 modified the method by measuring the ratio $R_p/R_s$ at different angles of incidence in order to overcome the difficulties of absolute reflectance measurement. The reflectance $R_p$ and $R_s$ are selected by introducing a polarizer into the path of incident beam. By rotating the polarizing device through 90°, intensity of incident and reflected beams in p and s state could be measured. Unlike the photometric method, polarimetric method deal with the measurement of phase different on reflection $\Delta$ between the s and p state of polarization. A commonly used setup called Michelson's interferometer was used. The incident beam was first polarized in either s or p state. After the interference pattern was recorded, the polarizer was rotated through 90°. After then, the fringe shift is produced and the phase difference $\Delta$ can be calculated. In order to solve for the values of both n and k, measurement of phase shift have to be done at different angle of incidence.

When compare the above methods, ellipsometry has a disadvantage that measurement has to be done at non-normal incidence while photometric and polarimetry can be performed at either normal or non-normal incidence. However, ellipsometry is comparatively a more powerful methods. First of all, during ellipsometry measurement, two parameters instead of one are determined in a single-measurement operation. Both the real and imagine part of the complex optical function of a bulk homogenous material can be obtained. Secondly,

ellipsometry deals with intensity-independent complex quantities[21]. It is relatively insensitive to the intensity fluctuations of the light source. Thirdly, ellipsometry method can be described as a double beam method in another point of view. It is because, the polarization of one component servers as an amplitude and phase reference for the other. The measurement of phase different makes ellipsometry generally more sensitive to surface conditions. The orthogonal components of the incident wave need not necessarily be in plane. For a null type ellipsometry, the linear polarized light was transformed to elliptical polarized light and then strike onto the sample. No matter what the state of the incoming wave is, what we measure is the change of the polarization state of the reflected wave. The general ellipsometer arrangement is shown in Figure 2.2.

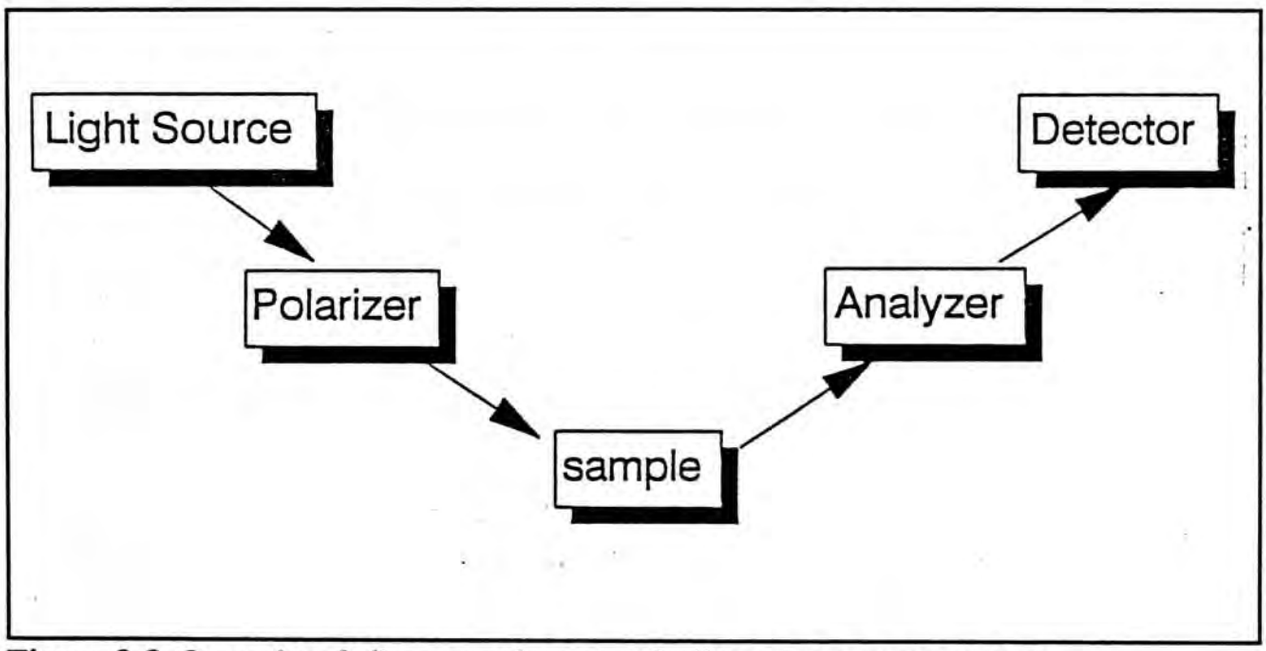


Figure 2.2 *Operational diagram of a general ellipsometer arrangement*

A continuous light was first polarized by the polarizer P. When the linear polarized light strike on the sample, its polarized state will change. Another polarizer and a detector were used to examine the elipticity and azimuth of the reflected light. Data obtained can be used to calculate the physical parameters of the specimen, such as refractive index, dielectric constant and the thickness of film.

## CHAPTER 3. MATHEMATICAL REPRESENTATION OF ELLIPSOMETRY

To understand the principle of ellipsometry, it should start from the relation of ellipsometric measurement to the electromagnetic theory of light in radiation. The objective of this chapter is to give a summary of principles necessary for interpretation of ellipsometric data, more extensive information should be referred to reference 13,14.

Firstly, we have to consider the wave formula despite of the medium used. If a plane wave travel in a medium in z-axis. According to the Maxwell's equation, the electric field vector E is given by equation 3.1

$$E = E_o \, e^{j(\omega t - N\chi z)} \tag{3.1}$$

$E_o$ defines the amplitude of wave, $\omega$ the angular frequency, t the time, N the complex refractive index of medium that EM wave passes thought, $\chi$ the wave vector and z the propagation direction. The complex refractive index N is denoted as

$$N = n + ik \tag{3.2}$$

where n = index of refraction of the medium

k = extinction coefficient of the medium

Similarly, the complex dielectric constant $\varepsilon$ is denoted by

$$\varepsilon = \varepsilon_1 + i\varepsilon_2 \tag{3.3}$$

and it can be related to the refractive index according to equation (3.4)

$$\varepsilon_1 = n^2 - k^2 \qquad and \qquad \varepsilon_2 = 2nk \tag{3.4}$$

After considering the above formula, we have to take into account the medium we employed. If a plane wave was strike at the planar interface between two semi-infinite media 0 and 1, the reflection and transmission of electromagnetic wave through the interface can

be described by Fresnel's equation which are derived from Maxwell's equations. Superscript +,- represent the incident and reflected EM wave at the interface between two media.

$$r_{01p} = \frac{E_{0p}^{-}}{E_{0p}^{+}} = \frac{n_1\cos\phi_0 - n_0\cos\phi_1}{n_0\cos\phi_1 + n_1\cos\phi_0} \tag{3.5}$$

$$r_{01s} = \frac{E_{0s}^{-}}{E_{0s}^{+}} = \frac{n_0\cos\phi_0 - n_1\cos\phi_1}{n_0\cos\phi_0 + n_1\cos\phi_1} \tag{3.6}$$

$$t_{01p} = \frac{E_{1p}^{+}}{E_{0p}^{+}} = \frac{2n_0\cos\phi_0}{n_0\cos\phi_1 + n_1\cos\phi_0} \tag{3.7}$$

$$t_{01s} = \frac{E_{1s}^{+}}{E_{0s}^{+}} = \frac{2n_0\cos\phi_0}{n_0\cos\phi_0 + n_1\cos\phi_1} \tag{3.8}$$

In order to satisfied the boundary conditions, the directions of all propagation of wave including incident, reflected and transmitted waves must lie on the plane of incidence. The angle of incidence $\phi_o$ and refraction $\phi_1$ can be related by the Snell's Law.

$$N_0\sin\phi_0 = N_1\sin\phi_1 \tag{3.9}$$

The vibration of polarized wave light are indicated by p and s. where p is the direction parallel to the plane of incidence and s represent the direction perpendicular to the plane of incidence.

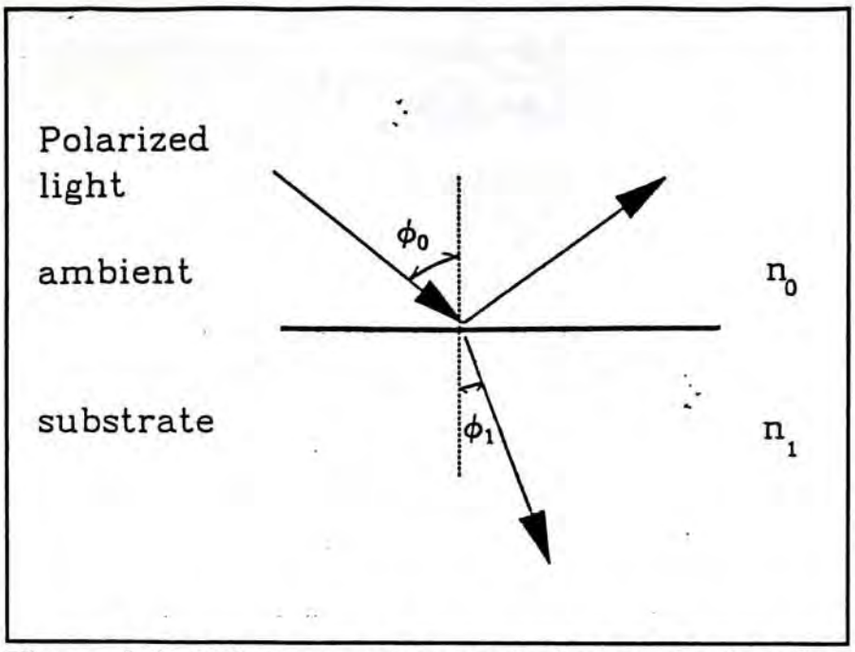


Figure 3.1 *Reflection and transmission at the interface between different dielectric media*

If media 0 and 1 are transparent , then both $N_0$, $N_1$ and $\phi_0$ and $\phi_1$ are real. It also implies that no phase shift between the incident wave and reflected or transmitted wave unless a phase is shifted by an integral multiple of $\pi$. Such an interface affect only the ratio of the amplitude of the reflected wave and therefore a linear polarized wave be transmitted if a linear polarized wave was reflected from the interface. The transmitted wave will have different azimuth. When either one or both media is absorbing, the angle $\phi_0$ and $\phi_1$, in general will become a complex value. By applying the Snell's Law to the Fresnel's equation, the Fresnel complex-amplitude reflection (r) and transmission(t) coefficient for p and s polarization will be recast into equation (3.10).

It shows that the reflection and transmission coefficient depends only on the angles of incidence $\phi_0$ and refraction $\phi_1$.

In order to deal with the reflection and transmission coefficients in amplitude and phase separately, we rewrite the complex Fresnel coefficient as equation (3.11).

The absolute value $r_p$, $t_p$ are the ratio of amplitude of the electric wave of the

$$r_p = \frac{\tan(\phi_0 - \phi_1)}{\tan(\phi_0 + \phi_1)}$$

$$r_s = \frac{-\sin(\phi_0 - \phi_1)}{\sin(\phi_0 + \phi_1)} \qquad (3.10)$$

$$t_p = \frac{2\sin\phi_1\cos\phi_0}{\sin(\phi_0 + \phi_1)\cos(\phi_0 - \phi_1)}$$

$$t_s = \frac{2\sin\phi_1\cos\phi_0}{\sin(\phi_0 + \phi_1)}$$

$$r_p = |r_p|\ e^{j\delta_{rp}}$$

$$r_s = |r_s|\ e^{j\delta_{rs}} \qquad (3.11)$$

$$t_p = |t_p|\ e^{j\delta_{tp}}$$

$$t_s = |t_s|\ e^{j\delta_{ts}}$$

reflection and transmission wave respectively.

$\delta_{r,p}$ and $\delta_{r,s}$ are the phase shifted between the reflected and the incidence wave parallel and perpendicular to the plane of incidence.

As reflection ellipsometry is a technique based on the measurement of the ratio of $r_p$ and $r_s$, therefore, from the experiment that have performed, the complex Fresnel reflection coefficient for the p and s polarizations can be derived as follows :

$$\rho = \frac{r_p}{r_s} \qquad (3.12)$$

$\rho$ can also be expressed in terms of ellipsometric angle $\psi$ and $\Delta$

$$\rho = \tan\psi\ e^{j\Delta} \qquad (3.13)$$

$\psi$ is the ratio of the amplitude of $r_p$ and $r_s$, $\Delta = \delta_{rp} - \delta_{rs}$ is the phase change of one component related to the other.

## Section 3.1 Ambient substrate system

From the above two equations, if we substitute $r_p$ and $r_s$ into Snell's Law, we can rewrite the equation of $N_1$ in terms of $\rho$ and $\phi_0$.

$$N_1 = N_0 \sin\phi_0 \left[1 + \left(\frac{1-\rho}{1+\rho}\right)^2 \tan^2\phi_0\right]^{1/2}$$
$$N_1 = N_0 \tan\phi_0 \left[1 - \frac{4\rho}{(1+\rho)^2} \sin^2\phi_0\right]^{1/2} \qquad (3.14)$$

In addition, reflectance $R_p$ and $R_s$ can be obtained by

$$R_p = |r_p|^2$$
$$R_s = |r_s|^2 \qquad (3.15)$$

$R_p$ and $R_s$ give the fraction of the total intensity of an incident plane wave that appear in the reflected wave for the p and s polarization.

It is obvious that the ellipsometry technique can be directly applied in the evaluation of the refractive index and the absorption coefficient of absorbing homogeneous sample whose thickness is large enough to prohibit multiple reflection in the sample. Such a measurement can be used to characterize the properties of bulk material. However, the result is affected by the presence of thin surface layers on wafer such as native oxide on wafer. Thus surface cleavage of the sample is essential before any measurement has been done.

## Section 3.2 Single layer (Ambient-film substrate)

Considering a single uniform film covered on a substrate, refractive wave will subsequently under multiple internal reflection between the parallel plane boundaries. If two boundaries are separated with film thickness d, there will exist infinite number of reflected and transmitted wave.

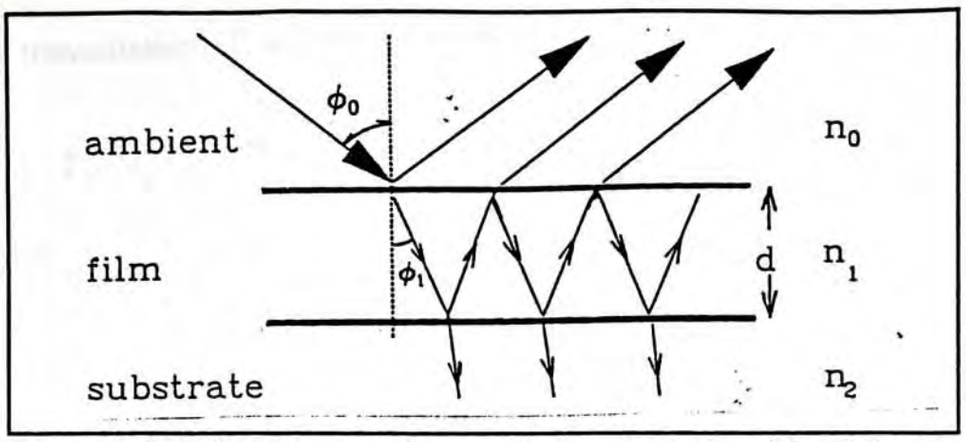


Figure 3.2 *Reflection at and transmission through a thin dielectric film*

Let $\beta$ be the phase change of multiple reflected wave inside the film experience and $\beta$ is given by

$$\beta = 2\pi \left(\frac{d_1}{\lambda}\right) N_1 \cos\phi_1$$

$$\beta = 2\pi \left(\frac{d_1}{\lambda}\right) (N_1^2 - N_0^2 \sin^2\phi_0)^{1/2} \qquad (3.16)$$

The total resulting reflection and transmission are in fact the summation of an infinite series

$$R = r_{01} + t_{01}t_{10}r_{12}\, e^{-j2\beta} + t_{01}t_{10}r_{10}r_{12}^2\, e^{-j4\beta} + t_{01}t_{10}r_{10}^2r_{12}^3\, e^{-j6\beta} + \ldots \qquad (3.17)$$

or

$$R = r_{01} + \frac{t_{01}t_{01}r_{12}\, e^{-j2\beta}}{1 - r_{10}r_{12}\, e^{-j2\beta}} \qquad (3.18)$$

Substitute $r_{10} = -r_{01}$ and $t_{01}t_{10} = 1 - r_{01}^2$

$$R = \frac{r_{01} + r_{12}\, e^{-j2\beta}}{1 + r_{01}r_{12}\, e^{-j2\beta}} \qquad (3.19)$$

Similarly, for transmission, T is given by the infinite geometric series.

$$T = t_{01}t_{12}\, e^{-j\beta} + t_{01}t_{12}r_{10}r_{12}\, e^{-j3\beta} + t_{01}t_{12}r_{10}^2r_{12}^2\, e^{-j5\beta} + \ldots \tag{3.20}$$

Summation give

$$T = \frac{t_{01}t_{12}\, e^{-j\beta}}{1 + r_{01}r_{12}\, e^{-j2\beta}} \tag{3.21}$$

Note that the Fresnel reflection and transmission coefficient at boundaries formed by 0 and 1 are denoted by $r_{01}$, $t_{01}$. Coefficients at the boundaries formed by media 1 and 2 are denoted by $r_{12}$ and $t_{12}$ and so on.

When we consider the parallel p and the perpendicular s wave to the plane of incident, subscript p and s are added to the coefficients and we have

$$R_p = \frac{r_{01p} + r_{12p}\, e^{-j2\beta}}{1 + r_{01p}r_{12p}\, e^{-j2\beta}} \tag{3.22}$$

$$R_s = \frac{r_{01s} + r_{12s}\, e^{-j2\beta}}{1 + r_{01s}r_{12s}\, e^{-j2\beta}}$$

In sum, reflection R and T can be written in terms of their absolute values and phases.

$$\begin{aligned} R_p &= |R_p|\, e^{j\Delta_{rp}} \\ R_s &= |R_s|\, e^{j\Delta_{rs}} \\ T_p &= |T_p|\, e^{j\Delta_{tp}} \\ T_s &= |T_s|\, e^{j\Delta_{ts}} \end{aligned} \tag{3.23}$$

Ratio of complex reflection coefficient $\rho$ are defined as

$$\rho = \frac{R_p}{R_s} = \tan\Psi \; e^{j\Delta} \tag{3.24}$$

As a result, what we have to measure in the experiment are the intensities and phases (state of polarization). If we consider a single layer model, equation of ratio of complex reflection coefficient will be in the form of equation (20).

$$\rho = \left[\frac{r_{01p} + r_{12p}\, e^{-j2\beta}}{1 + r_{01p} r_{12p}\, e^{-j2\beta}}\right]\left[\frac{1 + r_{01s} r_{12s}\, e^{-j2\beta}}{r_{01s} + r_{12s}\, e^{-j2\beta}}\right] \tag{3.25}$$

The single model is adequate for most applications. Function $\rho$ is depends on complex refractive index of ambient $N_0$, film $N_1$, substrate $N_2$ and film thickness $d_1$ as well as wavelength of incident light $\lambda$ and incident angle $\phi_0$ thus $\rho$ can then be written as equation (3.26).

$$\rho = \tan\psi \; e^{j\Delta} = \rho(N_0, N_1, N_2, d_1, \phi_0, \lambda) \tag{3.26}$$

In general, for a single layer thin film sandwished between the substrate and ambient, there are totally nine arguments for that system. Six parameters are from the refractive index of each medium and the remain three are $d_1, \rho_0, \lambda$. If we assumed that $N_0, N_2, \phi_0$ and $\lambda$ are known, three unknown variables remain in the equation ($d_1$, $n_1$ and $k_1$). It should be noticed that, we have to calculate three unknowns out of two ellipsometry data ($\psi, \Delta$). Therefore, if there is only one set of independent data, the thin film should be a non-aborting material or by some how one of the variables is known.

## Section 3.3 Multilayer system (Isotropic Stratified planer structure)

For a single layer structure, the above equation (3.26) is fully adequate for us to derive its optimal property. However, for multilayer structure, as there exist muti-reflection and refraction within layers, the simple mathematical equation cannot be applied to analyse specific characteristics of multilayer sample.

In order to overcome the above problem, a more elegant approach that employ 2x2 matrix which was first suggested by Abele's[23] was used. The principle is based on the fact that equations governing the propagation of light are linear and the continuity of tangential fields across an interface between two isotropic media can be regarded as a 2x2 linear matrix transformation.

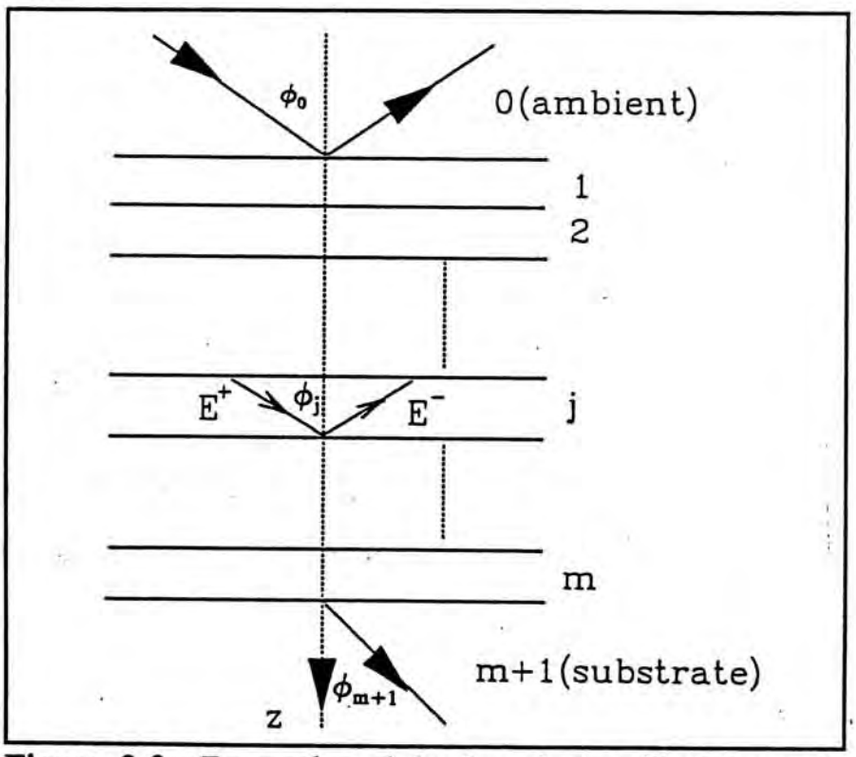


Figure 3.3. *Forward and backward travelling wave in multi-layer structure*

Considering a stratified structure that consists of a stack of m parallel layers sandwiched between two semi-infinite ambient and substrate. All media are homogeneous and isotropic. As shown in Figure 3.3, a forward travelling plane wave is denoted by superscript

(+) and backward travelling plane wave is denoted by superscript (-). Now, let $E^+(z)$ and $E^-(z)$ denote the complex amplitude of the forward and backward travelling plane wave at arbitrary plane z. The total field at z can then be written in the form of 2x1 column vector.

$$E(z) = \begin{bmatrix} E^+(z) \\ E^-(z) \end{bmatrix} \tag{3.27}$$

If we choose two parallel boundary Z' and Z", E(Z') and E(Z") can be written in linear equation format as follow :

$$\begin{bmatrix} E^+(Z') \\ E^-(Z') \end{bmatrix} = \begin{bmatrix} S_{11} & S_{12} \\ S_{21} & S_{22} \end{bmatrix} \begin{bmatrix} E^+(Z'') \\ E^-(Z'') \end{bmatrix} \tag{3.28}$$

or simply $E(Z') = S\,E(Z")$

where

$$S = \begin{bmatrix} S_{11} & S_{12} \\ S_{21} & S_{22} \end{bmatrix} \tag{3.29}$$

S represents the overall reflection and transmission properties of the stratified structure, so S is called scattering matrix. It is obvious that S must contain information about the interface between layers (I) and the layers (L) itself thus it can be expressed as a product of matrix I and L.

$$S = I_{01}L_1I_{12}L_2,\ldots\ I_{(i-1)}L_i,\ldots\ L_mI_{m(m+1)} \tag{3.30}$$

As Fresnel coefficients for forward and backward direction can be written as $r_{ba} = -r_{ab}$ and $t_{ba} = (1-r_{ab}^2)/t_{ab}$. $I_{ab}$ and L are expressed in the form of :

$$I_{ab} = \frac{1}{t_{ab}} \begin{bmatrix} 1 & r_{ab} \\ r_{ab} & 1 \end{bmatrix} \tag{3.31}$$

$$L = \begin{bmatrix} e^{j\beta} & 0 \\ 0 & e^{j\beta} \end{bmatrix} \tag{3.32}$$

Subscript a and b refer to the two media and thus $I_{ab}$ is the interface layer between a and b. The reflectance and transmittance are defined as

$$R = \frac{E_a^-}{E_a^+} = \frac{S_{21}}{S_{11}} \qquad T = \frac{E_s^+}{E_a^+} = \frac{1}{S_{21}} \tag{3.33}$$

Consider two components separately, we have equation (3.34)

$$R_p = \frac{S_{21p}}{S_{11p}} \qquad R_s = \frac{S_{21s}}{S_{11s}} \tag{3.34}$$

Finally we have the equation of complex reflective coefficient

$$\rho_r = \frac{R_p}{R_s} = \frac{S_{21p}\, S_{11s}}{S_{11p}\, S_{21s}} \tag{3.35}$$

The above procedure can be illustrated by taking an example. In case of single film sandwiched between ambient (air) and substrate, the scattering matrix S is given by

$$S = I_{01} L_1 I_{12} \tag{3.36}$$

Substitute corresponding equations into the above formula, we have

$$S = \frac{1}{t_{01}t_{12}} \begin{bmatrix} 1 & r_{01} \\ r_{01} & 1 \end{bmatrix} \begin{bmatrix} e^{j\beta} & 0 \\ 0 & e^{j\beta} \end{bmatrix} \begin{bmatrix} 1 & r_{12} \\ r_{12} & 1 \end{bmatrix} \tag{3.37}$$

or

$$S = \frac{e^{j\beta}}{t_{01}t_{12}} \begin{bmatrix} (1 + r_{01}r_{12}\, e^{-j2\beta}) & (r_{12} + r_{01}\, e^{-j2\beta}) \\ (r_{01} + r_{12}\, e^{-j2\beta}) & (r_{01}r_{12} + e^{-j2\beta}) \end{bmatrix} \tag{3.38}$$

When we expand the matrix by carrying out the multiplication, we get

$$\begin{aligned} S_{11} &= \frac{e^{j\beta}}{t_{21}t_{12}} (1 + r_{01}r_{12}\, e^{-j2\beta}) \\ S_{21} &= \frac{e^{j\beta}}{t_{01}t_{12}} (r_{01} + r_{12}\, e^{-j2\beta}) \end{aligned} \tag{3.39}$$

Put $S_{11}$ and $S_{21}$ into equation 3.33 yield

$$\begin{aligned} R &= \frac{r_{01} + r_{12}\, e^{-j2\beta}}{1 + r_{01}r_{12}\, e^{-j2\beta}} \\ T &= \frac{t_{01}t_{12}\, e^{-j\beta}}{r_{01} + r_{12}\, e^{-j2\beta}} \end{aligned} \tag{3.40}$$

Which are the same equations as calculated by using addition and multiplication shown previously in section 3.2 (single layer). In 1948, Crook also derive this equation by the method of adding and multiplying. However, the calculation was quite awkward and the situation will become even more complicated when the number of film is more than two. In contrast, method of scattering is simple and clear which can also be used in single layer case.

## CHAPTER 4. CLASSIFICATION OF ELLIPSOMETRY

Configuration of ellipsometer can be divided into two main classes, namely null ellipsometry and photometric ellipsometry. There are various kinds of construction modified from the traditional configuration. Difference between these two basic type configuration is that, for null type ellipsometer it is based on the measurement of the state of polarization by alternating the adjustment of polarizer and analyzer. Usually, we will adjust the angle of the first polarizer so that a linear polarized light was reflected from the sample's surface. The reflected light will then be blocked by an analyzer. By rotating the analyzer, the detect signal was minimized. Therefore, the polarization state was obtained indirectly from the azimuths of polarizer and analyzer. For a photometric type ellipsometry, state of polarization is determined by the direct measurement of elipticity of reflected wave while the angle of the polarizer was fixed. The operation principle of photometric type is based on the measurement of the change in output intensity for a given setting of the azimuth angle.

The earliest ellipsometer were all dependent on the determination of null position by human eye. At about 1939, Bor et al modified the instrument by replacing the eye with photocell. At that period, the measurement was confined at visible region. After then, the further development was approach towards the introduction of automatic adjustment.

Robert and Meadows made use of the feedback signal from photocell to adjust the null process by the mechanical operation of optical elements in 1974. Another means of automation is to employ the used of two Faraday cell[24] or Pockels cell[25]. The cells were mounted after the polarizer and before the analyzer. By applying feedback current to those cells, a magnetic field is established along the axis of the light path. Since the magnetic field can rotate the plane of polarization, the null process can be achieved by applying a suitable current to the cells. Instrument constructed with this configuration contain no motive

elements and thus successive measurements at a fixed photon energy can be obtained within 1ms. For the purpose of spectroscopic measurement, the spectrum can be acquired with few second.

The rotating element ellipsometer is the fundamental configuration of photometric type ellipsometer. The optical elements used is similar to that of null system except that the compensator is not necessary[12]. A typical instrument was constructed by D.E.Aspnes and A.A studna[26] in 1975 and it is still a standard in this field. The configuration of our spectroscopic is based on their design. The analyzer of such instrument mounted within the hollow shaft of a motor and rotated continuously at a stable mechanical frequency (50-100Hz). The complex reflectance coefficient $\rho$ can be acquired by using the Fourier analysis of the detected signal.

Moreover, there is a polarization-modulated ellipsometer which are constructed by replacing the compensator with a birefringent phase modulator such as Pockels cell or piezobirefringent plate[27,28]. The retardance varies sinusoidally with time rather than being fixed as in the null system. The sinusoidal signal can be analyzed by login amplifier[27,28] or by Fourier analysis[29]. Piezobirefringent modulator can be operated at fast as 100kHz and thus the speed of measurement can then be increased to about 10$\mu$s. However, there is still a drawback as the response of detector may not follow the signal's fluctuation. Aspnes[30] has analyzed the precision of few automatic systems and he found that no one system can has a major advantage over the others.

Another variation on the major type ellipsometer is the interference ellipsometer. It was modified from the Michelson's interferometer and was described by Hazebroek and Holscher[31]. An incident beam was divided into two by a beam splitter. One beam transmitted to and reflected back from the specimen while the other was sent along a reflecting arm

containing a standard reflector. The s and p components of the returning beam are selected and directed by a Woolastron prism to two matched detectors. The phase difference between two beams can be changed by adjusting the length of reflecting arm.

In recent years, a passive polarimeters was invented[32,33,38]. Instrument designed by Jellison was similar to that of interference ellipsometer which made use of beam splitter and Woolastron prisms. However, the beam was further divided into four parts whose individual intensities can be related to four Stokes parameters of the incident beam. Therefore, all parameters can be determined at once. Owing to the fact that the instrument contain no moving part, the speed of measurement was only limited by the responding time of detector.

Although there are different design and configuration of ellipsometer, most of them are modified from the null-type and photometric ellipsometer. A brief review of the two major type ellipsometers will be presented , then it will be followed by the reasons of choosing a particular construction.

**Section 4.1 Null-type ellipsometer**

Null type ellipsometer is a classical type configuration. Because of its simpler measurement of evaluation of algorithm, it has been widely use since 70's. Most of the design of commercially available equipment are still based on this technique.

A typical experimental arrangement for the instrument is shown in figure 4.1. It consists of two arms and a specimen table. Two arms place at left and right sides of specimen table are used to align laser light source, detector and optical components so that light path lie on the same plane. Null ellipsometer configuration is commonly called PRSA (Polarizer-Retarder-Sample-Analyzer) configuration. firstly, HeNe laser emit homogeneous light with wavelength 632.8nm. A compensator/retarder Q is then placed behind the polarizer so that the plane of s-wave is retarded relative to the p-wave. By adjusting the relative angle

of the polarizer and retarder (quarter-wave plane), a polarized beam with particular elipticity will incident onto the specimen.

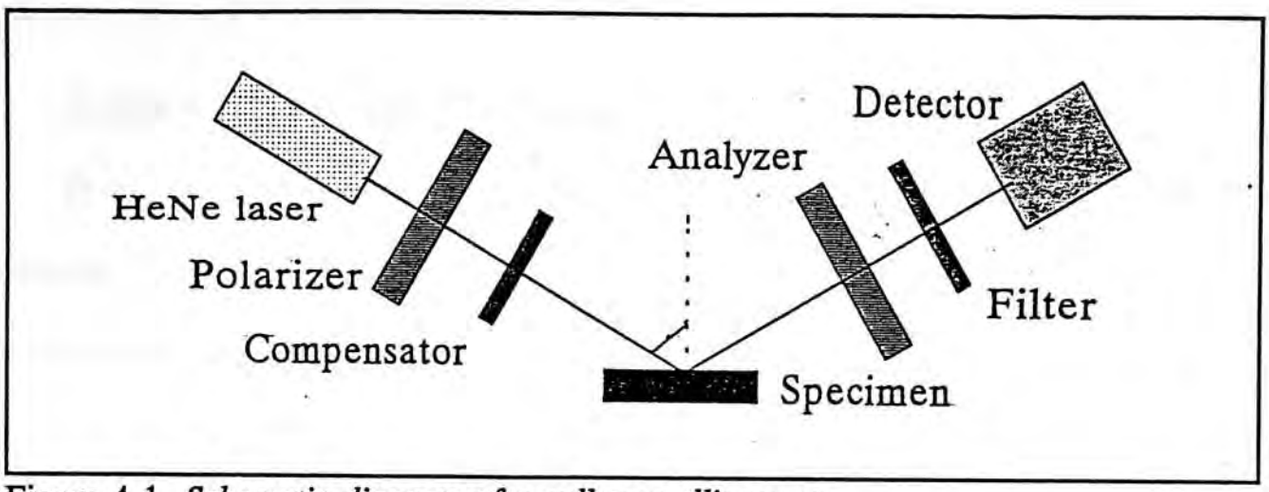


Figure 4.1. *Schematic diagram of a null-type ellipsometer*

If an appropriate elipticity was selected, after striking on sample surface, polarized beam will be converted into linear form. Intensity of the reflected wave will completely be extinguished by an analyzer. Measurement was independent on the beam intensity, thus intensity fluctuation of light source and environment light scattered into the optical path only have minor influence on the result. Hence, the complex reflection coefficient can be obtained from the elipticity angles of polarizer and analyzer. However, the alternating adjustment of polarizer and analyzer result in a long data acquisition time. Speed limitation affect the application of this technique for in situ monitoring of dynamic processes.

The compensator is set at a fixed angle to the plane of incidence. At that case, there will be two conjugate position of P and A which give null signal from the detector. The ellipsometer parameter is then equal to $\Delta=-(P_1+P_2)$ and $\psi=-(A_2-A_1)/2$ for retarder set at 45°. When retarder is set at -45°, $\Delta=(P_3+P_4)$ and $\psi=-(A_3-A_4)/2$. Usually, the retarder is keep fixed and thus only one set of P and A will be used. The method is then called two-zone averaging. The result obtained by using a null type ellipsometer (Gaernter L117) is used as a reference to check the accuracy of the spectroscopic ellipsometer. The ellipsometric

parameter acquired from that null ellipsometer is also based on the two zone method. If both sets of data are used, the method is called four-zone averaging. For detailed information refer to references 13,36.

**Section 4.2 Photometric Ellipsometer**

Photometric ellipsometry technique is based on the principle of polarization modulation. Intensity of the reflected beam is modulated by rotating analyzer and so this technique is also known as rotating analyzer ellipsometry. The modulated depth can be used to characterise the properties of the sample. Configuration of a rotating ellipsometer is similar to that of null type[12,26,37]. It also have two arms separated on left and right hand side of the specimen holder. This technique have higher speed and better accuracy. Light beam was polarized by a fixed polarizer. When a beam was reflected from the specimen surface, in general, an elliptical polarized wave was formed. The reflected wave will then be modulated by a rotating analyzer with twice the rotating frequency of the analyzer. The sinusoidal fluctuating intensity is measured by a suitable detector located behind the analyzer. If the beam incident on the analyzer is linearly polarized, detected signal will be a sine-square function with one maximum and one zero-intensity per half rotation cycle of analyzer. However, if there is no fluctuation, the incident beam should be circularly polarized. Therefore, the modulation depth is a function of elipticity of reflected light beam and the phase angle is related to the zero azimuth of the analyzer.

The incident angle is usually near the principle angle. The principle angle is defined as the angle of incidence at which a phase shift of $\pi/2$ occurs between two orthogonal components of the wave which are polarized in parallel and perpendicular to the plane of incidence, respectively. The Brewster angle will coincides with the principle angle if the light beam is reflected from a non-absorption material. Brewster angle is defined as the angle at

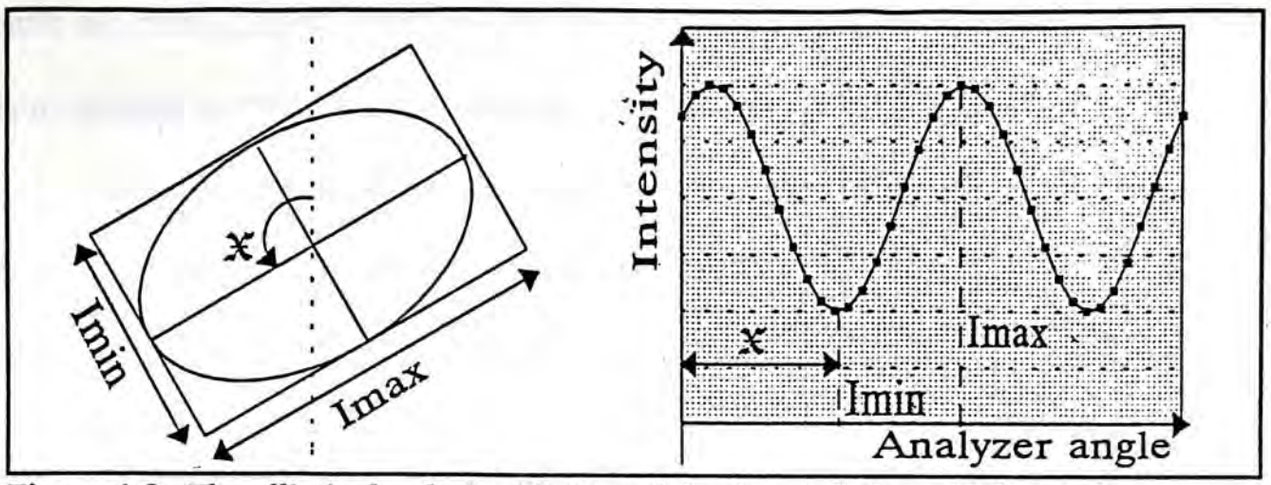

Figure 4.2. *The elliptical polarized light and the detected sinusoidal signal*

which only the component perpendicular to the plane of incidence will be reflected from the sample surface. If the substrate is absorbed, phase shift of few degrees will be introduced between the principle angle and the Brewster angle. If the angle of incidence is equal to the principle angle, then the elliptically polarized light will either have a major or minor axis parallel to the plane of incident. The elipticity of the reflected wave can be modified by the angle of the polarizer. If the polarizer's azimuth is equal to $\psi$, then a circularly polarized reflected beam will be resulted.

As mentioned before, the modulation depth and phase angle are related to the properties of the dielectric material, therefore, the next step is to extract the modulation depth and phase from the sinusoidal signal. Those parameters can be derived from the measured data by analog method or digital method. Since the modulation frequency was known, the amplitude of sinusoidal component could be measured by a lock-in-amplifier. Consider the digital methods, measured intensity was digitized for further processing. Results from the Fourier analysis of the digitized signal permitted us to calculate the complex reflection coefficient of the sample.

The photometric ellipsometry technique involved the measurement of the fluctuation of light intensity. The existence of stray light and scattering light will change the modulation

depth and finally affect the calculated result. In order to reduce the influence from stray light, suitable method should be done to compensate the effect.

The advantage of rotating analyzer ellipsometry is that the data acquisition time of this technique is shorter. Moreover, the simplified retarderless construction make rotating type favour for the spectroscopic investigation where a large number of data have to be acquired.

**Section 4.3 Spectroscopic ellipsometer**

The principle of ellipsometry has been known since 19th century. However, this technique was not widely used until the early 1960s. It is because, the evaluation of ellipsometric parameter is relatively complex. Equation involved Fresnel's formula can only be solved analytically in few special cases while in other cases, numerical approaches is needed.

At the end of 70s, the rapid development of computer technology successfully introduce the application of ellipsometry into industrial area. But the application was still limited on the thickness and refractive index measurement of non-absorption thin film on substrate with known optical properties. The endeavour in the determination of complex parameter in microelectronic industrial led to the development of the spectroscopic ellipsometry which use not only one wavelength of monochromatic light but it also need a number of measurements at different wavelengths.

Ellipsometry measurement at one wavelength $\lambda$ can only provide one set of optical parameter. Information can be used to determine the properties of a bulk material or a non-absorbing thin film. However, in general, there are three unknowns for each overlayer. If we want to find out the complex refractive index and the thickness of a overlayer, more than one set of optical parameters is needed. Multiple measurements at different wavelengths is a convenient way to increase the number of optical parameters and independent ellipsometric

equations. Measurement are usually taken within an interesting range of wavelength, mostly, within the entire visible spectrum. The ellipsometric parameters $\psi$ and $\Delta$ are now becoming the function of wavelength and therefore spectroscopic ellipsometry can determine a series of optical parameters from a complex multi-layer system.

# CHAPTER 5. CONSTRUCTION AND CALIBRATION OF SPECTROSCOPIC ELLIPSOMETER

The null type ellipsometer is a classical configuration. It is good enough to measure the optical properties and thickness of transparent thin film such as Silicon dioxide. However, the application of single-measurement ellipsometer is limited and the data acquisition time is long. Although the complex refractive index of a bulk material can be obtained directly from the ellipsometric parameters ($\psi$,$\Delta$), it cannot be applied to sample with absorbing thin film overlayer. Generally speaking, there are three unknowns for each layer of thin film, two from the complex refractive index and the other is the thickness of that layer. Therefore, only one pair of parameters obtained in a single-measurement ellipsometry is inadequate to find out all the unknowns. That is the reason why the application of null type ellipsometer is only limited in the measurement of transparent thin film previously. There is two ways to expand the ability of single-measurement ellipsometer. Firstly measurement can be repeated at different incidence angles so that the independent pair of parameters can be increased. There is a drawback that it is very time consuming especially when a null type ellipsometer is used. Optical properties of sample at a particular wavelength can be determined after multiple measurement. Moreover, a mathematical approach such as data fitting has to be involved in the calculation. The second method is to reduce the number of unknowns by measuring one of the parameter via other means. The most convenience way is the physical parameter (thickness) handling. This parameter can be determined by other method such as Alpha-Step. Theoretical speaking, two unknowns can be decided from two parameters. However, as the calculation consist of complex number, the solution is not unique. This phenomena has been studied and will be discussed in next chapter.

Owing to the above factors, it is better to construct a multi-measurement system to

modify the null ellipsometer.

**Section 5.1 Design and Construction of the ellipsometer**

Although the configuration of ellipsometer is classified into two main classes as we discussed in previous chapter, the ellipsometry measurement can be realized by different configuration and with different optical components. For a spectroscopic ellipsometry, measurement has to be repeated at different wavelength. Thus the difficulties in automation is one of a major consideration in constructing the ellipsometer. This is the reason why most of the SE nowadays fall in the photometric category.

Hauge and Dill[11] in 1973 constructed a basic computer-assisted rotating-analyzer ellipsometer unit. The configuration is similar to that of a null ellipsometer except the polarizer is fixed. The computer assisted the measurement and the position of the sample is adjusted by a computer controlled stepper-motor-driven x-y table. However, a laser light source is used in that instrument. Thus measurement can only be done at fixed photon energy. At the same year, Aspnes[12] replaced the laser source with a broad-band light source coupled to a computer controlled monochromator. The transmitted light intensity was analyzed based upon on-line Fourier by a minicomputer. After two years, Aspnes and Studna[26] modified the system and then reported a high-precision rotating analyzer instrument. The configuration of that instrument has become a performance standard in this field. The design of our SE system is therefore based on that standard configuration[11,12,26].

Besides the rotating element type ellipsometer, another choice for photometric system is the polarization-modulation type. The elipticity measurement of this is achieved by using Faraday cell or Pockell's cell while rotating type preformed with mechanical rotation of a polarizer. Both systems have their own advantage. For a real-time monitoring application such as fast electrochemical reaction at surface or in situ measurement of film growth, high

speed is a primary requirement. Polarization-modulation system is an appropriate choice. However, the use of compensator and modulator introduced a photon energy dependence element and thus the accessible spectral range is limited and the absolute accuracy will be reduced. On the other hand, if the primary requisite is the accuracy rather then the speed of measurement, the use of simple rotating analyzer ellipsometer is better.

Design of our spectroscopic ellipsometer is based on the rotating analyzer photometric type ellipsometer for the reason of its simplicity in construction and easier in automation. The ellipsometry system was interfaced to a micro-computer so that the operation was automated. Parameters $\psi$ and $\Delta$ will be measured as a function of wavelength and then stored in for further processing. The construction of a spectroscopic ellipsometer system (Figure 5.1) can be divided into three sub-systems (a) Optical assembly, (b) Electronic circuit, (c) Micro-computer(Software). Each sub-system will be discussed in below.

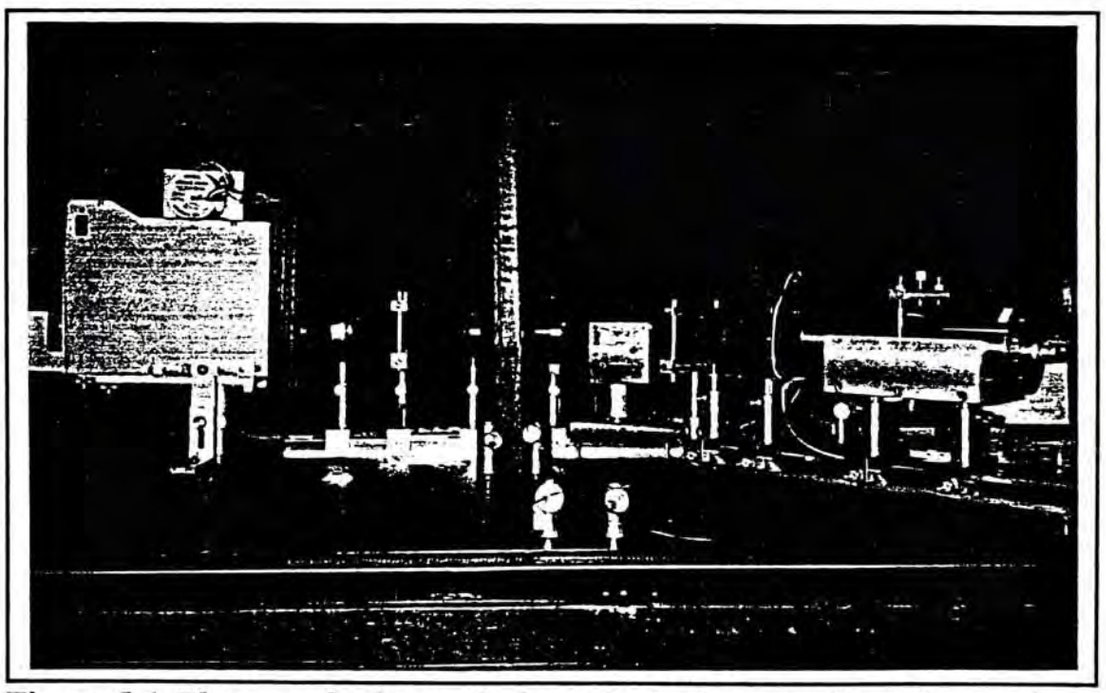

Figure 5.1 *Photograph shows all the optical elements of rotating-analyzer type spectroscopic ellipsometer*

**Section 5.1.1 Optical Assembly**

Spectroscopic Ellipsometer is basically an optical instrument that consists of a continuous light source, polarizer, analyzer, detector and various auxiliary optical components such as lens, iris and filter (figure 5.2).

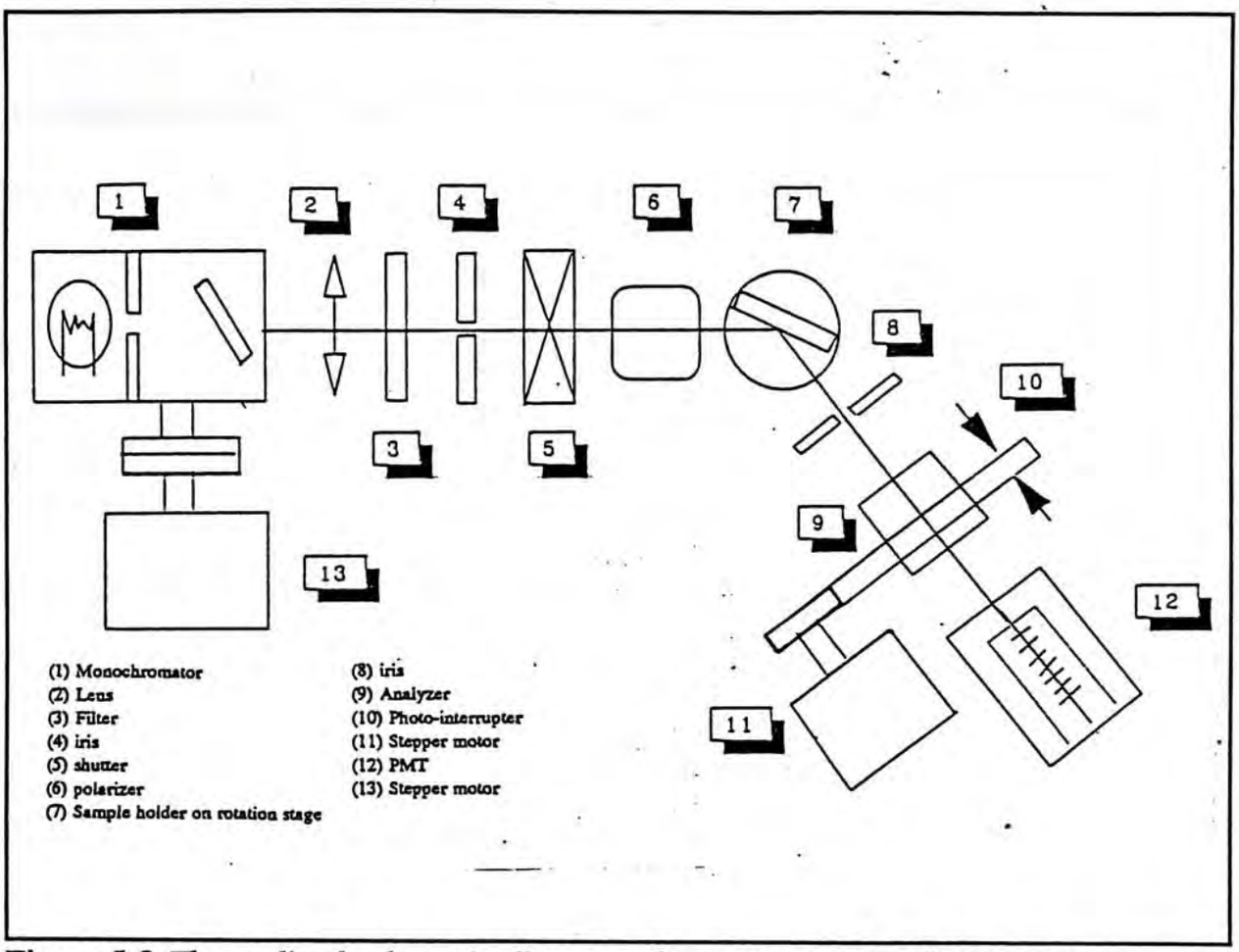


Figure 5.2 *The outlined schematic diagram of a spectroscopic ellipsometer*

A 35W tungsten (Quartz-iodine) lamp was installed in the lamp house to produce continuous light. The lamp house was collected to a monochromator which contain a grating of 1350 groove per millimetre. By turning the angle of grating, light beam with different colour can be selected. Measurement was taken only one wavelength at a time. When measurement was completed, another wavelength was selected and the measurement procedure would be repeated. The grating is operated in the visible region (350nm to 800nm) and blazed at 500nm. The monochromator has to be mounted before the fixed polarizer. It

is because, the throughput of the monochromator depends on the polarization state and thus it cannot be placed between the rotating analyzer and the detector.

Inside the monochromator, spectrum of light reflected from the grating was further spread by a concave mirror, thus light came out from the monochomator was divergent. Some commercial ellipsometer employ a collimator assembly to control the light beam within a divergence of about 2 mrad[35]. For the instrument designed by Aspnes and Studna[26], the apex angle of the light cone on the sample is about 1°. In order to reduce divergence and to increase the intensity of light beam, a "crown glass bi-convex" lens was used to collimate the monochromatic light into a parallel beam. The convex surface of these lens are symmetric with focal length which are equal to the radius of curvature. This has an advantage of minimizing in coma distortion and chromatic abberations. Moreover, a filter is placed behind the lens to cut out high order light from monochromator.

Diameter of the parallel light beam was then narrowed down into 1.5mm by using an adjustable aperture. The light beam was polarized by a Glan Tayler cube polarizer. Although a fixed polarizer is used in this instrument, it is mounted in a rotary stage and located behind the aperture so that the azimuth angle can be calibrated. However, the angle of these polarizer need not be changed frequently, so it was fixed at $45^0$ inclined to the plane of incident. Glan Tayler polarizer was made from natural calcite ($CaCo_3$) and the interface between the prisms was filled with air rather than cement. It gave high transmittance from 400nm to 2500nm. Besides this advantage, Glan Tayler polarizer has an extinctive ratio better than $10^{-5}$.

Sample was mounted on a tilt table which placed on top of a rotating state (Figure 5.3) so that the sample surface can be aligned. The rotational stage can turn along an axis perpendicular to the plane of incidence. For reasons of simplicity, the polarizer and analyzer

were mounted at an angle of 135°, thus the angle of incidence is equal to 67.5°.[26]

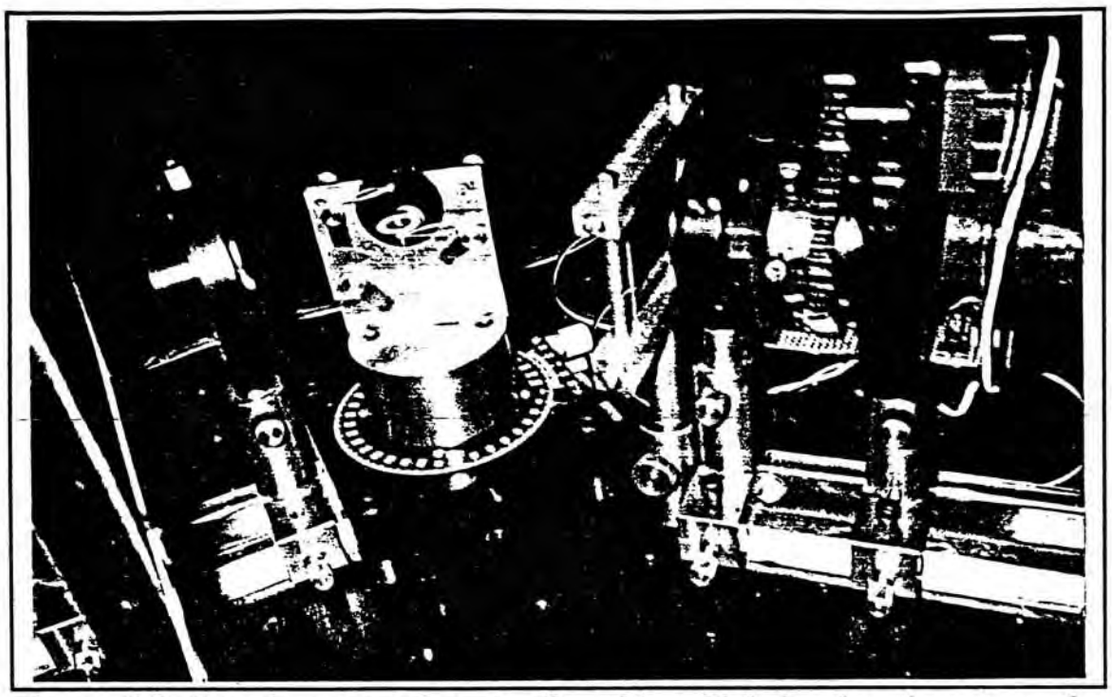

Figure 5.3 *Sample mounted on a tile table which is placed on top of a rotation stage.*

Usually, beam reflected from the sample would be elliptically polarized. The elipticity is then analyzed by an analyzer (Second Glan Tayler polarizer). A special rotary stage held the analyzer and rotated in an axis parallel to the propagation of reflected beam. The rotary stage was driven by a stepper motor. Step increment was equal to 0.36° per step. Rotation of analyzer was slow down by a 3 to 1 gear. To complete one cycle of motion, three hundred steps have to be moved. Another adjustable diaphragm was placed in front of the analyzer to cuts off any possible parasitic beam.

When an elliptical polarized light passed though a rotating analyzer, a sinusoidal fluctuating signal would result. Light intensity at the minimum point might be week or even close to zero. Therefore, photo-multiplier tube was chosen to be the detector for its sensitivity towards week light.

The photo-multiplier tube was biased by using a divider network (figure 5.4) which consisted of a series of resistors between the earth and high potential. Potential added across

dynodes create an electrostatic field so that electrons could accelerate in the cascade between successive dynodes and thereby providing current amplification.

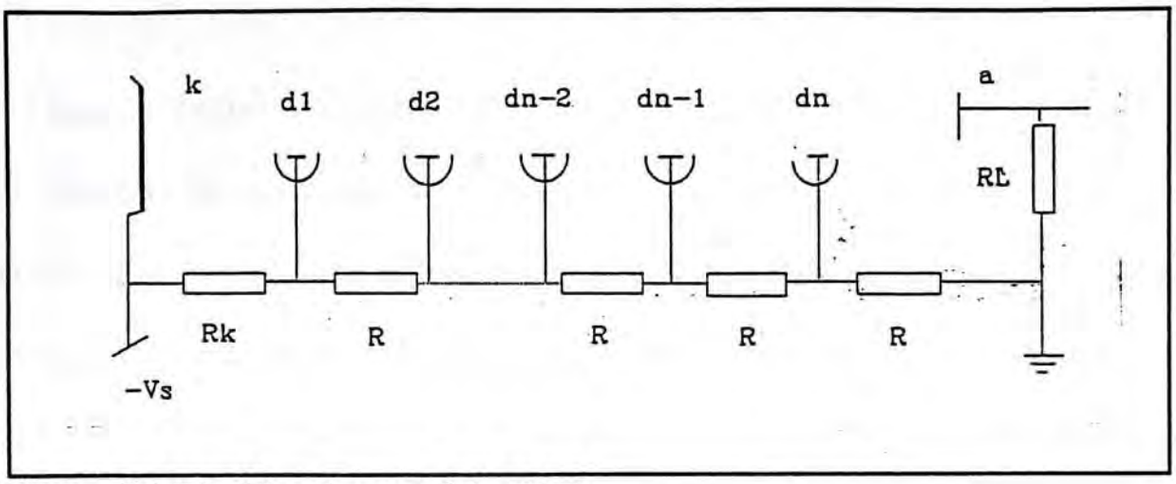


Figure 5.4 *The biased network in PMT*

All resistors except $R_k$ and $R_l$ were selected to have the same value so that a uniform voltage divider networks was provided. Value of $R_k$ double the others to provide a higher operating voltage between cathode and the first dynode. A uniform networks can provide a maximum current Ia of 10$\mu$A.

PMT is an extremely sensitive photodetector. It can not be exposed to room light when EHT is applied on it. The whole system is therefore placed inside a black box to protect the PMT. The dark environment can also reduce stray light enter into the light path. All optical components were placed on an optical table which was made of a 1/2" metal plate. The optical table has been drilled with 1/4" threads.

Although stray light and scattering light can be reduced, it is still unavoidable. Offset cause by those parasitic light will appear in the detected signal. A simple way to measure the intensity of parasitic light is to block the light beam and then do the measurement. The unwanted offset will then be cancelled out by adjusting the offset of the amplifier circuit.

**Section 5.1.2 Electronic circuit**

A micro-computer is used to control the operation of instrument. The interface

circuitry that interface computer and the ellipsometer can be divided into two main parts, Stepper Controller and Signal amplifier and digitalize. Figure 5.5 shows the block diagram of the interfacing circuit. The circuit diagrams are placed at appendix.

Monochromator and rotation of analyzer are both driven by two similar stepper motors. The activate signal sent from computer via a programmable input/output interface card (8255 PPI). Shaft of motor will rotate a precise angular amount when it receive an activate signal. The angular displacement can simply be convert from the number of steps sent from the computer. The direction of motion can be reversed by reversing the sequence of activation signals. Since the outport port of PPI cannot provide enough power to drive the stepper motor, an interface circuit for stepper motor is needed (Appendix R1,R2).

Scanning range of the monochromator was defined by the user. Once the scanning is completed, stepper motor would drive the monochromator back to its initial position. A photo-interrupter (Appendix R3) is used to check the initial azimuth of the analyzer. A pin blocker is installed on the rotation stage that hold the analyzer. Once the photo-interrupter is blocked, a HIGH signal would sent to computer via PPI and no activation signal would be sent to the motor that drive the analyzer. Position of analyzer is therefore reset.

Light intensity is converted into electrical signal by PMT. Signal is then amplified by an amplifier which composed of three OP Amps (Appendix R4). Output impedance of PMT was so high that it must be buffered by a OP Amp follower. Dark current of PMT and scattering light from the surrounding introduced an offset to the signal. Offset was compensated by applying a suitable voltage at the non-inverting terminal of the second OP Amp. Voltage gain was realize in the last stage. Amount of amplification was set in manual mode or auto mode. When auto mode was selected, voltage gain was adjusted automatically by an auto gain control circuitry (Appendix R5). In order to maintain the high performance

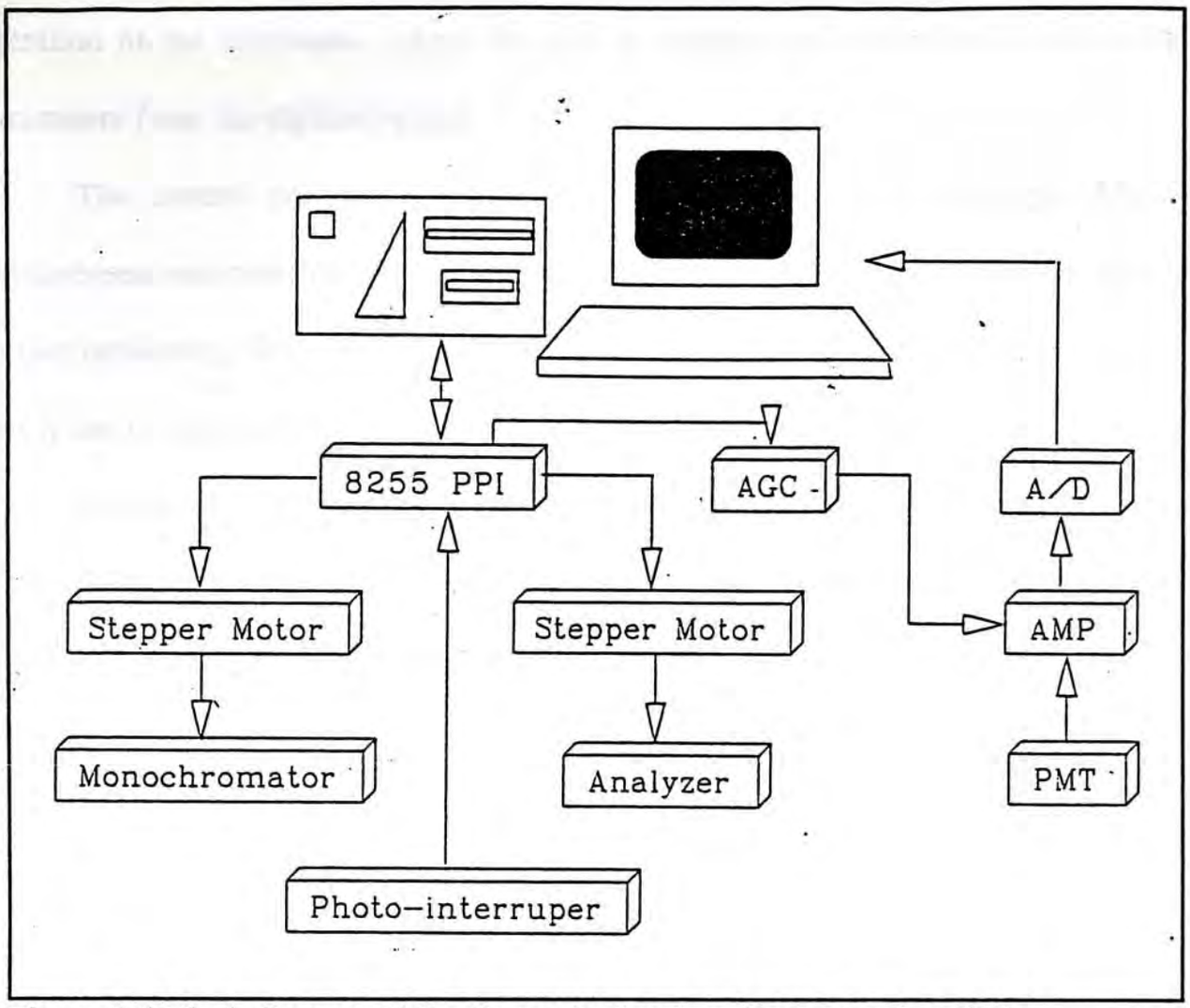


Figure 5.5 *Block diagram of the electronic circuit and computer interfacing*

of the amplify circuit, the input signal to A/D has to be set to a maximum level without overflow[42]. Since, the response of PMT is not linear throughout the spectrum, the gain has to be varied when measurement was done at different photon energy. Finally, the amplified signal was digitised and transferred to the computer by an analog to digital converter (A/D). The 1612 A/D card can converted analog signal into 12 bits digital signal. Thus it can provide a resolution of 4096 stages and the accuracy is equal to 0.024%. It has high input impedance (5MΩ) and fast conversion time (typical 25$\mu$s). Differential input mode was selected to reduce the induced noise.

**Section 5.1.3 Micro-computer (Software)**

An micro-computer system is in fact the brain of the ellipsometer. It control the

operation of the instrument, adjust the gain of amplifier and calculate the ellipsometric parameters from the digitized signal.

The control program was written by using turbo C++ language. After the measurement was completed, the result would display on screen. Data can then be stored for further processing. The ellipsometric parameters $\psi(\lambda),\Delta(\lambda)$ are stored in ASCII format so that it can be easily read by other software such as Lotus and Matlab.

As mentioned before, the ellipsometric parameters are calculated from the modulation depth and the phase angle of the detected sinusoidal signal. Flux variation detected by PMT can be expressed in a mathematical form[11,12]

$$I(t) = I_o\ (1 + A\cos 2\theta + B\sin 2\theta) \tag{5.1}$$

or

$$I(t) = I_0\ [\ 1 + e\ \cos(\ 2\theta+\Phi\ )\ ] \tag{5.2}$$

where

$$\theta = \theta(t) = 2\pi f_o t + \theta_o \tag{5.3}$$

$$e = (A^2 + B^2)^{\frac{1}{2}} \qquad \Phi = \tan^{-1}(-\frac{b}{a}) \tag{5.4}$$

$I_o$ is the average intensity and $\theta$ is the instantaneous azimuth angle of analyzer. $f_o$ is the modulated frequency which is equal to twice the mechanical rotation frequency. A and B are the normalized Fourier coefficient which describe the phases and the amplitudes of the AC components of the flux incident onto the detector. Theoretically speaking, there is only one signal in the frequency domain after the Fourier transform. However, owing to by system defect and noise induced, it may cause higher order Fourier coefficients[43]. In addition, the coefficient derived from two sets of half mechanical cycles (0°-180° and 180°-360°) should

be identical. But in practice, the misalignment of rotation axis of analyzer cause difference between both signals. This phenomena will be discussed in next section. Value of A and B can then be calculated according to the following equations[11,12]

$$A = \frac{2\sum (I_n \cos\frac{2\pi n}{N})}{\sum I_n} \qquad B = \frac{2\sum (I_n \sin\frac{2\pi n}{N})}{\sum I_n} \tag{5.5}$$

From the Fourier coefficients, the ellipsometric parameters can be obtained by the equation 5.6.[11,12]

$$\psi_m = \frac{1}{2}\cos^{-1}(A) \qquad \Delta_m = \cos^{-1}\left(\frac{B}{\sqrt{1 - A^2}}\right) \tag{5.6}$$

Subscript m represent the measured result.

**Section 5.1.4 Modification of configuration**

The design of the spectroscopic ellipsometer (SE) system is based on what have been done by Aspnes, Studna, Hauge and Dill[11,12,26] for the reason of its simplicity in the construction and automation. However, the electronic circuit for signal processing and the system control algorithm are designed by our own. The SE system we constructed is a photometric type ellipsometer which is operating with a rotating analyzer. The rotation of analyzer in our system is controlled by a stepper motor rather than a D.C. motor. The use of stepper motor have three major advantages.

(1) The rotation speed can be directly controlled by a mini-computer.

(2) Measurement can be taken at a definite azimuth angle of the analyzer.

(3) The signal acquisition circuit can be simplified by eliminated the sample and hold circuit and the trigger circuit for rotation of analyzer.

In order to reduce noise pick-up from the power line, the rotation speed of analyzer is usually selected to be different from the oscillation frequency of A.C. power. If the rotation of analyzer is low fast, the modulation frequency of signal will be too high for the detector to response. On the hand, it is difficult to have a stable control for a slow rotation. Thus, a tradeoff is exist in the choosing of rotation speed of the analyzer. For a D.C. motor drive analyzer, the measurement process is triggered by the tooth or holds on the disc which is mounted on the rotator. However, during the measurement of light intensity, the rotation of analyzer is keep on-going and therefore a phase shift existed between the detected signal and the azimuth angle of analyzer. Aspnes[26] has found that, the rate of change of signal voltage is about 7mV/$\mu$s for an optical frequency of 150Hz. If a ADC card with 10$\mu$s conversion time is used, the change of signal during the A/D process will become 70mV. One way to solve this problem is to make use of a sample-and-hold circuit. It has been discovered that if that circuit is omitted, large error will occurs. The typical conversion time of our ADC is about 22$\mu$s, that means longer time is needed to complete a successive-approximation module. Although the conversion time can be reduced when lower resolution is used, the faster conversion we achieved is about 17$\mu$s for 8 bits resolution. The method we used is to replace the D.C. motor by a stepper motor. The rotation speed is directly controlled by the computer via the PPI interface. Unlike the way we used when an D.C. motor was employed, the data is taken while the analyzer was stopped at a particular angle. A reading will be given out after averaging the data from a multiple measurements at the same angle. After then, the analyzer will be driven to the next step and the measurement process repeat again until one or more mechanical cycle is completed. Since the step angle

of a stepper motor is well known and the measurement operation and motion of analyzer is controlled by the same instrument - computer, a trigger circuit is not needed. Analyzer can wait until the measurement and A/D conversion process complete. It is suitable for a system in which a longer time is needed in signal processing. Moreover, the electronic circuit and the calibration process can be simplified because the phase delay between the detected signal and the angle of analyzer is no longer exist.

**Section 5.2 Alignment and Calibration**

Ellipsometer is an optical instrument. The procedure of alignment is therefore generally used in other optical apparatus except for the adjustment of the polarizer (P) and analyzer (A). Alignment processes is mainly depends on the design and construction of the instrument. Although the procedure is machine depended, their principle are the same. More intended information on the alignment of sample can be found in ref. 39,40,41. Aspnes[12] and P.S.Hauge[11] also have a brief discussion on the procedure in the alignment of optical elements for their own systems. Azzam and Bashara[13] have summarized nearly fifteen factors that can affect the determination of the ellipsometric parameters $\psi,\Delta$ for a general ellipsometer. Some factors are caused by the particular optical components that we have not used such as compensator and cell windows. Some factors affect both the values of $\psi$ and $\Delta$, thus points are overlapped.

**Section 5.2.1 Alignment the optical units**

Excluding the alignment of grating of monochromator, the alignment of spectroscopic ellipsometer emphasised on three major parts

(i) Incidence angle ($\phi$)

(ii) Azimuth angle of Polarizer (P) and Analyzer (A)

(iii) Rotation axis of Analyzer

Some literature mentioned that the alignment of ellipsometer is not too critical for the measurement of thickness and refractive index of thin film, but the accuracy of setting (i) to (iii) was found to have a significant influence on the measured data. The ellipsometer was first aligned with the help of a He-Ne laser and then it was calibrated by measuring various kind of samples.

As shown in Figure 5.2 optical components such as lens, iris, polarizer etc are mounted on two rails which are inclined at a angle of 135°. A silicon wafer coated with aluminum was mounted on the sample holder. This specimen act as a mirror and it can be used to calibrate the angle of rotation stage on which the sample holder was mounted.

The rotation stage was rotated to a position that the surface of mirror is perpendicular to the propagation direction of the incidence beam. The angle of normal incidence is then calibrated by fine turning the rotation stage and the tilt table. When the reflected light propagate in the same path as the incidence beam but in opposite direction, the incidence angle is equal to zero degree. Once the normal incidence was found, an appropriate incidence angle can be selected by rotating the stage. For the reason of convenience in setting up the second rail which carry the analyzer and detector, we rotate the stage with 67.5°. Beam reflected from the specimen(mirror) is then used to adjust the position of optical components on the second rail. It has been found that incidence angle around 70° can increase the variation of ellipsometric parameters ($\delta\psi$ and $\delta\Delta$) with respect to wavelength of light beam. In other words, the sensitivity can be optimized when an appropriate incidence angle was used.

The ellipsometric parameters $\psi$ and $\Delta$ are calculated from the relative amplitude of Fourier coefficients A and B. Their relation are given by equation 5.5. The spectroscopic ellipsometer is an instrument contain no retarder, thus the complex reflective coefficient can

be written as equation 5.7. P is the azimuth angle of polarizer.

$$\tan\psi\ e^{(j\Delta)} = \tan P \left( \frac{1 + e\cos\Phi}{-e\sin\Phi \pm j(1-e^2)^{\frac{1}{2}}} \right) \tag{5.7}$$

Expressions of $\psi$ and $\Delta$ can be derived from equation 5.6 and re-written as equations 5.8 and 5.9

$$\tan\psi = \tan P \frac{(1 - e^2\cos^2\Phi)^{\frac{1}{2}}}{1 - e\cos\Phi} \tag{5.8}$$

$$\tan\Delta = \pm\frac{(1-e^2)^{\frac{1}{2}}}{e\sin\Phi} \tag{5.9}$$

It is obvious that values of $\psi$ and $\Delta$ are depends on the azimuth angle of polarizer and the Fourier coefficients A and B. If the polarizer azimuth P is equal to 45°, the magnitude of the orthogonal components of the incidence light will be the same. According to equation 5.8, $\psi$ will depends on A and B only.

The Glan Taylor polarizer was mounted on a vertical rotation stage. Owing to the fact that polarizer is composed of two prisms, the diagonal of it's square surface is equal to 45° of polarization. The angle P is therefore roughly aligned by setting the diagonal of prism surface parallel to the plane of incidence. The precision of the angle P have a great influence on the value of $\psi$. Error of $\pm 1°$ in P will introduce an error of about 3.5% on the value of $\tan\psi$. Fine adjustment of angle P was done by measuring the modulation signal of some known specimen.

Besides the azimuth angles, rotation-axis misalignment will also affect the detected signal, especially in the alignment of analyzer. Equation (5.1) are derived under the assumption that the polarizes are rotated about the beam as axis. David C. Nick and Azzam[44]

have shown that in reality, the axis of devices will not exactly coincide with the beam axis. The influence of small angular misalignment of the rotation axis of analyzer with respect to the light beam axis is that odd harmonics signal will be introduced in the detected signal. Figure 5.6 show a normal signal measured by the PMT. The sinusoidal dots represent the noisy signal and the solid line is the re-generated signal from the coefficients obtained by the Fourier analysis of the noisy dots signal.

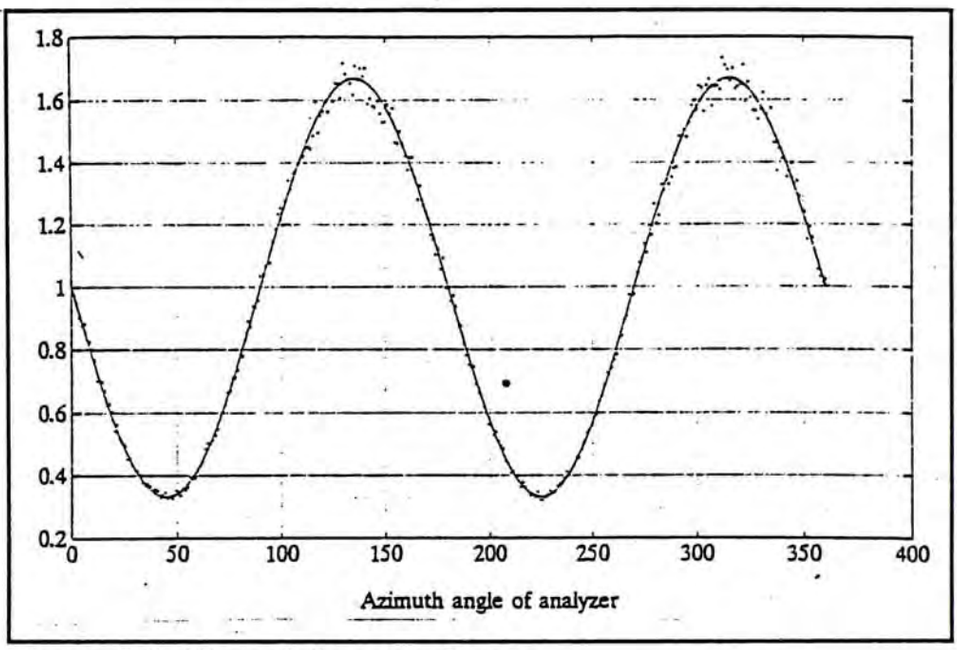


Figure 5.6. *Normal detector signal*

If misalignment of rotation axis exist, distortion due to the presence of the first and third harmonics will occur. As shown in figure 5.7, the peak magnitude of second cycle is lower than that of the first cycle. It also showed the reason why we have to measure the modulate signal through a complete rotation the analyzer in a cycle. The rotating stage that hold the analyzer is especially designed for the alignment of rotation axis.

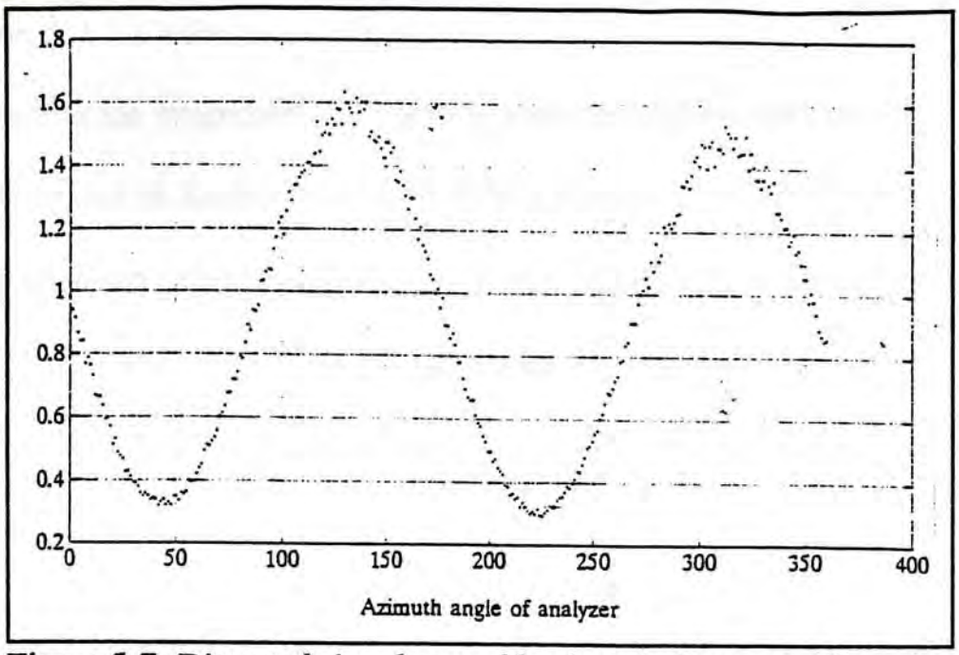


Figure 5.7. *Distorted signal caused by the misalignment of rotation axis of analyzer*

In fact, polarizer and analyzer are first calibrated with the help of He-Ne laser. Position of polarizer and analyzer are tuned so that the light beam reflected from the surface of the Glan taylor polarizer are coincide with the path of incidence light but with opposite direction. Afterwards, they are rotated such that we can investigate the displacement of reflected beam from the path of incidence light beam. Unlike polarizer (azimuth angle is fixed), analyzer have to rotate about the light beam. The influence of misalignment of analyzer will larger than that of the polarizer.

The polarization of axis of analyzer was set perpendicularly to the plane of incidence and analyzer rotate in anti-clockwise direction when looking into the beam[43]. Fine adjustment of azimuth of polarizer and analyzer are done by measuring a bare silicon wafer. The detected signal was compared with the ideal generated signal of a bare silicon wafer. The azimuth angles were adjusted so that the measured signal match with the calculated one.

**Section 5.2.2 Calibration of the system**

The calibration procedures for rotating analyzer ellipsometer was first described by Meulen and Hien and by Aspnes in 1974. Aspnes's method include the first-order corrections to the values caused by the optical activity of the quartz Rochon polarizer. A later article reported by Aspnes and Studna[26] added the corrections of systematic errors caused by the transfer characteristics of the detection circuitry. In fact, another attempt has been made to eliminate error by using a mechanical chopper to modulated a carrier frequency higher than the optical frequency imposed by the rotation of an analyzer, however, the performance of such a light chopping arrangement has bot been justified. In contrast, Meulen and Hien[24] use another approach to perform the calibration. A silicon oxide with particular thickness on crystal Si wafer was used. It has been found that the sensitivity can be optimized when $\Delta$ is near 90°. Meulen and Hien calibrated the system at photon energy 1.96eV with a oxide of about 1350-1400Å. Two standard industrial fabricated samples with oxide thickness of about 1000Å are used to verify the measured result of our system. Before the measurement of the standard samples, a bare silicon wafer is used to have a fine alignment of the system.

The bare silicon specimen is a one inch p-type $<111>$ silicon wafer. It was cleaned by standard RCA method and the wafer was dried by purging it with nitrogen gas. It has been found that a silicon oxide overlayer will immediately formed on a cleaned wafer. The oxide layer formed by the natural process is assumed to be uniform and perfect. The sample was first measured by a commercial monochromatic Gaertner Ellipsometer and a native oxide of about 20Å thick was found. A spectrum of ellipsometric parameters $\psi_c(\lambda)$ and $\Delta_c(\lambda)$ of 20Å $SiO_2$ on silicon substrate at incidence angle of 67.5° were generated by a program based on the theory mentioned in Chapter 3 (Figure 5.8). The generated values of ellipsometric parameters are further transformed to the Fourier coefficients which are used to represent the

detected sinusoidal signal. Signal generated by theoretical means is then used to compare with the experimental one.

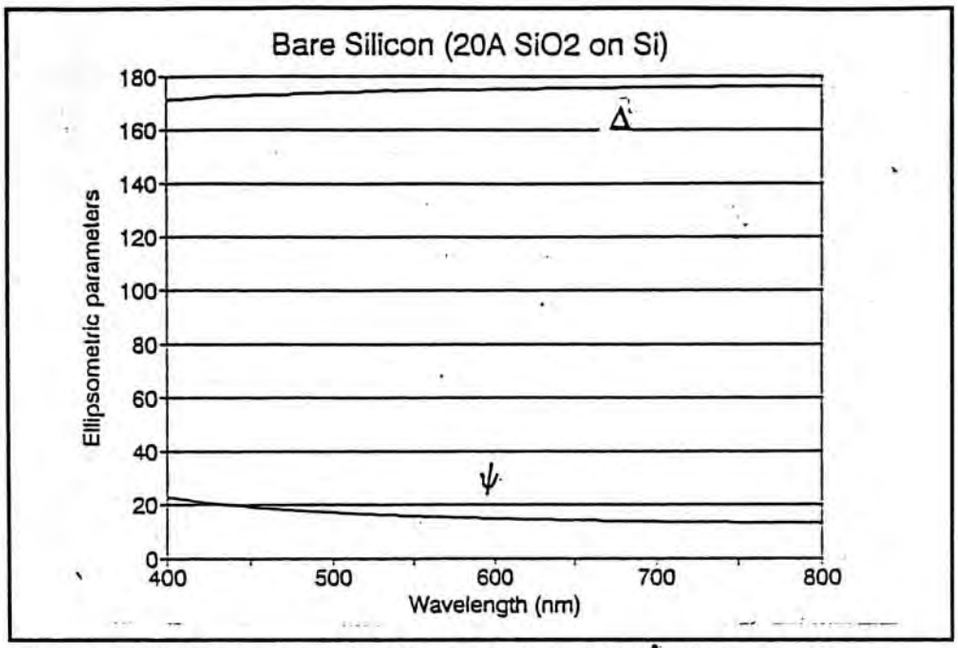


Figure 5.8 *Spectrum of $\psi(\lambda)$ and $\Delta(\lambda)$ of 20Å $SiO_2$ on silicon*

The modulated signal at 633nm was generated by reversing the equations 5.6. [$\psi$(633nm) = 14.41486° and $\Delta$(633nm) = 175.4658°]. The ideal modulated signal was represented by solid line in Figure 5.9, dots represented the measured signal. The azimuth angles of polarizer and analyzer were adjusted so that the detected signal (dots) matched well with the generated signal (solid line). Light reflected from a bare silicon is linearly polarized. It is because Imin of modulated signal in figure 5.9 is close to zero. But, the polarization is no longer 45° inclined to the plane of incidence. Moreover, phase shift of about $0.32\pi$ was resulted when light beam was reflected from the bare silicon. Although the analyzer is symmetric, the direction of its rotation must be concerted. The analyzer must rotate in anti-clockwise direction when facing the incoming light beam, otherwise the Fourier coefficients calculated based on equations described in Chapter 3 will be faulty.

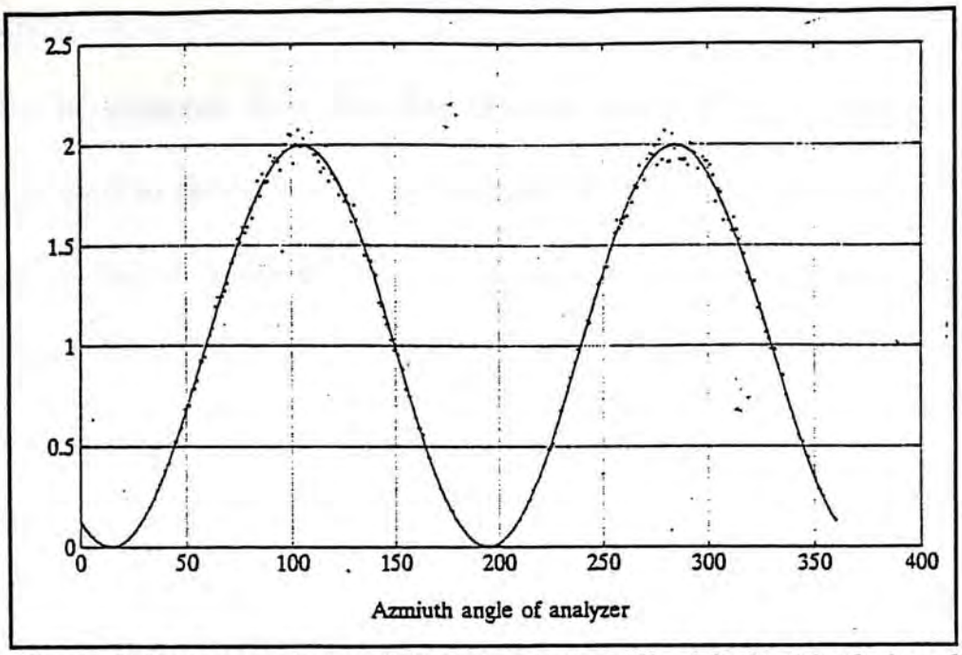


Figure 5.9 *Detected signal (Dots) match well with the ideal signal (Solid line)*

If misalignment of polarizer and analyzer exist, the phase and modulation depth of detected signal will different from that of ideal signal. An example was shown in Figure 5.10. If -4.4% error was introduced in $\psi$ ($\Delta$ no change) phase shift of -5° will occur between the detected signal and the original signal.

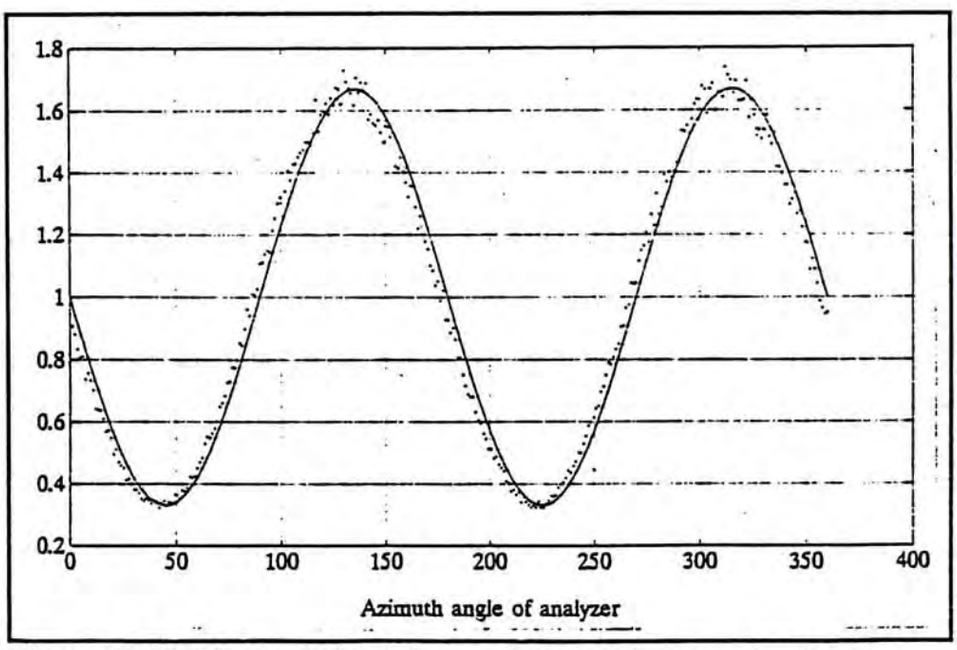


Figure 5.10 *Phase shift of detected signal due to misalignment*

Sinusoidal signal is the result of light intensity modulated by a rotating analyzer. The initial position of analyzer is in fact the azimuth angle of that components. A photo-interrupter was used to check the angular position of analyzer. Azimuth angle of analyzer was calibrated by adjusting the position of the blocking pin which was used to block the signal from the photo-detector. Every time when the measurement begin, the azimuth angle of analyzer will be resisted so that the initial angle of analyzer is correct.

**Section 5.2.3 Standard Samples measurement**

According to the Aspnes's calculation, the precision in determination of ellipsometric parameters $\psi$ and $\Delta$ will decrease when $|\Delta|$ approaches 0° or 180°. The performance of a rotating analyzer ellipsometer will be degraded. It is because the value of $\Delta$ will suffer from the random and systematic errors[43]. Aspnes defined a term called "residual function" to represent the deviation of Fourier coefficients. These characteristic behaviour also appear in our experimental result. From figure 5.12 and 5.13, the measured result match well with the calculated one in the region at where the value of $\Delta$ is near 90°. However, when the $\Delta$ approach 180°, larger deviation will appear. This phenomena can be explained by using equation 5.6. When $\Delta$ approach 180°, the value of $\psi$ will trends to 90°. According to equation 5.6, Fourier coefficient A will be near to one and $\cos(\Delta)$ will be related to a very small denominator and dominator. Therefore, larger error will occurs in the value of $\Delta$.

In order to verify the system, two factory fabricated standard samples were measured. Both samples have silicon oxide layer on silicon substrate.

Sample (1) : 972Å $SiO_2$ (Reg. no. 5863)

Sample (2) : 1180Å $SiO_2$ (Reg. no. 1237)

Standard samples were immersed in 95% alcohol solution and then ultra-sonic cleaned for 30 minutes. After then they have been purged to dry by nitrogen gas, their optical

parameters were checked again by using the monochromatic null ellipsometer (Gaertner L117). Angle of incidence is equal to 70°. The following tables summarized the measured result.

| **Sample 1** | P1 | A1 | P2 | A2 | thickness | refractive index (n) | Period |
|---|---|---|---|---|---|---|---|
| trial 1 | 96.1 | 39.9 | 185.9 | 139.7 | 966Å | 1.475 | 2784Å |
| trial 2 | 95.6 | 40.2 | 186.1 | 139.7 | 972Å | 1.471 | 2797Å |
| trial 3 | 95.6 | 40.1 | 186.3 | 140.2 | 964Å | 1.473 | 2788Å |
| **Mean** | | | | | **967.3Å** | **1.473** | |

| **Sample 2** | P1 | A1 | P2 | A2 | thickness | Refractive index (n) | Period |
|---|---|---|---|---|---|---|---|
| trial 1 | 93.6 | 55.1 | 184.5 | 125.2 | 1175Å | 1.465 | 2816 |
| trial 2 | 93.6 | 55.1 | 184.5 | 125.3 | 1174Å | 1.465 | 2816 |
| trial 3 | 93.4 | 55.4 | 184.4 | 124.7 | 1180Å | 1.464 | 2819 |
| **Mean** | | | | | **1176.3Å** | **1.4646** | |

Values of PSI($\psi$) and DEL($\Delta$) were calculated from P1,P2,A1 and A2. Their relationship are governed by equations 5.10

$$\Psi = \frac{180^o-(A2-A1)}{2} \qquad \Delta = 360^o-(P1+P2) \tag{5.10}$$

Silicon oxide is a non-absorption film (ie the extinction coefficient k is near zero). Thickness (d) and real part of refractive index (n) are the only unknown for a single layer film. The unknowns were then calculated by a HP85 computer by the method of interpolation.

We cannot directly compare the values of $\psi$ and $\Delta$ between the spectroscopic ellipsometer (SE) and the Gaertner ellipsometer. It is because their incidence angle are different. The spectra of ellipsometric parameters of sample (1) and (2) are plotted in the

same graphic and show in figure 5.11.

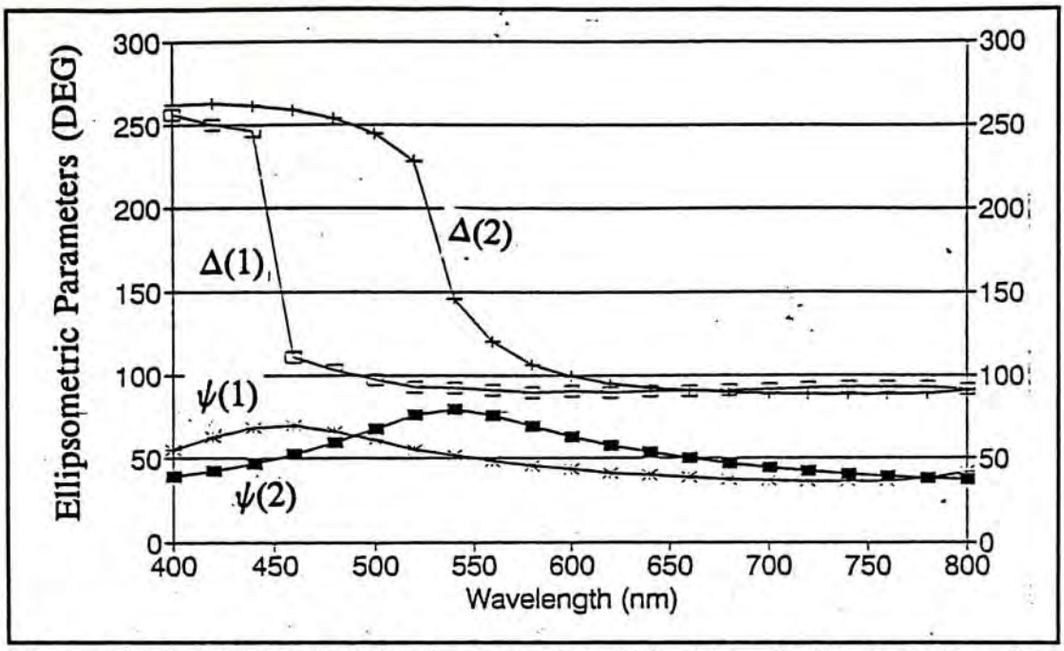


Figure 5.11 *ψ(λ) and Δ(λ) of standard sample (1) and (2) plotted against wavelength of incidence light*

According to equation 3.24 the value of DEL(Δ) is related to the phase different between two orthogonal components while PSI($\psi$) is corresponded to the ratio of the magnitude of those components. The falling edge of DEL(Δ) curve will shift towards higher wavelength when thickness of silicon oxide layer increase. If thickness of oxide layer further increase, value of tan(Δ) will oscillate between positive and negative.

The spectroscopic ellipsometry data was fitted by searching a set of optical parameters (n,d for single layer non-absorption film) such that the selected model matched with the experimental result. The least-square error was minimized with the help of Levenberg-Marquardt method. The fitting procedure will be discussed in next section. The best fit result of sample (1) and (2) from the spectroscopic ellipsometry data were shown in figure 5.12 and 5.13 respectively.

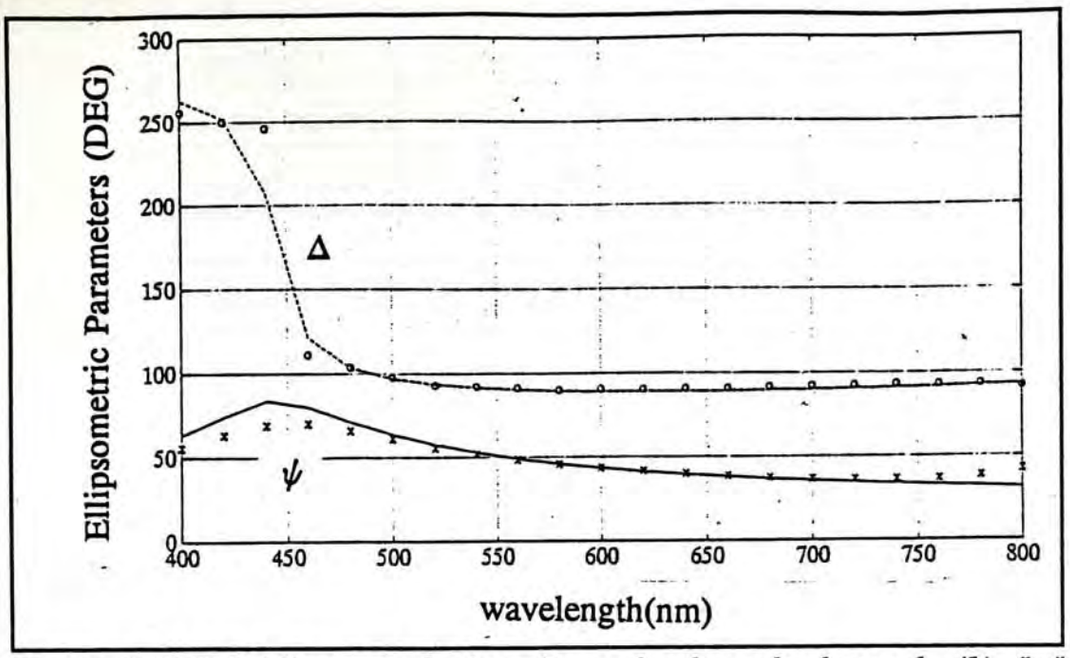


Figure 5.12 *Solid lines are the best fit result of standard sample (1), "o" and "x" represent the experimental values of ψ and Δ*

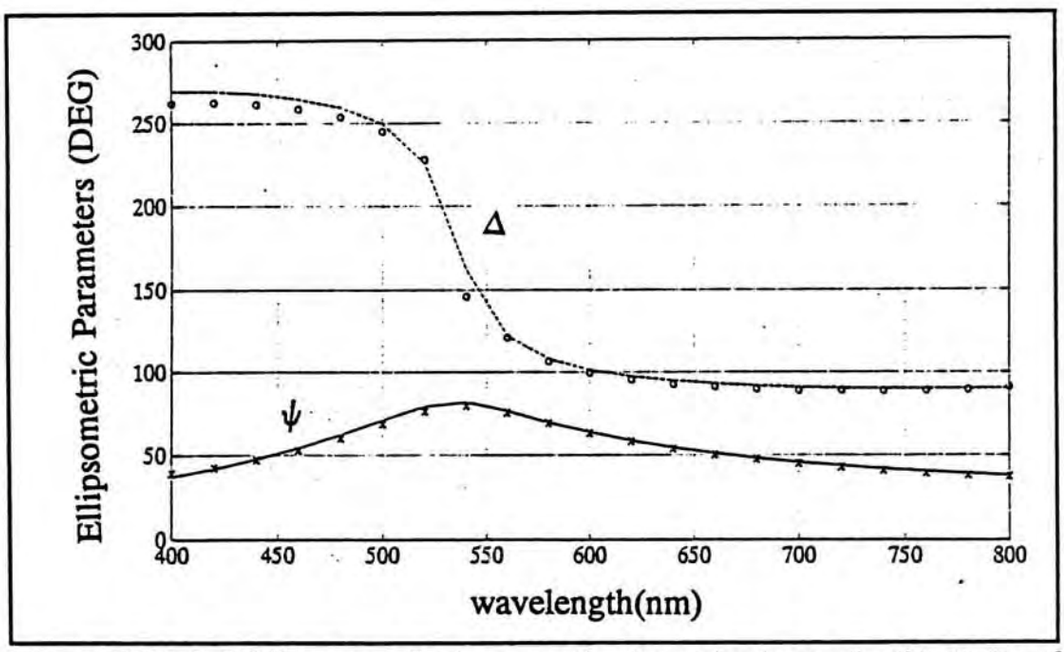


Figure 5.15 *Solid lines are the best result of standard sample (2). "o" and "x" represent the experimental values of ψ and Δ.*

The selection of an appropriate initial model is an essential problem. If the deviation of initial model is large, the fitting result may be diverged. Owing to the simple structure of sample (1) and (2), their optical parameters can be verified by Gaertner ellipsometer. The initial guessing of the spectroscopic ellipsometry data is therefore based on the verified result.

| Sample (1) | Refractive index (n) | Thickness (Å) |
|---|---|---|
| Input value | 1.47 | 967 |
| Output result | 1.4827 | 954.36 |

| Sample (2) | Refractive index (n) | Thickness (Å) |
|---|---|---|
| Input value | 1.46 | 1180 |
| Output result | 1.4638 | 1174 |

Spectroscopic ellipsometry data was measured with incidence angle 67.5° and PMT voltage 700V. The following table compare the percentage error of the commercial Gaertner ellipsometer and the home made spectroscopic ellipsometer. The verified result (Mean value) obtained from Gaertner ellipsometer were used as a reference.

| Percentage error (thickness) | Gaertner ellipsometer | Spectroscopic ellipsometer |
|---|---|---|
| Sample (1) | 0.48% | 1.3% |
| Sample (2) | 0.31% | 0.51% |

| Percentage error (Refractive index) | Gaertner ellipsometer | Spectroscopic ellipsometer |
|---|---|---|
| Sample (1) | 0.1358% | 0.6585% |
| Sample (2) | 0.0273% | -0.0546% |

One of a pioneer in the study of ellipsometry - Mo Dang has measured the ellipsometric spectra of $SiO^2$ films of several thickness on silicon[45]. Results measured by using spectroscopic ellipsometer were also compared with the data obtained from null-type ellipsometry. The percentage error of thickness lies between 0.9% and 3.6% and the results obtained from both methods were declared to be matched. The largest error in thickness of our system is 1.3% and therefore we can claim that data obtained by our system are reliable.

The advantages of spectroscopic ellipsometry (SE) over the null type technique is that the relation of n,k and $\lambda$ can be directly calculated from SE data when no overlayer present on the sample's surface and thereby the optical band gap of material can be obtained from the extinction coefficient k. Moreover, for a single non-absorption film, the film thickness can be determined without period ambiguity.

# CHAPTER 6. ANALYSIS OF ELLIPSOMETRIC PARAMETERS

$\psi(\lambda)$ and $\Delta(\lambda)$ are the ellipsometric parameters measured at different wavelengths. As mentioned before, $\psi$ is related to the ratio of magnitude to orthogonal components sensed by the detector and $\Delta$ is related to the phase difference between the components. Both parameters have close relationship with the properties of the sample. In order to acquire the optical parameters of the specimen, we have to convert $\psi$ and $\Delta$ into physical quantities such as refractive index and film thickness. The dielectric function or refractive index describes the response of a material to electromagnetic radiation. Data analysis of SE data can be categorised into two types : (1) bulk samples, (2) layered structures

## Section 6.1 Optical properties of bulk material

Ellipsometry is a valuable technique for the determination of the optical properties of materials such as refractive index and dielectric constants. It is particularly useful in the wavelength regions where the materials are strongly absorbing, so that transmission measurement is precluded.

If the samples constitute a bulk phase, light is reflected from the interface between the substrate and the ambient of known optical properties. It is obvious that the ambient should be transparent (light transmitting) and do not perturb the substrate. Vacuum and inert gas are ideal selections for the ambient. For non-inert ambient, additional modification of the substrate at the interface is needed. Some factors may cause error in the determination of optical properties of a bulk sample.

(1) The presence of contaminant or oxide film[49] (e.g. native oxide),

(2) Surface with high density of dislocation (stressed layer) due to mechanical forces involved in the preparation,

(3) Surface roughness[46,47] (e.g. samples grown by liquid phase epitaxy LPE)

The real and imaginary parts of the complex dielectric function are both functions of frequency. Kramers and Kronig in 1926 introduced a relation which enable us to find the real part of $\epsilon$ if we know the imaginary part of $\epsilon$ at all frequency, and vice versa[21]. Pierce and Spicer measure the reflectivity (R) of samples in a wide range of wavelength (energy from 0.4eV to 11.8eV) and then n and k were calculated by using the this relation. The disadvantage of using the Kramers-Kronig relation is that the calculation involve the integration of reflectivity of wide range of wavelength. Reflectivity at the wavelength beyond the measured region can only be obtained by estimation or in other case ignored[36].

In spectroscopic application, both real and imaginary parts of the complex refractive index or dielectric constants can be determined as a function of wavelength. The relationship between the ellipsometry data and the optical parameters have been derived[23] and it is based on the Fresnel's equation, Snell's law and the equation of complex reflection coefficient. Refractive index can be written in terms of ellipsometry data ($\psi$, $\Delta$) and incidence angle ($\phi_i$). If the condition $n^2(1+\kappa^2) \gg 1$ is satisfied, where refractive index $N = n(1+\kappa)$.

$$n = \frac{\sin\phi_i \tan\phi_i \cos 2\psi}{1 + \sin 2\psi \cos\Delta} \tag{6.1}$$

$$\kappa \simeq \tan 2\psi \sin\Delta \tag{6.2}$$

In a particular case when the measurement was done at the principal angle of incidence $\phi'$, then $\Delta = -\pi/2$ and $\psi = \psi'$, equations (6.1) and (6.2) reduced to

$$n \simeq -\sin\phi_i' \tan\phi_i' \cos 2\psi' \tag{6.3}$$

$$\kappa \simeq -\tan 2\psi' \tag{6.4}$$

Dielectric constants $\epsilon = \epsilon_1 + j\epsilon_2$ can be obtained from the following equations[23,50]

$$\epsilon_1 = n^2(1 - \kappa^2)$$
$$= \sin^2\phi_1 + \frac{\sin^2\phi_i \tan^2\phi_i(\cos^2 2\psi - \sin^2 2\psi \sin^2\Delta)}{(1 + \sin 2\psi \cos\Delta)^2} \quad (6.5)$$

$$\epsilon_2 = 2n^2\kappa$$
$$= \frac{\sin^2\phi_i \tan^2\phi_i(2\sin 2\psi \cos 2\psi \sin\Delta)}{(1 + \sin 2\psi \cos\Delta)^2} \quad (6.6)$$

The method discussed above can be extended to highly absorbing film. If the thickness of an absorbing film is larger than the penetration depth of the incidence electromagnetic radiation, then the film can be regarded as a semi-infinite material. It is because radiation reflected from the interface between the film and substrate is negligible. The penetration depth of a dielectric material depends on the wavelength of the incident light and the extinction coefficient k. The larger the value of k or the shorter the wavelength, the smaller will be the penetration depth[51].

**Section 6.2 Optical properties of thin films**

In the previous section, what we concerned are the optical properties of a bulk sample or an absorbing layer on a substrate. When there exist a thin film or more than one overlayer of small or zero extinction coefficient on a substrate, the method described above is not appropriate. The refractive electromagnetic wave inside the film subsequently suffers multiple internal reflection between the boundaries. Reflected wave is therefore the resultant of an infinite number of reflected and transmitted wave.

For a single transparent thin film, a single wavelength measurement can provide adequate information to determined the film characteristics, if the interface is abrupt[48]. When the film is absorbing or the number of film exceeds one, spectroscopic measurement is needed. Spectroscopic measurement can provide additional information to allow the optical

properties of the films to be determined along with its thickness. Unfortunately, the analysis of the spectra of ellipsometry data are quite complicated that we cannot calculate the parameters directly from the data. Numerical analysis of least-squares fitting procedures has to be used for the accurate determination of the refractive indices ($N_i$) and the thicknesses ($d_i$) of a layered structure. The fitted results not only depend on the accuracy of the instrument but also depend on the model of the structure we assumed.

Procedures involved in the analysis of the spectra of ellipsometric parameters $\psi(\lambda)$ and $\Delta(\lambda)$ are summarised as in figure 6.1.

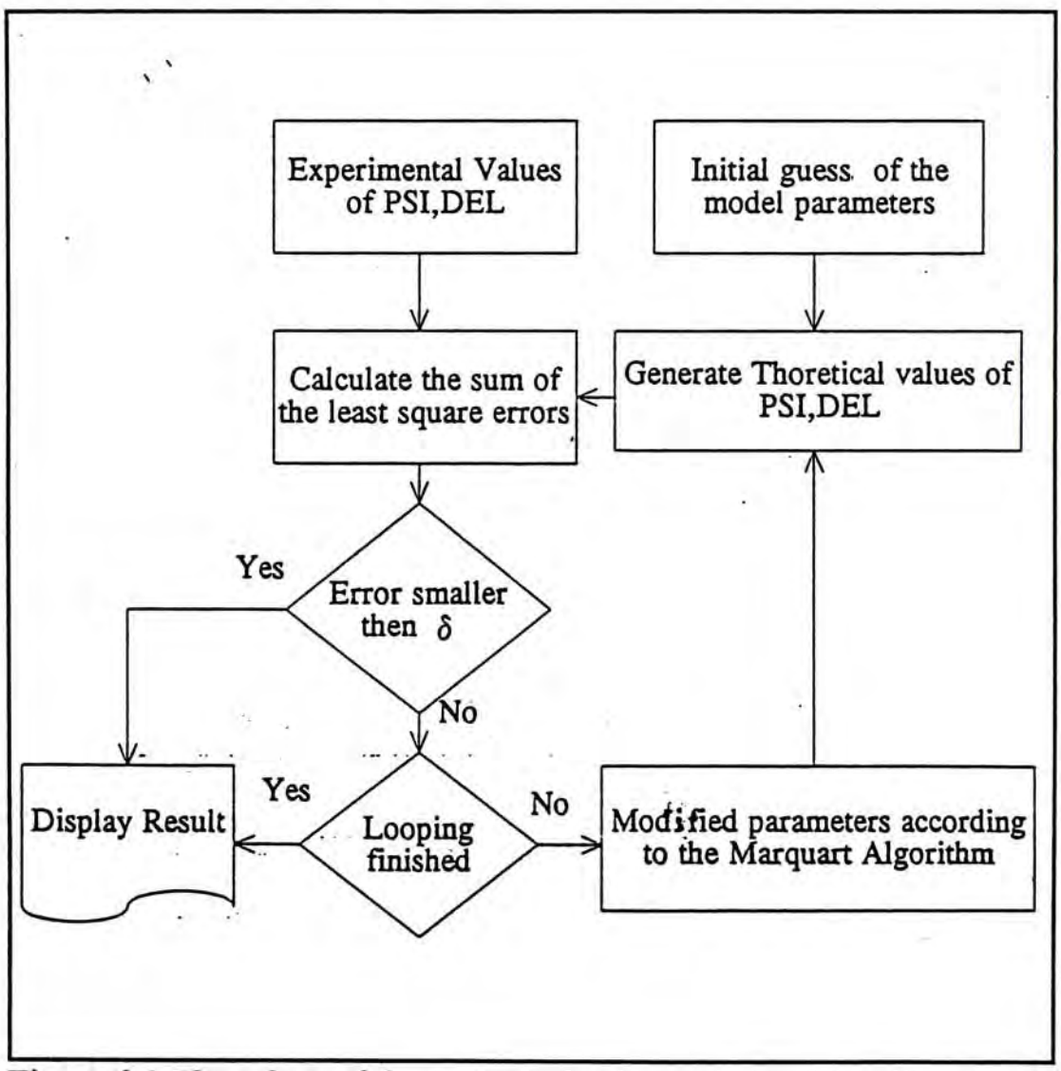


Figure 6.1 *Flow chart of the program for the analysis of the ellipsometric spectra. The inputs are the experimental values of $\psi_m$ and $\Delta_m$.*

Spectra of $\psi_m(\lambda)$ and $\Delta_m(\lambda)$ are the measured results from the Spectroscopic

Ellipsometer. An appropriate model and relevant initial guess of the model parameters have to be input. The theoretical values of $\psi_c$ and $\Delta_c$ are calculated according to the equations described in Chapter 3. The experimental data are compared with the calculated ones to see whether the initial guess is correct or not. If the difference between the two sets of data is larger than a preset limit, the initial parameters will be modified according to the Marquart Algorithm. A new set of ellipsometric parameters will then be generated by using a subroutine which will be discussed in the next section. The new calculated values are then compared with the experimental values again. The procedures of comparison and parameters modification will be repeated until the difference between the calculated and the experimental data is minimized or the number of looping exceeds a limit. An unbiased estimator is used to describe the agreement between the experimental data and the modelling data (calculated). Unbiased estimator exists in various forms. The rate of convergence can be improved if an appropriate estimator was selected. The choice of the unbiased estimator will be discussed in the next section.

### 4.2.1 Parameter generator

The modelling data $\psi_c(\lambda)$ and $\Delta_c(\lambda)$ are generated based on the theory discussed in section 3.2 and 3.3. The program was written by using Pro-Matlab for its great ability in complex matrix handling. Programs are executed on a DEC workstation in UNIX environment so that the "multi-windows" function can facilitate the display of texts and graphics at the same time.

The generation programs can be further divided into two sub-programs. One of them is mainly for the generation of ellipsometry data for multi-layer structures. PSI($\psi$) and DEL($\Delta$) are generated as functions of wavelength. Another program was written to extend the ability of the monochromatic ellipsometer (Gaertner) so that a single absorbing thin film

of known thickness can be measured. PSI($\psi$) and DEL($\Delta$) are generated as functions of the real part and the imaginary part of the refractive index.

As we mentioned before, the application of single wavelength measurement approach is limited. Since we have only one set of data ($\psi$,$\Delta$), information provided is only adequate to analyses a single non-absorbing thin film (i.e., k=0). If in some cases, the thickness of a single absorbing film is known, then in principle we can obtain n and k from the ellipsometry data.

The generation program was verified by comparing the generated data at $\lambda$=6328Å with the values on the "Ellipsometric Table" provided by Gaertner Scientific Corporation. The following table shows the result of comparison for a sample of thickness 1000Å and refractive index 1.45 at an angle of 70°

| Incidence angle | Table | Program |
|---|---|---|
| 70 | $\psi_T$ = 40.609<br>$\Delta_T$ = 80.013 | $\psi_c$ = 40.6087<br>$\Delta_c$ = 80.0125 |
| 50 | $\psi_T$ = 43.992<br>$\Delta_T$ = 141.749 | $\psi_c$ = 43.9926<br>$\Delta_c$ = 141.7486 |
| 30 | $\psi_T$ = 45.495<br>$\Delta_T$ = 171.274 | $\psi_c$ = 45.4947<br>$\Delta_c$ = 171.2740 |

Figure 6.2 shows a plot of DEL($\Delta$) against PSI($\psi$) for a 4680Å thin film with unknown refractive index on silicon substrate. The real part of the refractive index changes from 2 to 4 with a step increment of 0.01 and the extinction coefficient k varying from -0.5 to -0.2 with a step increment of 0.05. Graphs like figure 6.2 can help to estimate the initial values for the fitting program from which a more precise result will be calculated. Dealing with an absorbing film is more complicated then a non-absorbing one for two reasons. Firstly, we have to handle complex calculation if the value of k is not equal to zero (k=0

in transparent thin film). Secondly, the solution for an absorbing film is not unique. More then one set of optical parameters can sometimes match the experimental ellipsometry data. Figure 6.3 shows a plot of cos(DEL) against tan(DEL) for a 1000Å thin film. It is obvious that the curves generated cross each other at some values of PSI and DEL. If the experimental data fall on the cross point region, the n,k values obtained are not unique.The obtained results will depend on the direction of search and the values of the initial guess. An example will be given in Chapter 7. There are two possible solutions for the refractive index of an amorphous carbon thin film from the measurement at a single wavelength of $\lambda$=6328Å. It will also be shown that the correct result can be determined using spectroscopic ellipsometry .

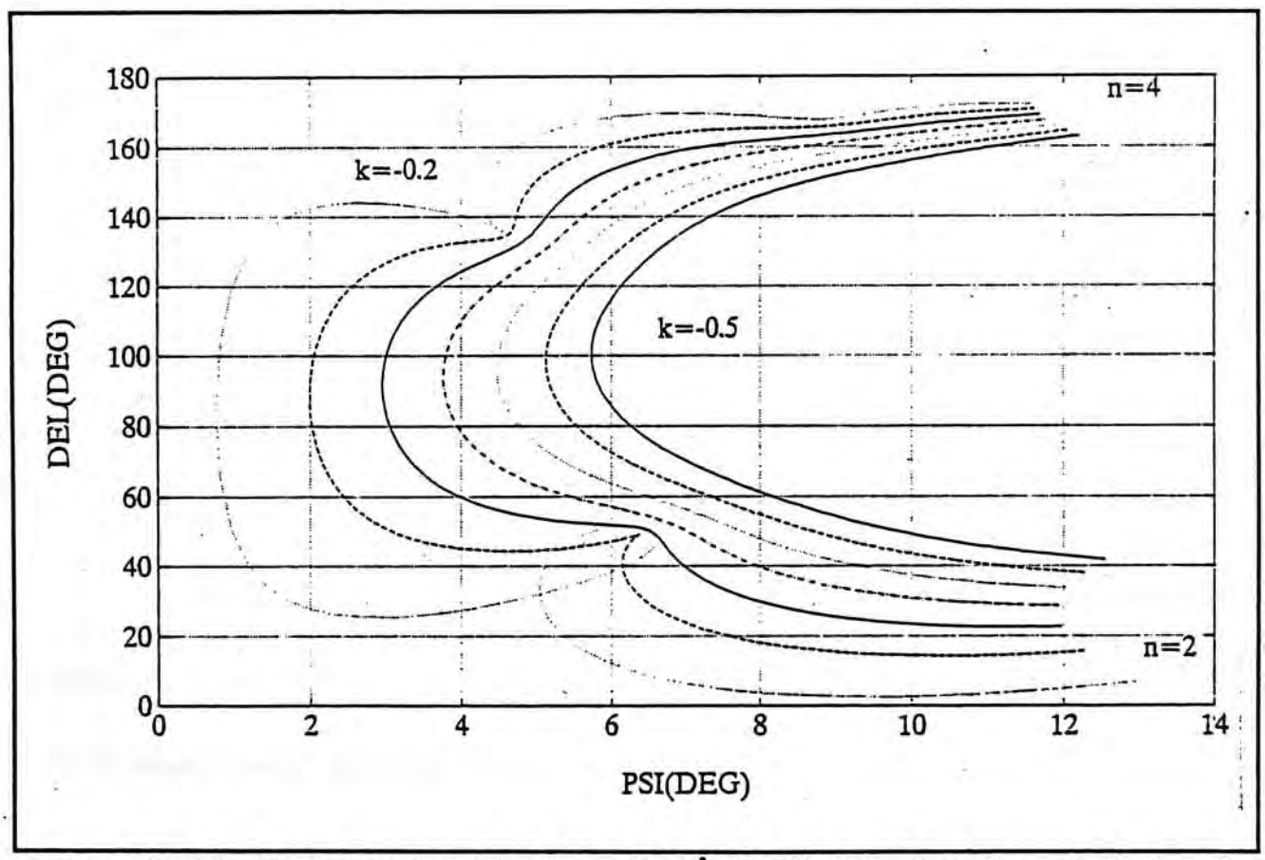


Figure 6.2. *$\Delta(n,k)$ plot against $\psi(n,k)$ for 4680Å thin film (n=2 to 4 step 0.01; k=-0.5 to -0.2 step 0.05)*

Another sub programs generates PSI($\lambda$) and DEL($\lambda$) of layered structures using the method of 2x2 scattering matrix which has been described in section 3.3. The spectroscopic

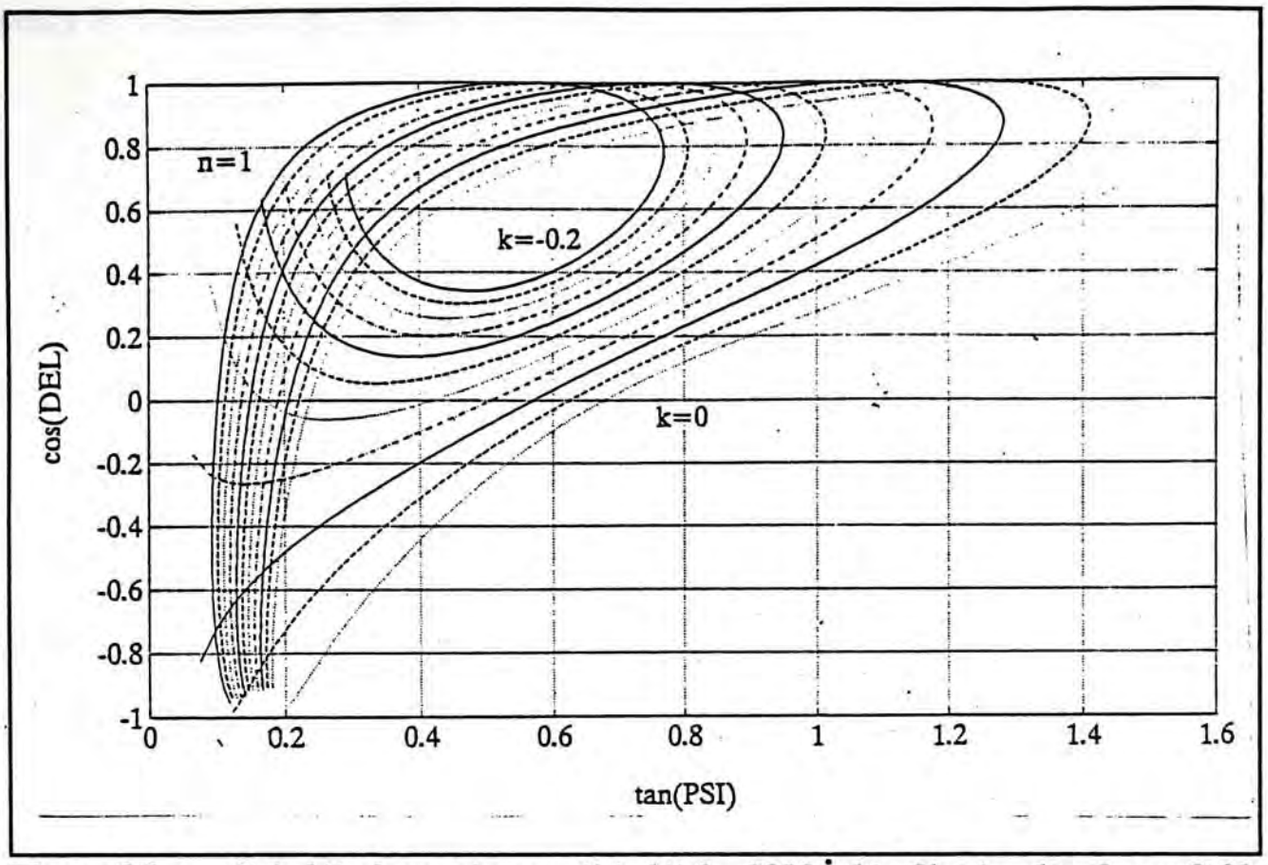


Figure 6.3. *cos(Δ(n,k)) plot against tan(ψ(n,k)) for 1000Å thin film (n=1 to 3 step 0.01; k=-0.2 to 0 step 0.02)*

ellipsometry data generator has been verified by comparing the generated data with the results from other papers. The program allows the user to vary the incident angle, the wavelength range, the step increment of wavelength, the number of overlayers and the relevant parameters for each layer.

**Section 6.2.2 Least Square fitting**

Let $\rho^m_i$ denote the complex ratio of the reflection coefficient from $i^{th}$ measurement on a stratified isotropic planar system and $\rho^c_i$ be the computed value. The computed values were calculated according to a given set of values of the unknown parameters. The computational problem involves the searching for a set of optical parameters ($N_1, N_2, N_3, \ldots N_L, d_1, d_2, d_3, \ldots d_L$) that characterize the optical system under measurement such that the

quantity F in equation (6.7) below is minimized.

$$F = \sum_{i=1}^{M} \left| \rho_i^m - \rho_i^c(N_o, N_1, N_2, N_3, \ldots N_L, N_s, d_1, d_2, d_3, \ldots d_L, \phi_o, \lambda) \right|^2 \qquad (6.7)$$

where $N_1, N_2, \ldots N_M$ are the complex refractive indices of the thin film and $d_1, d_2, \ldots d_L$ are the thicknesses of the layers. L is the number of layers, $N_o$ and $N_s$ are the refractive indices of the ambient and the substrate respectively, M is the number of measurements at different wavelengths and $\phi_o$ is the angle of incidence.

For instance, measurements are repeated M times at M different wavelengths. Each measurement provides two real quantities $\psi$ and $\Delta$, thus the number of independent measured quantities is 2M. The refractive indices of the ambient and the substrate is usually known. There are at most three unknowns for each layer $(n_i, k_i, d_i)$. Therefore, normally we should have $2M \geq 3L$ in order to be able to determine the unknowns.

The program which performs the fitting procedures permits the users to fix certain sets of parameters so that the values of these sets of data will not be varied. If we know that the thin films of the sample are non-absorbing or we know the thicknesses of the films, we can fix the values of k or d at the particular values. The computation time will be greatly reduced if some of the variables were fixed. Moreover, the computation error will also be diminished if less parameters are involved in the calculation.

The fitting procedures cannot guarantee that the final output converges to the solution. The final result may sometimes get trapped in a local minimum point if the deviation of the initial guess from the true solution is large. In an ideal situation where there are no experimental errors, truncation errors nor model errors, it should be possible to compute the value of the unknown optical parameters such that F will equal to zero. However,

instrumental, model imperfection and truncation errors are unavoidable, a finite minimum value of F is expected. In some cases, different results corresponding to different local minimum point of F will be obtained if different values of initial parameters were used. As an example, the SE data of the standard sample (1) is fit again here using another set of initial parameters for comparison :

Initial guess : n=1.46, k=0, d=980Å

Output value after 20 looping : n=1.4527, k=0, d=989.82Å (Figure 6.4)

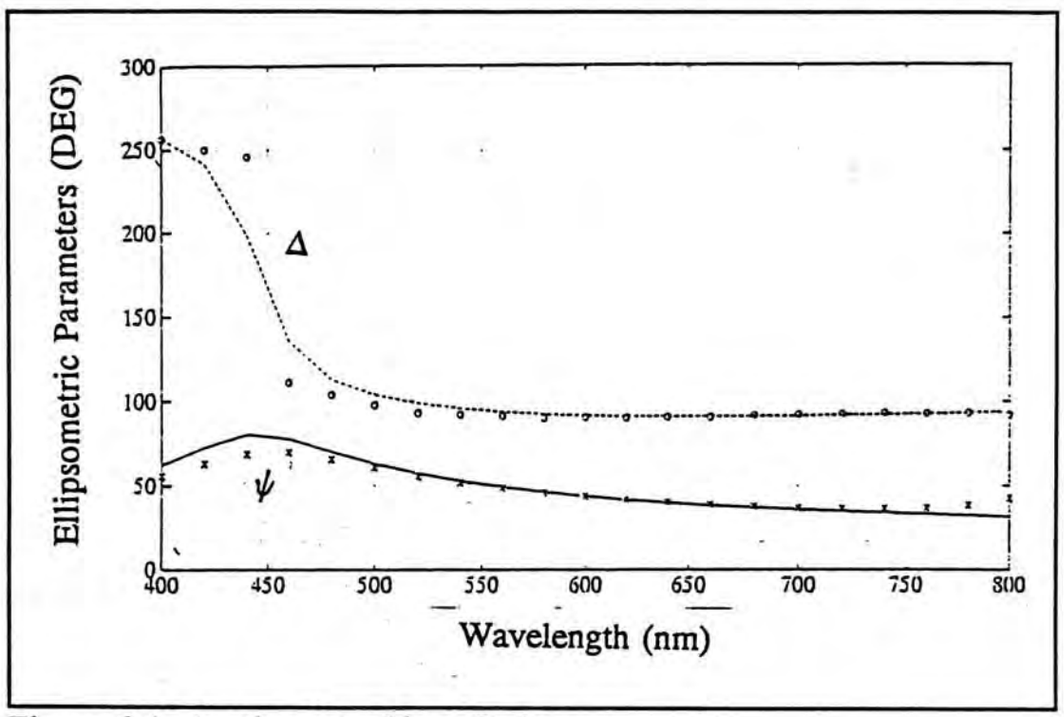


Figure 6.4. *Another set of best fit data*

Although the best fit data of the refractive index and the thin film thickness obtained are different from the previous one (Figure 5.14), their least square error are more or less the same. Therefore a set of data which have a more reasonable values was selected.

Spectroscopic ellipsometry is a powerful tool. Ellipsometry data are sensitive to the change of the optical functions of the material. However, the interpretations of the SE data are model dependent. The fitting process can help to estimate a more reasonable set of parameters for a model, but the fitting itself cannot determine whether the established model

is correct or not. This means that a good fitting to the SE data does not necessarily prove the reality of the corresponding model. However those models that do not fit the data well, can reasonably be eliminated.

**Section 6.3.2 Choice of error function (unbiased estimator)**

Error functions are usually in the form of a sum of a series of square forms. $F(x) = \Sigma f_i^2(x)$. The accuracy of the fitting is determined by the value obtained by the estimator $\sigma$ which is given by

$$\sigma = \left(\frac{F}{2n - p}\right)^{\frac{1}{2}} \qquad (6.8)$$

Where n is number of measurements and p is the number of parameters.

If the weighting of different variables of the error function is equal, it is called unbiased estimator, otherwise it is called a biased estimator[52]. Unbiased estimator is not unique. The choice of these function can affect the rate of convergence of the fitting and the final result[53]. If a poor error function was used, larger deviation will happen in the calculated parameters. Sometimes the regression will become divergent or the calculated values are found to be bounding back and forth around a local minimum rather than converging to the answer. Various types of error functions that commonly used were tested so that an appropriate estimator can be selected.

Three mean square functions, equation (6.9) to (6.11) given below, were used to fit the same set of data.

$$F_1 = \sum_{i=1}^{M} \left[ (\Delta_i^c - \Delta_i^m)^2 + (\psi_i^2 - \psi_i^2)^2 \right] \tag{6.9}$$

$$F_2 = \sum_{i=1}^{M} \left[ (\psi_i^c - \psi_i^m)^2 + (\cos\Delta_i^c - \cos\Delta_i^m)^2 \right] \tag{6.10}$$

$$F_3 = \sum_{i=1}^{M} \left[ (\tan\psi_i^c - \tan\psi_i^m)^2 + (\cos\Delta_i^c - \cos\Delta_i^m)^2 \right] \tag{6.11}$$

The set of synthesised data was generated using the parameters shown in the following table.

| | |
|---|---|
| Incident angle | 70 DEG |
| Start Wavelength | 300 nm |
| Stop Wavelength | 800 nm |
| Step increment | 20 nm/step |
| Number of film | 1 layer |
| Refractive index of ambient | 1 (air) |
| Refractive index of film | 1.46 |
| Refractive index of substrate | 3.85-0.02j |
| Thickness of film | 1580Å |

In order to test the performance of the fitting program. The initial input parameters are deviated from the ideal parameters shown in the above table. Figure 6.5 to 6.8 are the result where "x" and "o" represent the generated spectra of PSI($\psi$) and DEL($\Delta$) respectively and the solid line and the dashed line represent the results from the fitting program.

Typical numerical values of the testing results are listed.

(i) Initial value : n=1.465, k=0.01, d=1600Å, number of looping = 50

| | $F_1$ | $F_2$ | $F_3$ |
|---|---|---|---|
| Output result | n=1.467, k=0.00987, d=1497.05Å | n=1.49, k=-0.0123, d=1680Å | n=1.46, k=$4.3\times10^{-9}$, d=1580Å |
| Mean square deviation | 1497.05 | 2.50445 | negligible |

The final results of the fitting using error function $F_3$ match very well with the generated data. When comparing the mean square deviations, the performance of $F_1$ is the worse. Figure 6.5 and 6.6 plot the output results of $F_3$ and $F_2$ respectively together with the ideal data for comparison.

The rate of convergence of using error function $F_1$ is slow. If the parameters adjustment procedure (looping) is doubled, the fitting result of using $F_1$ is similar to the result shown in the above table. There is only a slight reduction of about 0.53% in the mean square deviation.

Although the deviation of using function $F_2$ is not too large in value, the accuracy of the output value is poor. Moreover, as the error function $F_2$ deal with $\cos(\Delta)$ rather then $\Delta$, the variation of the result should be larger than the numerical value when compared with the result using function $F_3$. A more conspicuous examples is show in figure 6.7 and 6.8. We fixed two set of the parameters (n and k) and the remained variable is the thickness d. The initial value of the thickness used was d = 2000Å. After 50 times of looping, the mean square deviation of using function $F_2$ is 7.92692. However, in the case of using function $F_3$, the deviation slim down to 0.001132 within 4 looping. Therefore the rate of convergence and the accuracy of using $F_3$ as an error function is better than the other two.

The goodness of fitting is not only dependent on the model but also relied on the initial guess of the values of the parameters. We have found that the parameters may not always converge to the solution and the value of the unbiased estimator may sometimes bound back and forth around the local minimum point. If the deviation of the initial values from the true values is too large, it may even lead to diverged result.

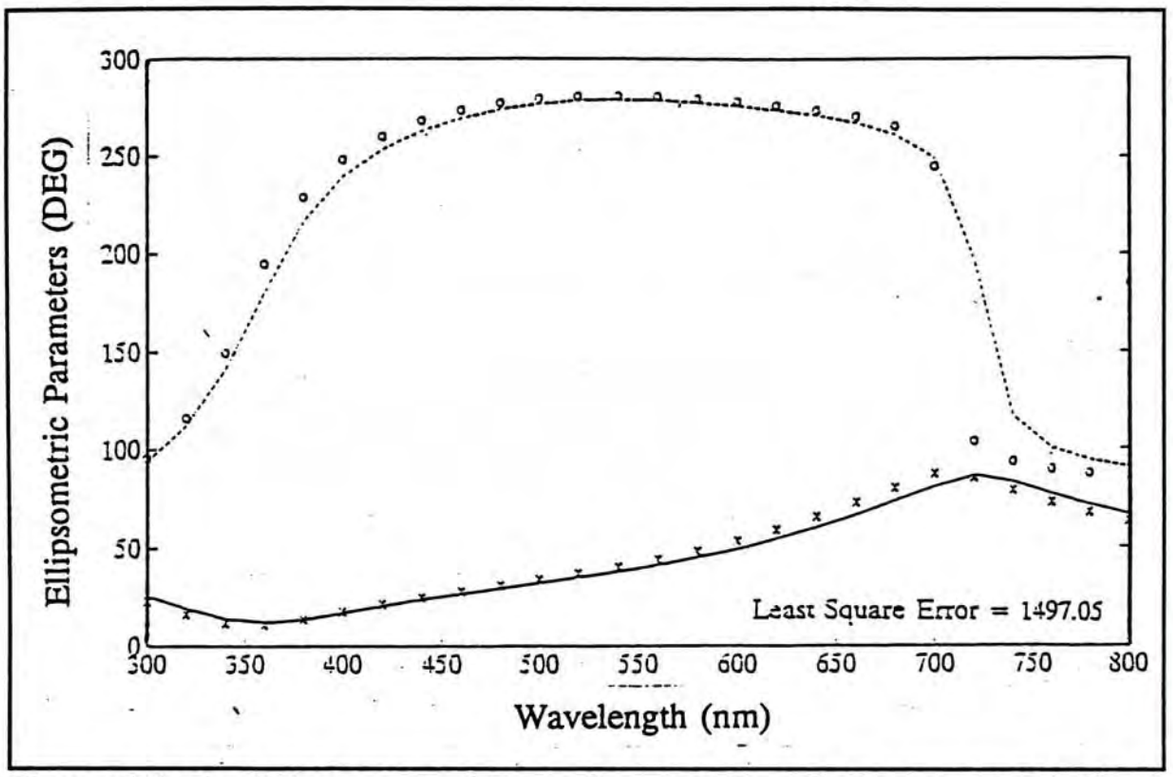


Figure 6.5 *The fitting result of Error Function $F_1$ and no parameter is fixed. When the number of looping increase to 100, error will be reduced to 1489.16*

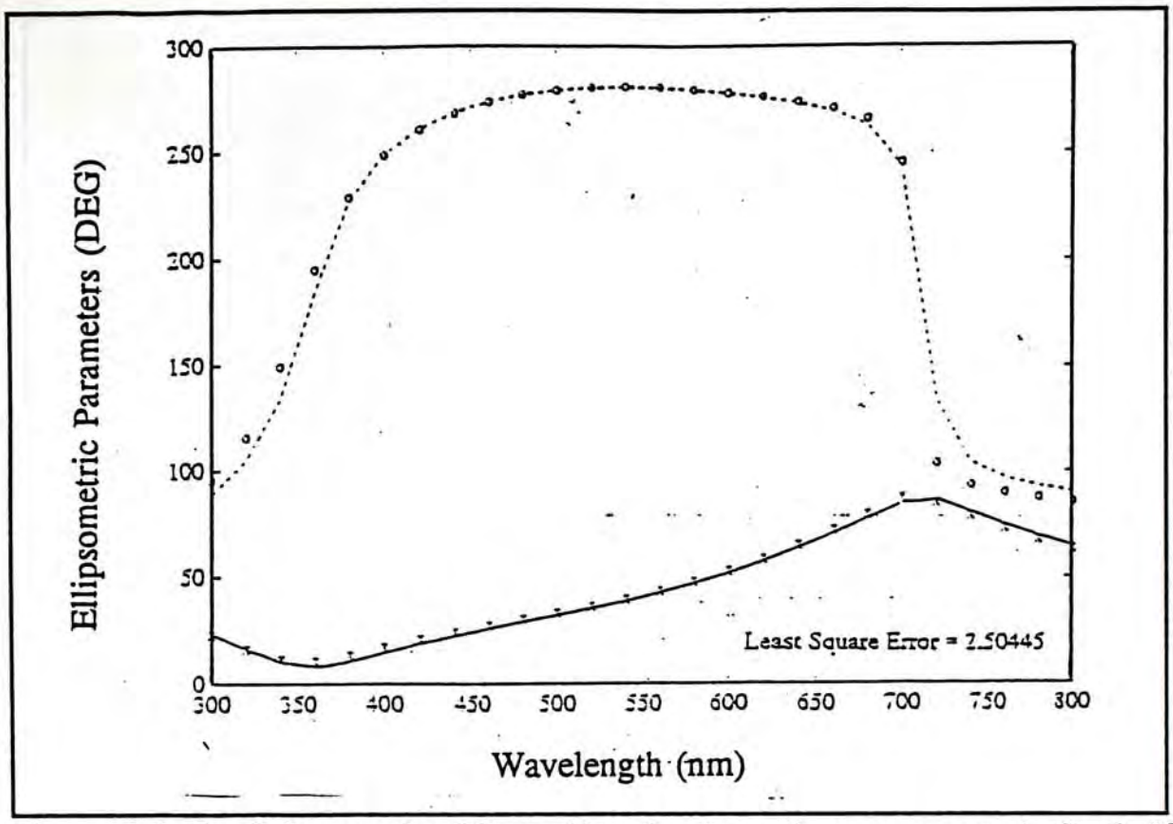


Figure 6.6 *The fitting result of Error Function $F_2$ and no parameter is fixed. If refractive index is fixed, error can be reduced.*

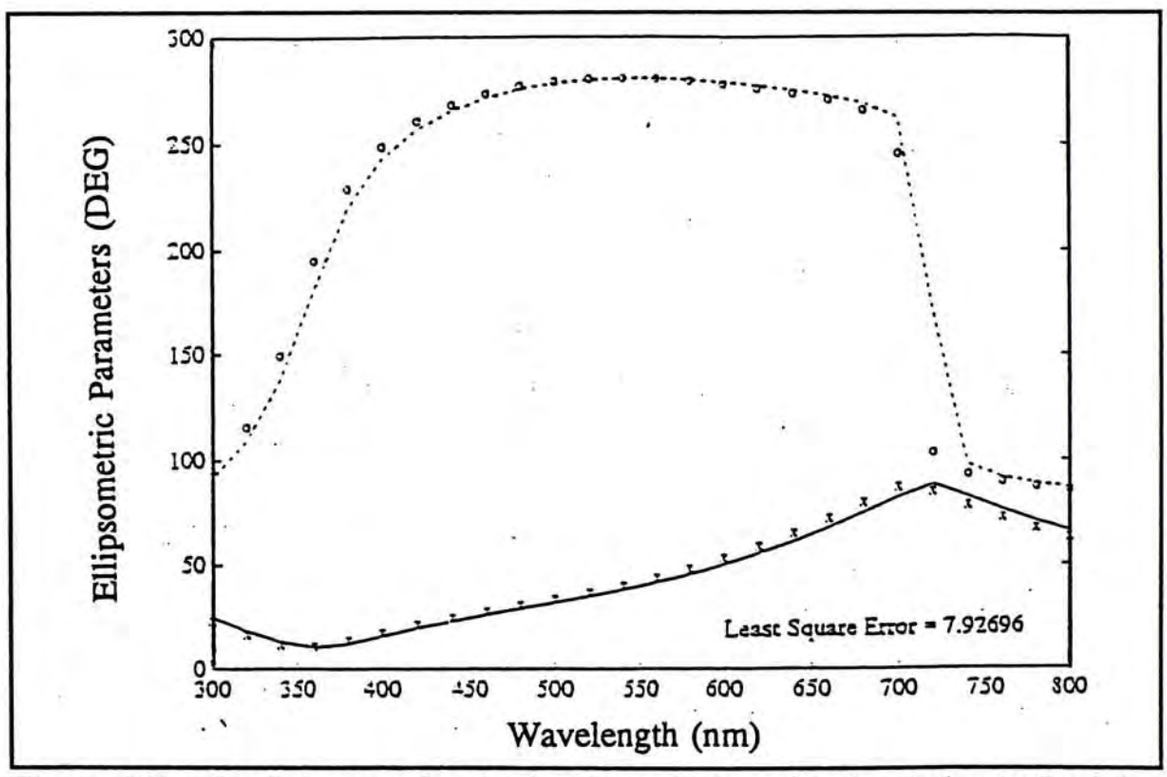


Figure 6.7. *The fitting result of using $F_2$ and the refractive index is fixed but larger deviation was introduced in the initial value of thickness.*

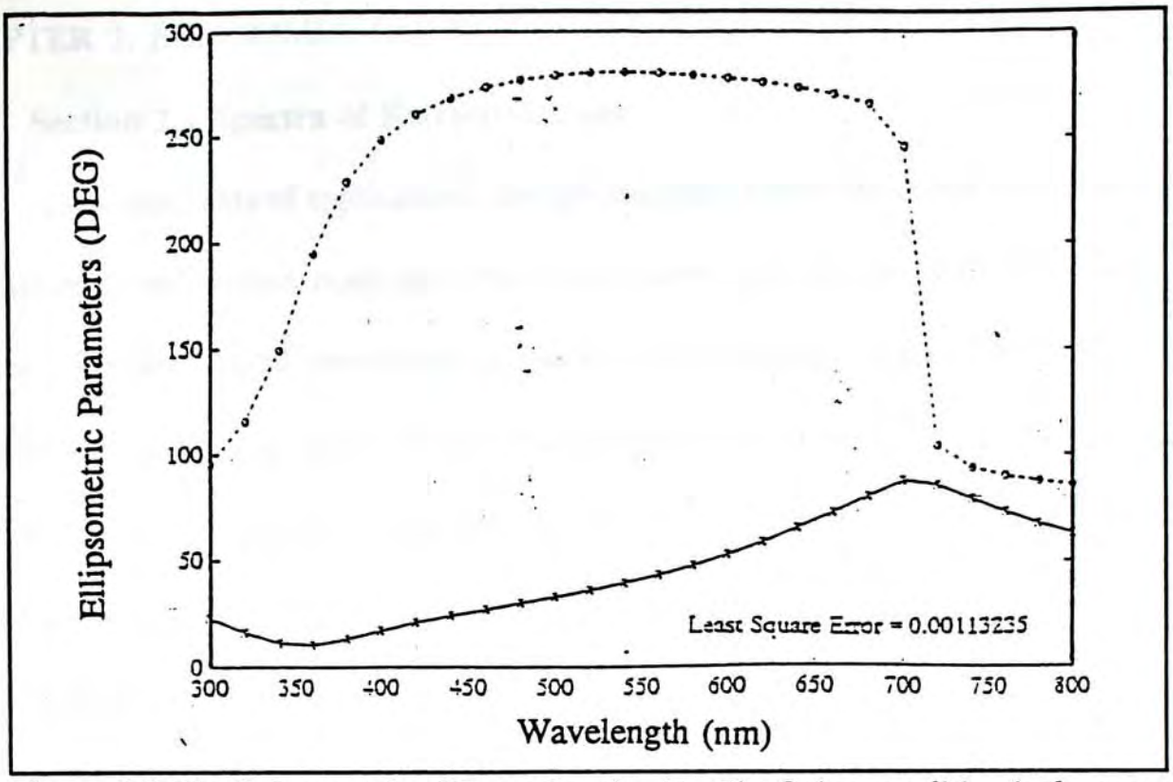


Figure 6.8 *The fitting result of Error function $F_3$. The fitting condition is the same as in Figure 6.7 but it converges within four times of looping.*

# CHAPTER 7. EXPERIMENTAL RESULT

## Section 7.1 Spectra of Refractive index

As an examples of applications, the spectroscopic ellipsometer has been used to make measurements on various materials. For a bulk material or sample with a thick absorbing surface layer, the optical properties can be calculated from the ellipsometric parameters by using equations (6.1) to (6.6). If the measurement repeated at different wavelengths, the complex refractive index and dielectric constant can be obtained as a function of wavelength. In this section, three materials which has no certain optical properties have been measured and the results are summaries as below.

### Section 7.1.1 GaAs layer grown by Molecular Beam Epitaxy (MBE) at low temperature on GaAs substrate

GaAs layers grown at low substrate temperature of around 200°C by MBE have been shown to have unique properties which are of great interest in both device application and fundamental research. It was first found by Smith and Calawa that a buffer layer in GaAs field effect transistor (FET) formed by low temperature grown GaAs (LT-GaAs) can lead to a significantly reduction in backgating and sidegating effect. The increase in trap filled limited voltage ($V_{TFL}$) for such layers provide an effective way of increasing the isolation between devices such as MESFET and HEMT based integrated circuits[54,55,56]. Further study also shows that LT-GaAs is a non-stoichiometric material. The amount of arsenic atoms was found to have 1% to 2% in excess. The resistivity was found to increase with decreasing growth temperature.

The properties of LT-GaAs has been studied by various methods such as the DLTS, PL, PICTS and EPR. However the optical properties such as the refractive index and the dielectric constant have not been fully studied.

Ellipsometry measurements on a LT-GaAs layer of known thickness of about 4680Å was grown on GaAs substrate at 200°C by MBE have been performed by both the null ellipsometer and the Spectroscopic Ellipsometer. The results are presented and discussed as follows.

(i) Measurement by the Null ellipsometer

Incidence angle = 70°; Wavelength = 632.8nm

| P1 | P2 | A1 | A2 |
|---|---|---|---|
| 54.2° | 144.3° | 11.0° | 169.1° |

From equation (5.10), we have

PSI ($\psi_m$) = 10.95° DEL ($\Delta_m$) = 161.5°

Now, if we assume that the penetration depth of the LT-GaAs layer is smaller than its thickness, then the electromagnetic wave reflected from the interface between the LT-GaAs layer and the substrate can be precluded. The refractive index of the LT-GaAs layer can be calculated by taking the sample as a bulk sample. Thus, we have

N(LT-GaAs,Bulk) = 3.822 - 0.458j

In order to verify the above assumption, we fixed the thickness of the LT-GaAs layer and then calculate the complex refractive index by using the method described in section 6.2.1. Making use of figure 6.2, the solution was estimated by matching $\psi_m$ and $\Delta_m$ to the graph. The estimation was then used as an initial guess for the least square fitting program such that a more accuracy result will be obtained.

We can also calculated the result by using layer phase with film thickness equal to 4680Å : N(LT-GaAs,Layer) = 3.8248 - 0.4580j

N(GaAs) = 3.8554 - 0.1954j

The answer matches very well with those acquired in the bulk mode. Thus the assumption is correct. The refractive index of normal GaAs at wavelength 632.8nm was quoted for comparison.

(ii) Measured by Spectroscopic ellipsometer

Incidence angle = 67.5° PMT voltage = 700V

Wavelength range = 400 nm to 800 nm

Figure 7.1 show the spectroscopic ellipsometric data of a 4680Å LT-GaAs layer on GaAs substrate.

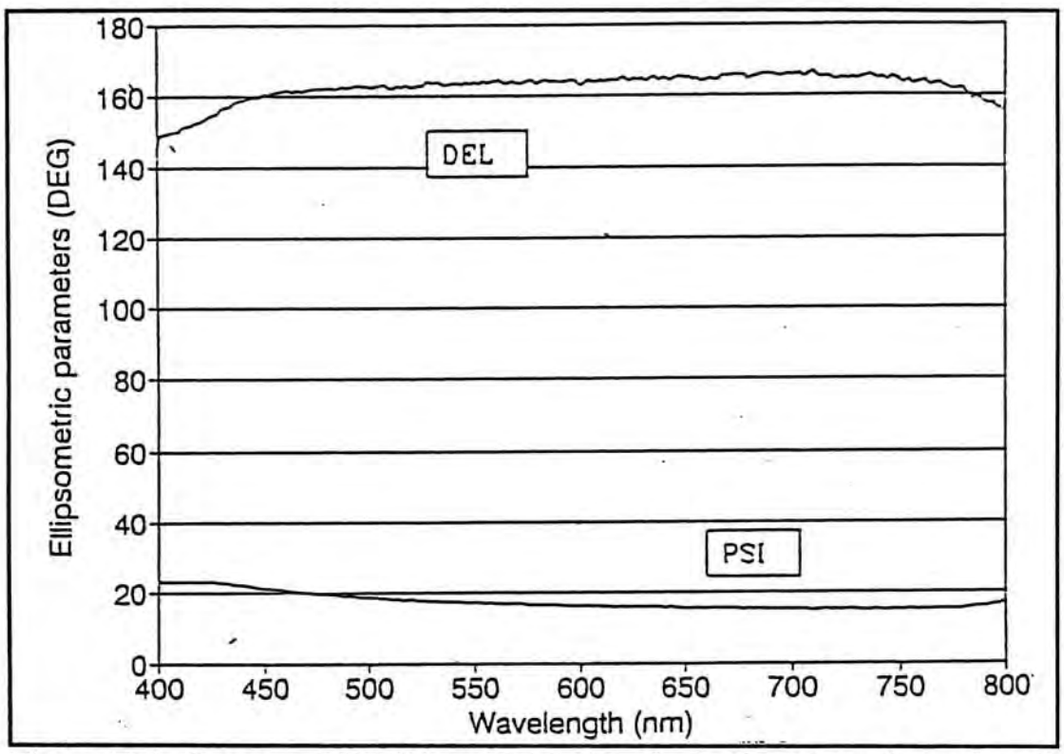


Figure 7.1. *Spectra of PSI(ψ) and DEL (Δ) plot as function of wavelength for GaAs growth by MBE on low-temperature substrate.*

The complex refractive index (N) and dielectric constants (ϵ) of LT-GaAs were then calculated by using equations (6.1),(6.2) and (6.5),(6.6). The results are plotted on the same graph (Figure 7.2) where the y-axis on the left side indicates the values of N and that on the right side indicates the relative dielectric constants. The optical properties of crystalline GaAs within the visible region were plotted in figure 7.3 as a reference[21].

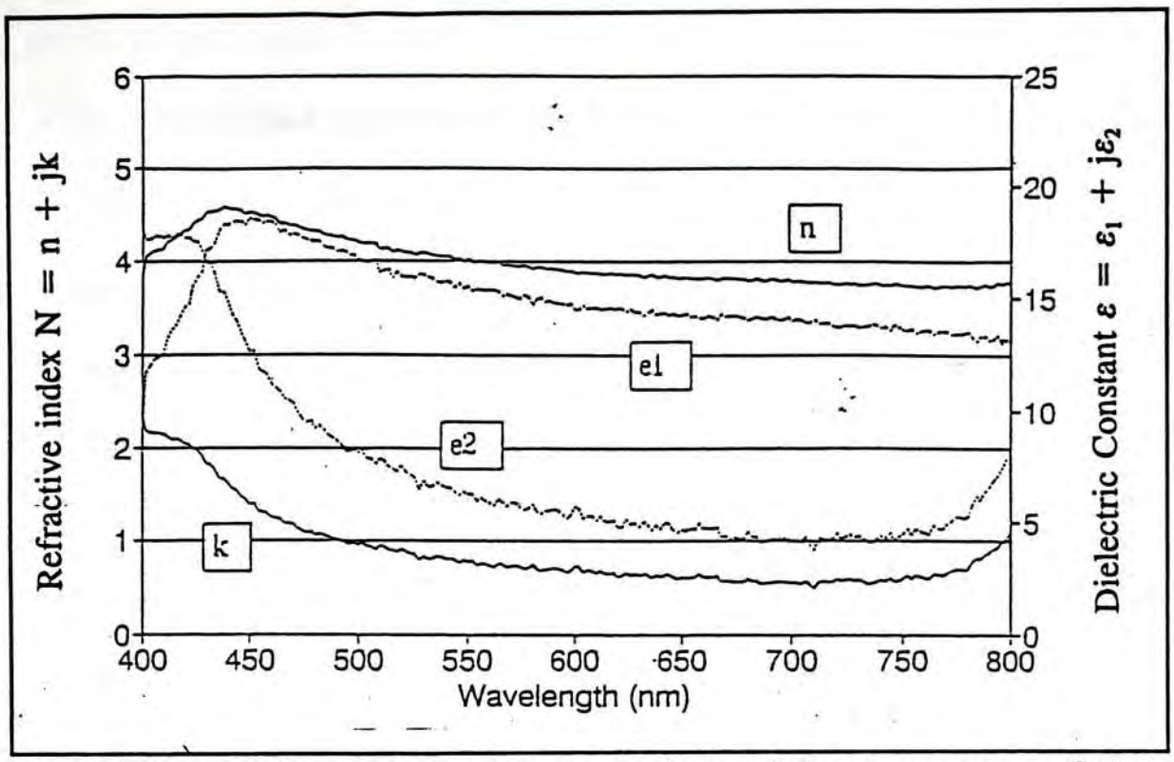


Figure 7.2. *Complex refractive index and relative dielectric constants of GaAs growth by MBE on low temperature GaAs substrate.*

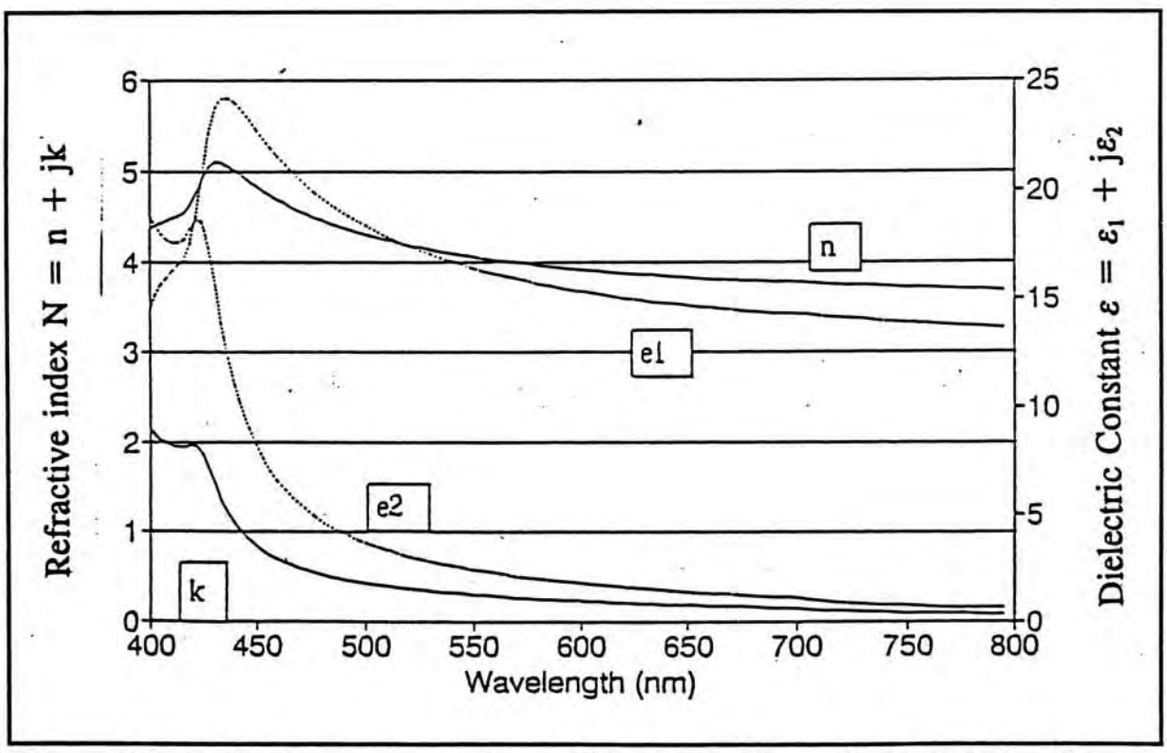


Figure 7.3. *Optical parameters of crystalline GaAs. Data obtained from reference (21)*

By comparing figure 7.2 and 7.3, the shape of the optical parameters spectra of normal GaAs and LT-GaAs are similar but their amplitudes are different. Similar to the result obtained by the null ellipsometer at 6328Å, the real part of the refractive index of LT-GaAs is smaller than that of normal GaAs by about 0.8%.

However the imaginary part of the refractive index shows a significant increase in magnitude. The highly absorbing behaviour of the LT-GaAs layer may be due to the off-stoichiometric effect and the excess point defects introduced during growth.

### 7.1.2 Amorphous Carbon thin film

In this section we shall give an example to demonstrate that a single wavelength measurement is insufficient to determine the optical properties of an absorbing thin film even when we have an idea on the film thickness.

The sample is an amorphous carbon thin film of about 1500Å deposited on a silicon substrate by RF sputtering. Since the structure of this specimen is simple (a single layer film on a semi-infinite media), we first measured it by null ellipsometry. The result is as follow

Incidence Angle = 70° Wavelength = 632.8 nm

| P1 | P2 | A1 | A2 |
|---|---|---|---|
| 67.2° | 157° | 10.4° | 169° |

$PSI(\psi_m) = 10.7°$ $DEL(\Delta_m) = 135.8°$

If the bulk mode is used, the effective complex refractive index is equal to

N(Bulk) = 3.38 - 0.856j

Figure 7.4 show $PSI(\psi_c)$ plot against $DEL(\Delta_c)$ as n and k vary. When we try to match the value $\psi_m$, $\Delta_m$ to the graph, we found that the experimental values lie in the "overlapped" region. Therefore, there are two possible solutions.

| Initial estimation | Least square fitting results |
|---|---|
| $N_1 = 2.5 - 0.02j$ | $N_1 = 2.5145 - 0.0214j$ |
| $N_2 = 3.1 - 0.9j$ | $N_2 = 3.4096 - 0.8329j$ |

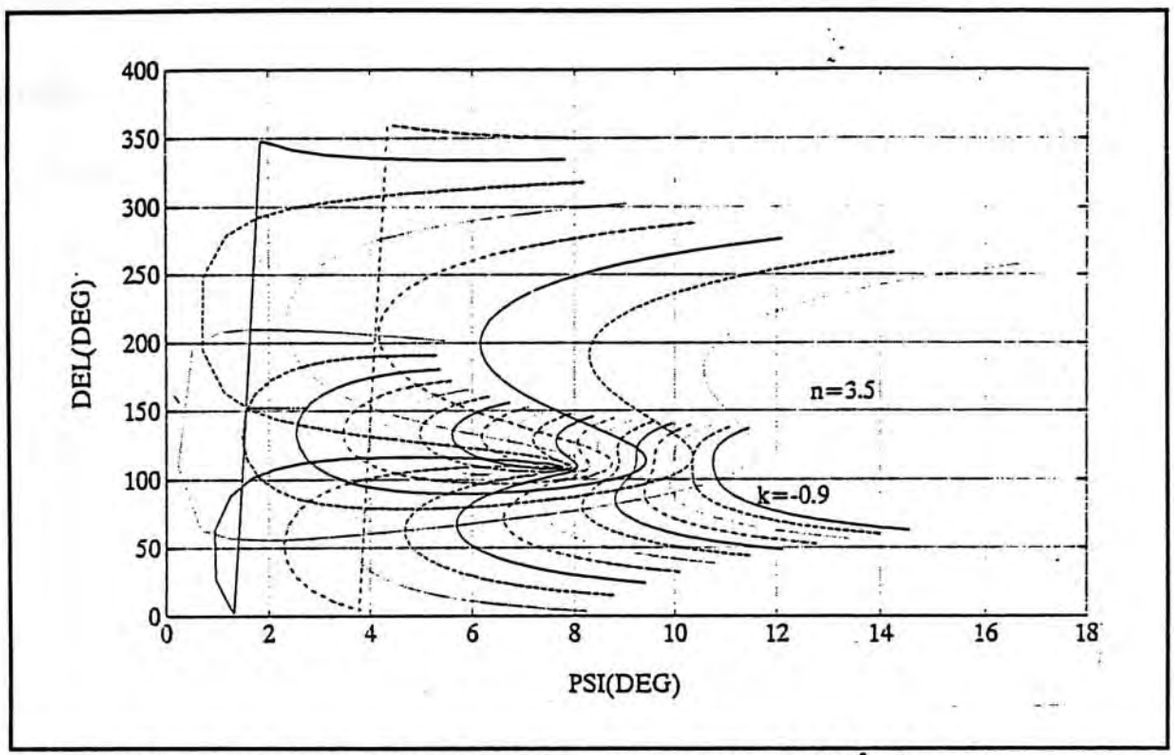


Figure 7.4. *A plot of DEL($\Delta$) against PSI($\psi$) for 1500Å thin film on silicon substrate. (n=2 to 3.5 step 0.02; k=-0.9 to 0 step 0.05)*

To determine which answer is correct, we fit the spectroscopic ellipsometric data by using both set of solution as a initial guess and then compare the fitness with the experimental SE data. In figure 7.5 and 7.6 the symbols "o" and "x" represent the experimental data of $\Delta_m$ and $\psi_m$, respectively and the dashed line and the solid line represent the calculated $\Delta_c$ and $\psi_c$.

| Initial guess | SE fitting result | Figure |
|---|---|---|
| $N_1 = 2.5 - 0.02j$ | $N_1 = 2.4832 - 0.015443j$ $d_1 = 1511.8$Å | Fig. 7.5 |
| $N_2 = 3.1 - 0.9j$ | $N_2 = 3.11168 - 0.84126j$ $d_2 = 1531$Å | Fig. 7.6 |

SE data generated by using N = 2.5 - 0.02j are in sawtooth shape (Figure 7.5). It matches the experimental result at wavelength 475nm and 620nm but deviates a lot from the experimental data at other wavelength region. When we use $N_2$ as the initial parameters (Figure 7.6), the results converge and match quite well with the experimental data. Thus , the confusion caused by the single wavelength measurement can be eliminated. The discrepancy between the calculated and the experimental spectra as seen in Figure 7.6 is due to our use of a non-dispersive refractive index (N) value for the amorphous carbon thin film which is clearly an over simplified assumption.

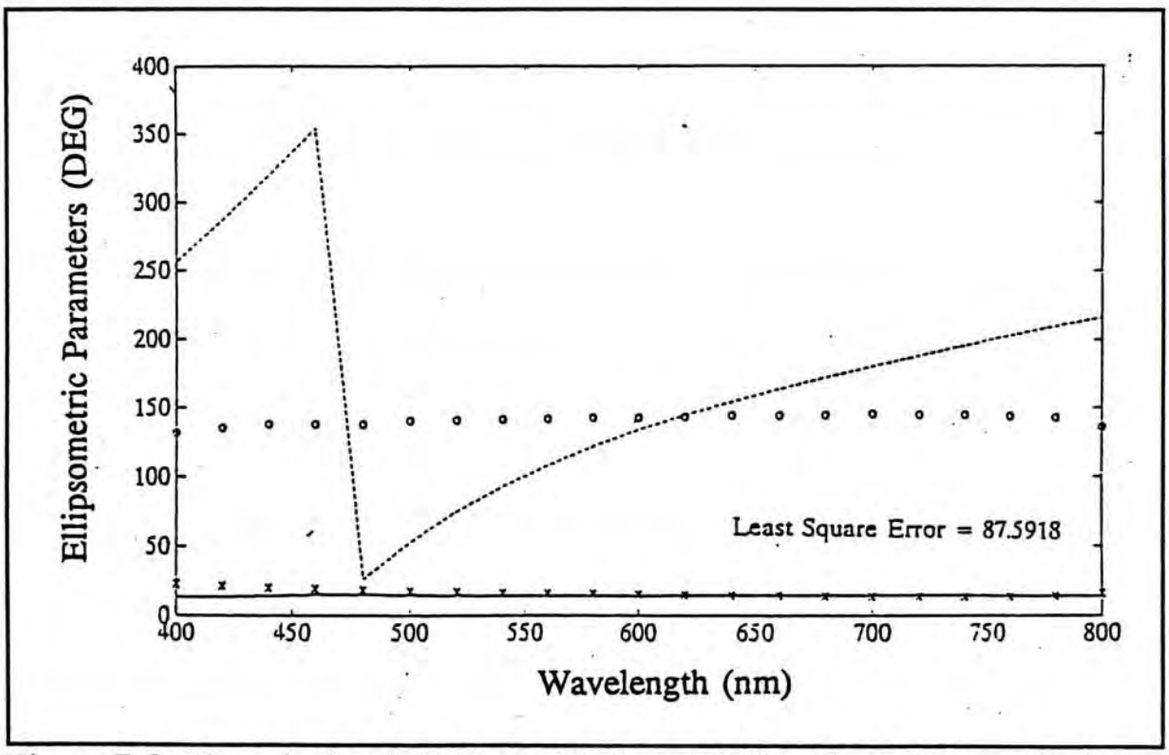


Figure 7.5. *The calculated SE data with N=2.5-0.02j. The fitting results do not match the experimental data for the amorphous carbon on silicon sample.*

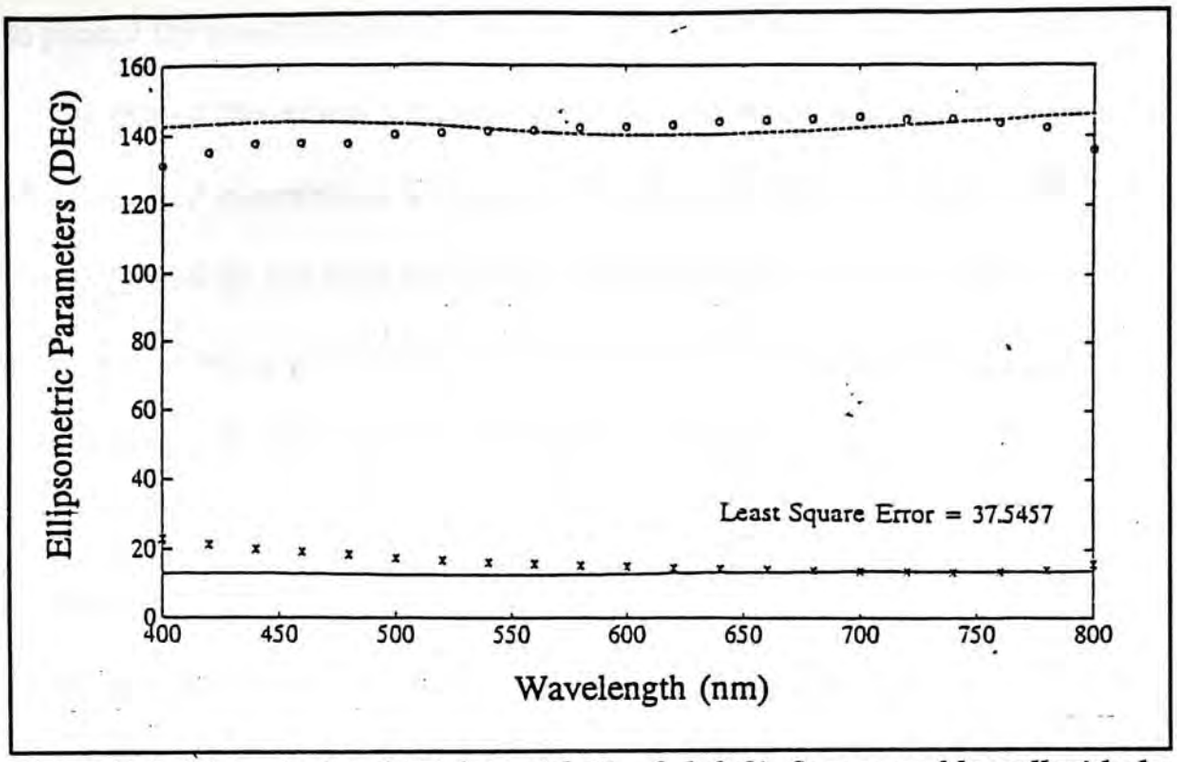


Figure 7.6. *The calculated SE data with $N_2$=3.1-0.9j, fit reasonably well with the experimental data for the amorphous carbon on silicon sample.*

### 7.1.3 High order x $Al_xGa_{1-x}As$ with different cooling rate

AlGaAs/GaAs alloy is a potentially useful material for high-speed electronics and optoelectronic devices. The optical constants n, k are therefore two utmost important parameters. The optical properties of $Al_xGa_{1-x}As$ with Al concentration varying from x=0 to x=0.8 in step of 0.1 has been reported by S.Adachi[58] and D.A. Aspnes[57]. Adachi calculated the real part of the refractive index from the Exciton Rydberg energy G and the direct-gap energy $E_o$ of AlGaAs while Aspnes calculated the complex refractive index from the spectroscopic ellipsometric data. The experimental values obtained by Aspnes from SE measurement[57] do not match well with the theoretical values calculated by Adachi [58] especially when the concentration of aluminum is high. (Fig. 7.14). The experimental values of the refractive index are the derived quantity from the SE data by means of a ambient-substrate model. However, a perfectly abrupt and clean surface can never be achieved in practice. The thickness and properties of the residual surface layers are not known, the best

way to present the results is directly report the properties of the samples in pseudo form[57,59].

The data of the optical properties of $Al_xGa_{1-x}As$ alloys for energies from 1.5 to 6 eV and wide range of composition x (from x=0 to x=0.9) have been reported[57,58]. However, at present, we still do not have reliable experimental results of the properties of $Al_xGa_{1-x}As$ at x=0.9. This is because the $Al_xGa_{1-x}As$ samples with composition near x=0.9 are so active that surface film will form quickly just after the chemical cleaning. Nevertheless, the real part of refractive index of $Al_xGa_{1-x}Ga$ at x=0.9 was calculated theoretically by Asachi[58] and it can be used as a reference spectrum (Figure. 7.14).

As an application of the spectroscopic ellipsometer, we try to measure the ellipsometric spectra of high Al concentration $Al_xGa_{1-x}As$ which were prepared by liquid phase epitaxy with different cooling rate (0.1°C/min. to 0.5°C/min.) The concentration of aluminium was measured by X-ray diffraction methods and the value of x was found to be about 0.88. No treatment such as polishing and stripping has been done on the samples' surface. The measured results of a bare sample are directly reported. Samples were first measured by null ellipsometer at 6328Å. The data obtained were then analyzed using the ambient-substrate model and the layer-substrate model. The experimental results are listed below.

| Cooling rate °C/min. | Thickness $\mu$m | P1 | A1 | P2 | A2 | $\psi$ | $\Delta$ |
|---|---|---|---|---|---|---|---|
| 0.1 | 8.0 | 62.4 | 6.5 | 151.7 | 173.9 | 6.3 | 145.9 |
| 0.2 | 6.08 | 53.4 | 6.6 | 143.1 | 174.1 | 6.25 | 163.5 |
| 0.3 | 4.26 | 58.1 | 4.7 | 148.1 | 176 | 4.35 | 153.8 |
| 0.4 | 3.45 | 55.4 | 4.8 | 145 | 175.6 | 4.6 | 159.6 |
| 0.5 | 2.74 | 54.7 | 5.0 | 144.1 | 175.2 | 4.9 | 161.2 |

The thickness of the AlGaAs layer was obtained by measuring the cross-section of the

sample by using optical microscopy. From the above table, it is clear that thicknesses of the above samples are in the order of micron. We can forecast that the optical parameters obtained using ambient-substrate should be very close to the true values. Thus, refractive index of the samples calculated by ambient-substrate(bulk) model were used as the initial parameters for the least square fitting program when layer-substrate(layer) mode analysis was used[60]. Both set of results are shown in the table.

| Cooling rate °C/min. | N (Bulk mode) | N (Layer mode) |
|---|---|---|
| 0.1 | 3.213 - 0.369j | 3.2135 - 0.3688j |
| 0.2 | 3.315 - 0.192j | 3.3161 - 0.1921j |
| 0.3 | 3.097 - 0.189j | 3.0982 - 0.1901j |
| 0.4 | 3.141 - 0.161j | 3.1412 - 0.1615j |
| 0.5 | 3.175 - 0.161j | 3.1746 - 0.1612j |

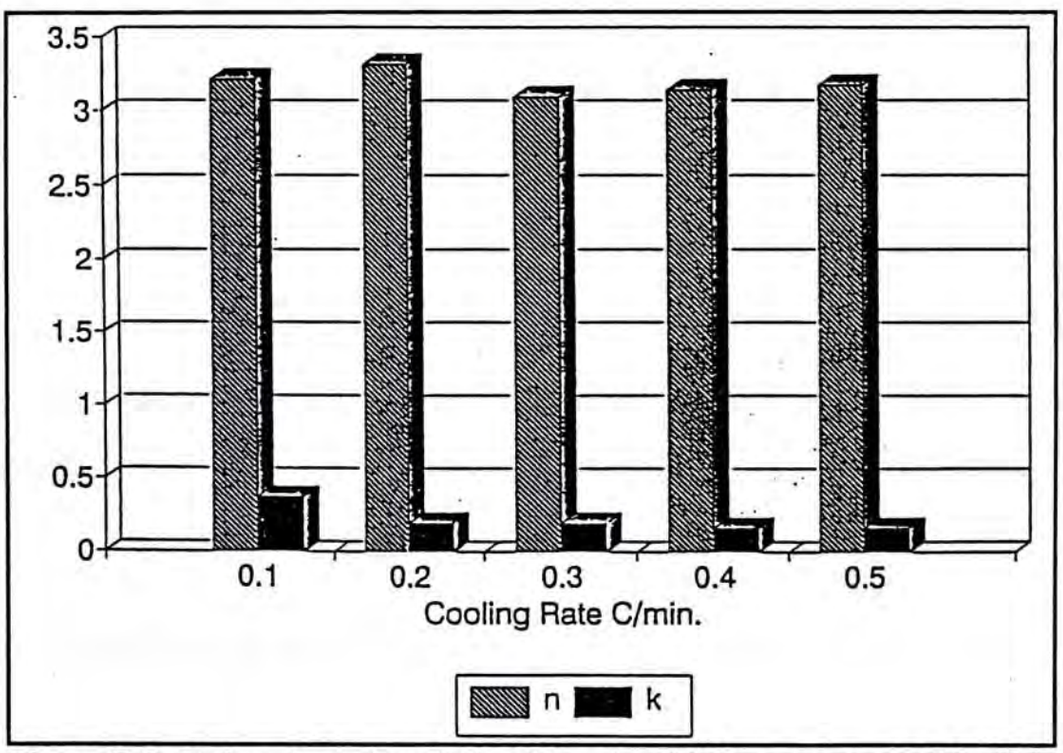


Figure 7.7. *Refractive index of $Al_{0.88}Ga_{0.12}As$ which were prepared by LPE with cooling rate varying from 0.1°C/min. to 0.5°C/min.*

No matter which model is used, the calculation is based on the same set of data

obtained by the null ellipsometer. If the surface layer can be regarded as a semi-infinite dielectric material then the optical properties reckoned from either the bulk mode or the layer mode will be the same. The AlGaAs layer grown by LPE is usually thick enough so that optical parameters obtained by ambient-substrate model and layer-substrate model are equal[51]. Since the film thickness is much larger than the penetration depth of incident light, thickness of the AlGaAs layer is not important in the calculation of the refractive index. During the measurement on our samples, we observed that the reflected laser beam was scattered seriously by the sample surface. It means that the sample surface is not smooth (Fig. 7.16 to Fig. 7.19) and the smoothest region was selected for the measurement.

In principally we expect that there exists a relationship between the optical properties and the cooling rate of the samples. If the duration of the cooling process is long, the AlGaAs layer can re-crystallize with less defect. However, according to our experimental results, the refractive index of the samples do not show any simple correlation with the cooling rate.

Referring to the theoretical values calculated by Aspnes (Fig.7.14), the AlGaAs layer should be non-absorbing at a wavelength of 633nm. In contrast, our experimental result of the extinction coefficients (k) are much larger than expected. It has also been found that the results are dependent on the surface roughness of the samples. Experimental data will be different for different regions of the sample surface. The measured results are significantly influenced by the roughness of the surface of the samples. Since the degree of roughness is different from sample to sample, the "cooling rate" dependence may be obstructed by the imperfect surface condition. Figure 7.8 and 7.9 are the spectroscopic ellipsometry spectra ($\psi(\lambda),\Delta(\lambda)$) of the LPE grown AlGaAs layer. The ellipsometric data of the samples prepared with different cooling rate are plotted on the same graph.

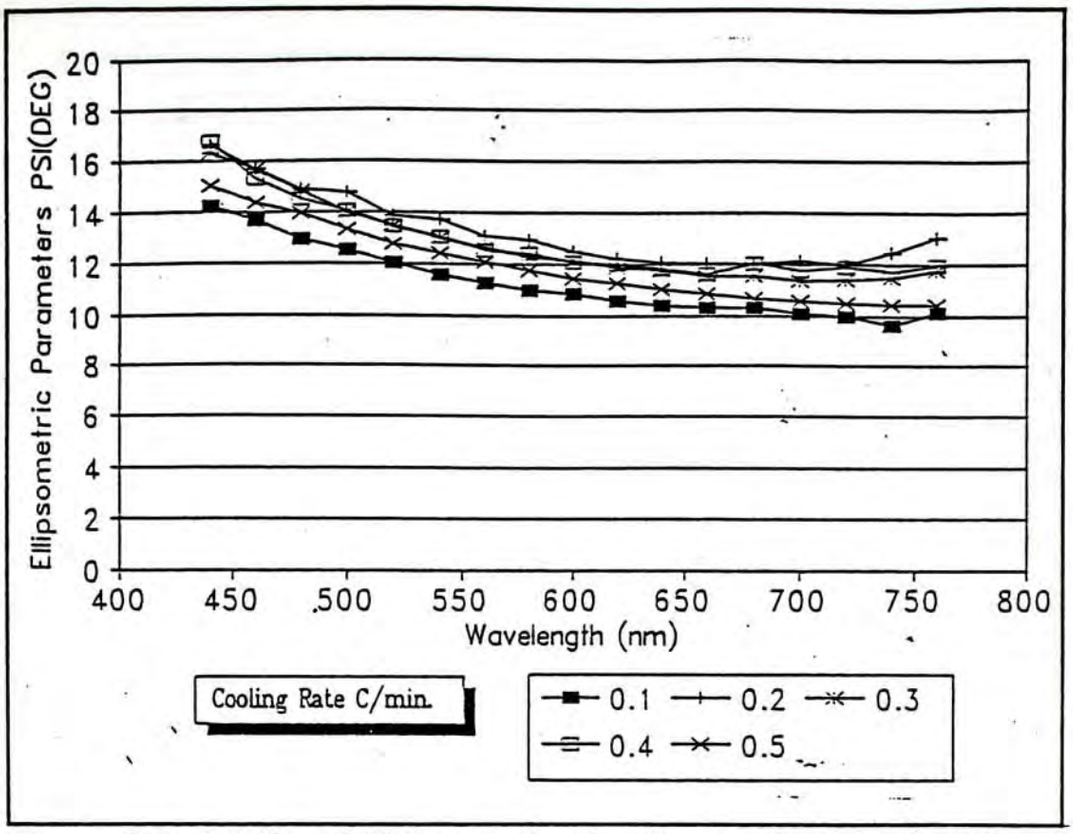


Figure 7.8. *PSI(ψ) of LPE growth $Al_{0.88}Ga_{0.12}As$ layer with different cooling rate.*

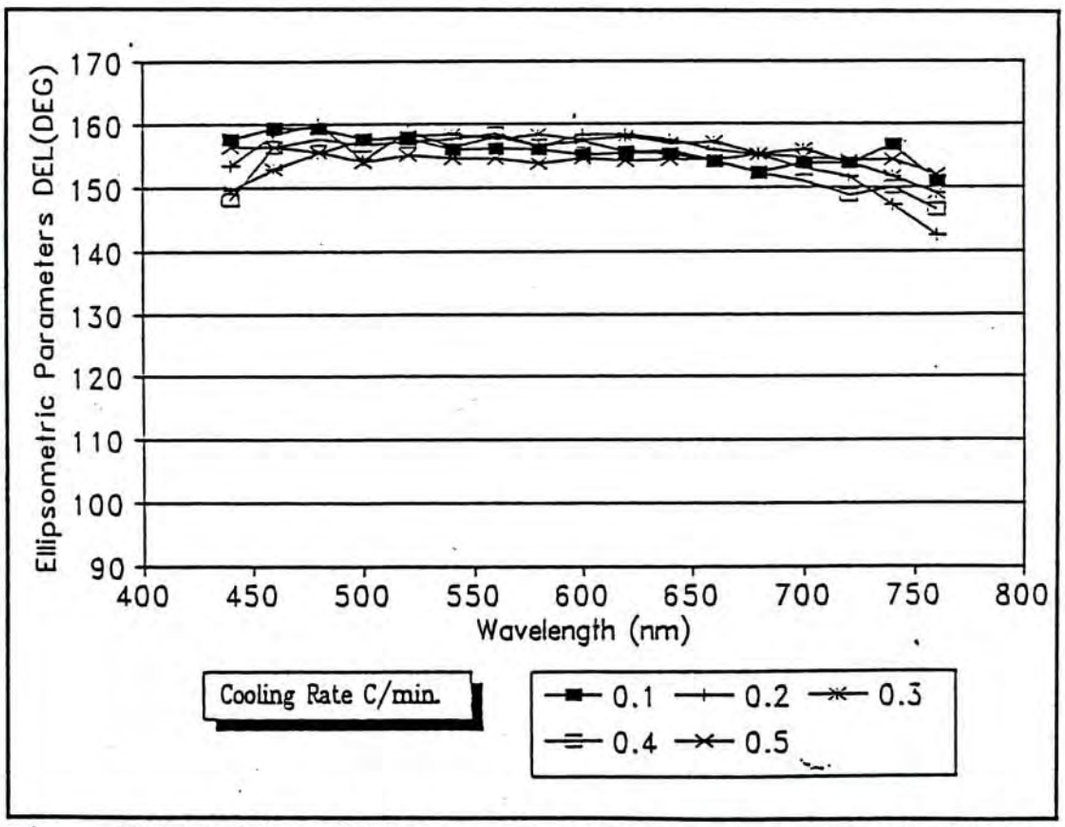


Figure 7.9 *DEL(Δ) of LPE growth $AL_{0.88}Ga_{0.12}As$ layer with different cooling rate*

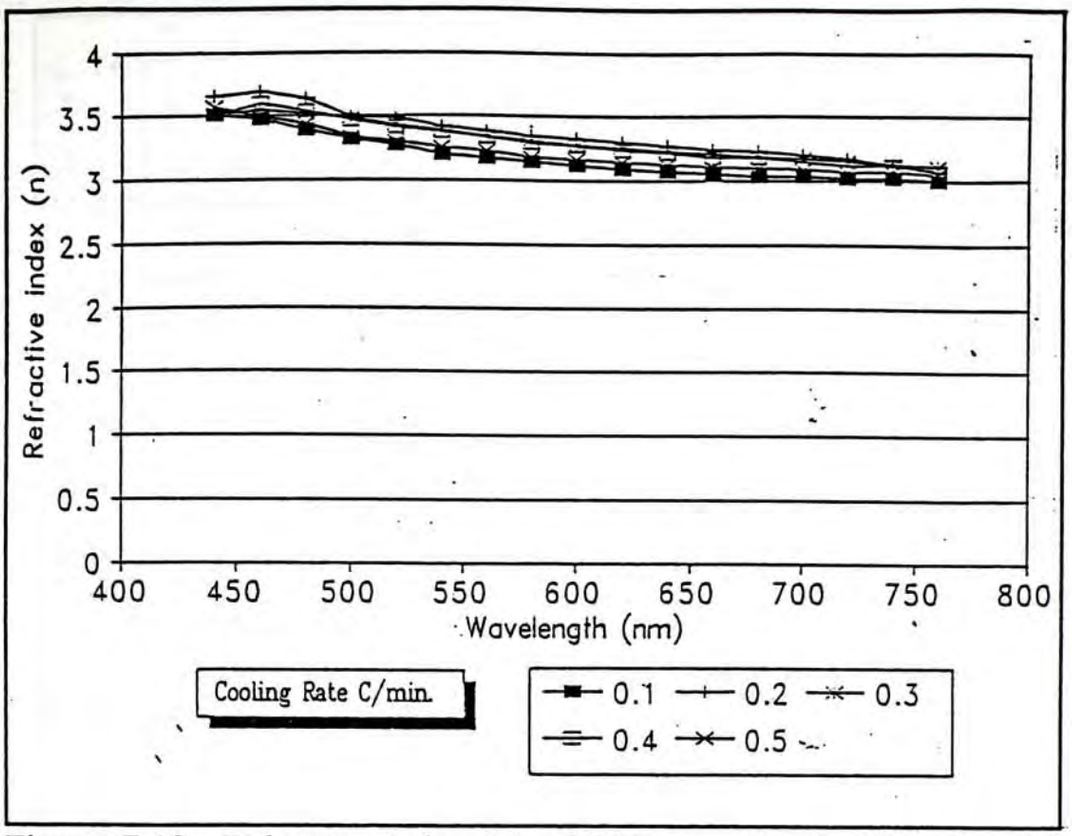


Figure 7.10. *Refractive index (n) of LPE growth $Al_{0.88}Ga_{0.12}As$ with different cooling rate.*

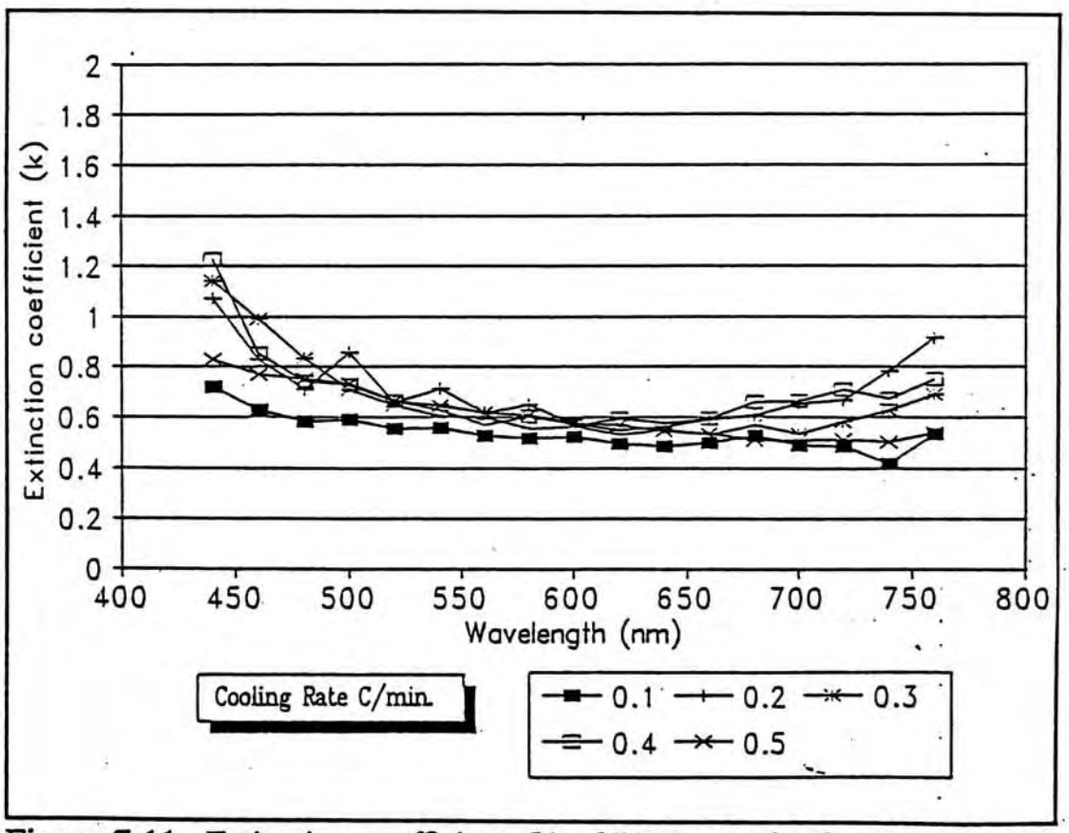


Figure 7.11. *Extinction coefficient (k) of LPE growth $Al_{0.88}Ga_{0.12}As$ with different cooling rate.*

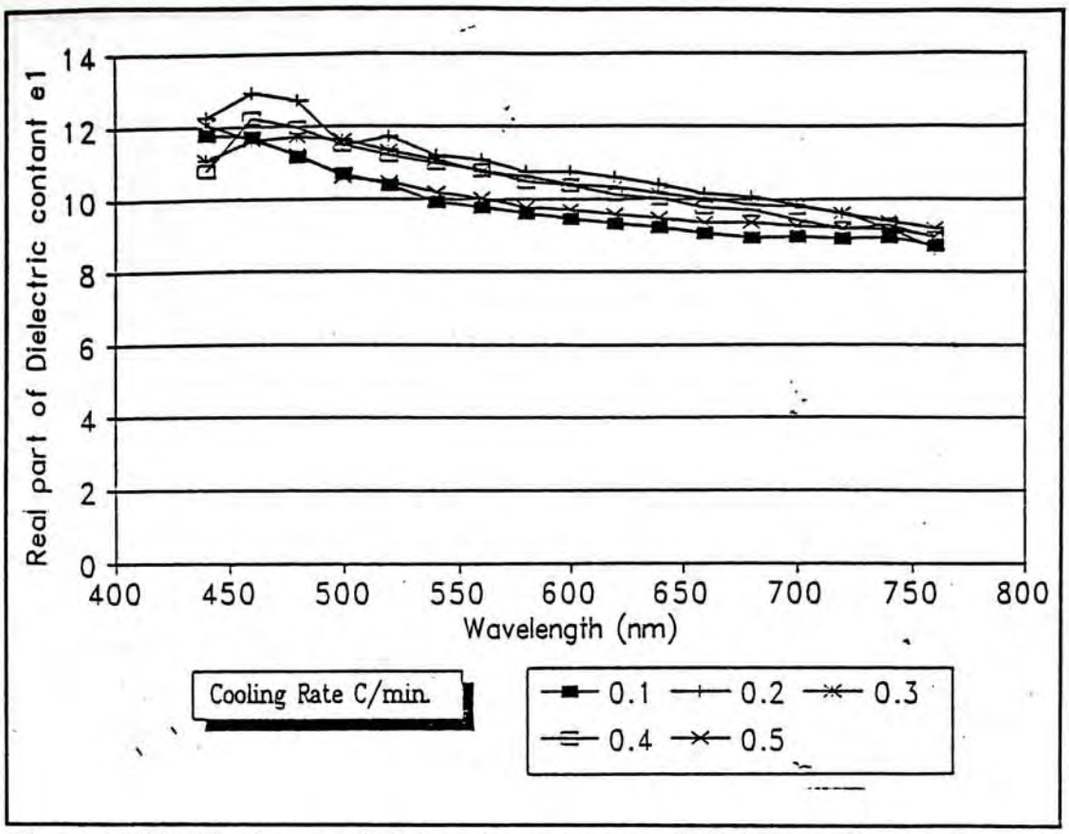


Figure 7.12. *Real part of dielectric constants of LPE growth $Al_{0.88}Ga_{0.12}As$ with different cooling rate.*

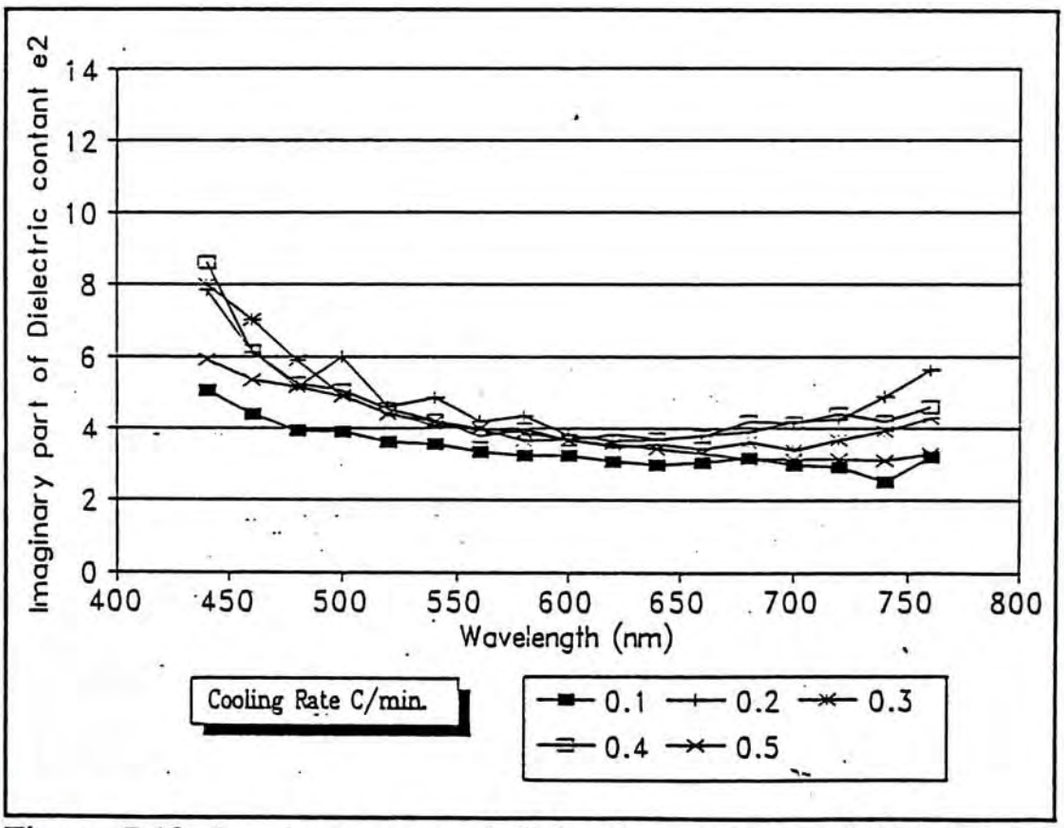


Figure 7.13 *Imaginary part of dielectric constants of LPE growth $Al_{0.88}Ga_{0.12}As$ with different cooling rate.*

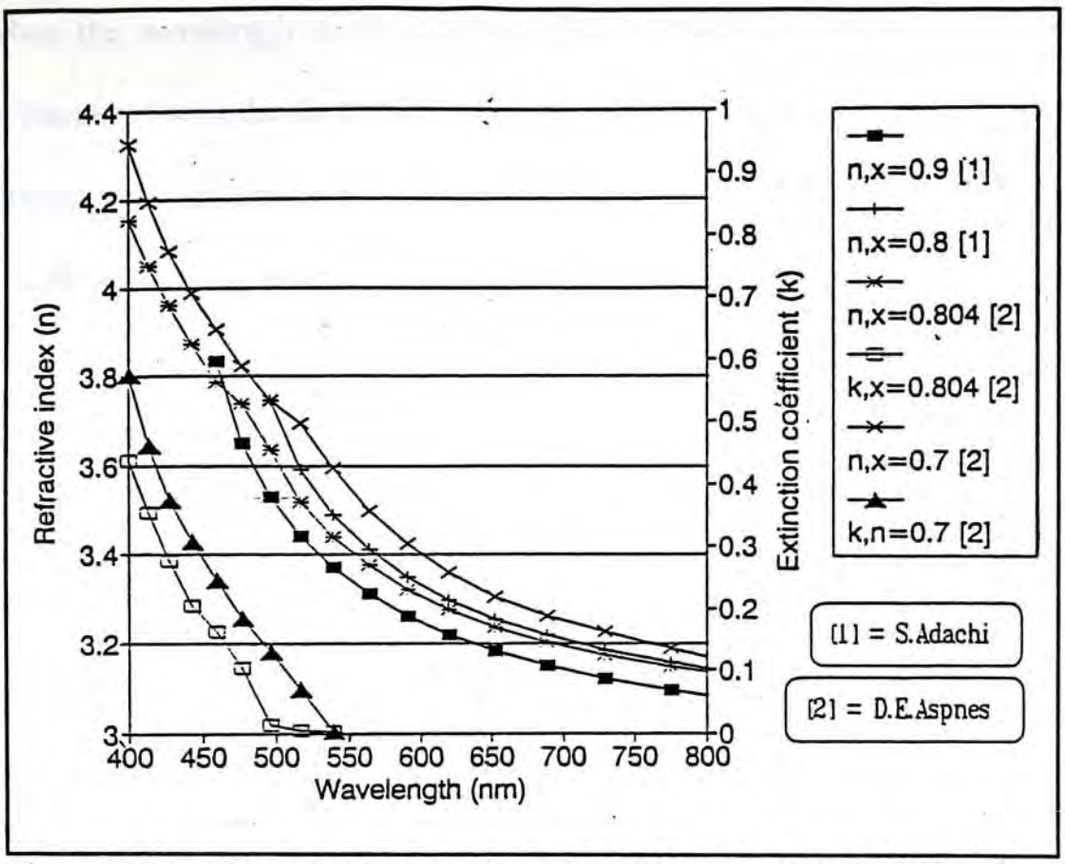


Figure 7.14. *The optical properties n,k of Al concentrated AlGaAs from [1] S.Adachi (Calculation); [2] D.E.Aspnes (Spectroscopic Ellipsometry)*

The optical properties of the samples are derived from the ellipsometric data by means of an ambient-substrate model.If the surface is rough, error will be introduced into the measured data[46,47]. Nevertheless, the optical and electrical parameters of the samples which derived from these ellipsometric data by means of an ambient-substrate model are shown in Figure 7.10 to Figure 7.13. When compare our experimental data with those obtained by Aspnes, the values of the refractive index(n) of our samples are close but those of the extinction coefficient (k) are quite different especially in the long wavelength region.

According to the results reported by Aspnes[57] and Adachi[58], the real part and imagine part of the complex refractive index decrease as the concentration of Al in $Al_xGa_{1-x}As$ increases. Moreover, both values should also decrease gradually with increasing wavelength of the incident light. From our experimental data (fig.7.10), we observed that the refractive index of sample which were prepared with different cooling rate varied from about 3.6 to 3

3.6 to 3 when the wavelength of the incident light increase from 440nm to 760nm. When comparing the result with the theoretical value of $Al_xGa_{1-x}As$ at x=0.9, the refractive index (n) of our result is lower. However, if we regard the refractive index as a pseudofunction of the wavelength and then compare with those acquired by Aspnes (x=0.7 and x=0.9), the trends of the curves are matched and the experimental values are close.

Owing to the non-prefect sample surface and the existence of dusts and particles on the sample surface, scattering light is unavoidable. The HeNe laser beam used in the null ellipsometer is narrow and bright enough to be noticed, thus the position of samples can be adjusted with the help of the light source so that the scattering effect was minimized. This is the reason why the extinction coefficient (k) obtained by the null ellipsometer is usually a little bit smaller than those acquired by the spectroscopic ellipsometer.

Therefore, when sample surface is rough like the LPE grown $Al_xGa_{1-x}As$ layers, deviation between the value of k obtained by the null type and the rotating-analyzer type ellipsometer will be larger. Although the diameter of the light beam used in the SE system is narrowed down by a diaphragm, the surface area of the sample shined by the light beam is still larger than using a laser light source. Moreover, the intensity of incident light produced from a quartz lamp is lower than the intensity of a laser light source, it is difficult to align the sample as we did in the single wavelength measurement by the null ellipsometer. If the dimension of the sample is small, measurement is usually taken at the central region of the sample in order to ensure that the incident light will not strike on the sample holder.

According to the data we have in the single wavelength approach, the optical result obtained by bulk mode analysis match with those using layer model, we know that the $Al_xGa_{1-x}As$ layer is an absorbing layer at 633nm. The SE result also show that the samples prepared at different cooling rate have a great absorbability near the blue region. However,

the values of the extinction coefficients (k) do not reduce significantly when the wavelength of the incident light increases. The values of k keep at about 0.5 throughout the whole measured region. This phenomena seems to imply that the imagine part of the refractive index of the samples is independent to the wavelength of the incident light. The strange behaviour of our LPE grown highly Al concentrated $Al_xGa_{1-x}As$ layer may be caused by two major factors.

(i) Physical mixture of oxide and $Al_xGa_{1-x}As$ alloy on the samples surface

The sample surface of a highly Al concentrated $Al_xGa_{1-x}As$ was found to be so reactive that an oxide layer will immediately formed after the chemical cleaning. According to the result obtained by Aspnes, when the concentration of Al is high ($x>0.6$), chemical cleaning is not adequate to remove the surface layer completely and thus the result will show systematic discrepancies. When the content of Al increase to $x=0.9$, the sample surface will become very active. Oxidation of a highly Al concentrated surface will proceed via local penetration rather than along a uniform front. The reactive layer may probably be formed by the mixture of $Al_2O_3$, $As_2O_3$ and $Ga_2O_3$, but the exact composition is difficult to determine[57]. Moreover, the optical properties and thickness of such a layer are unknown and therefore, up to now we still do not have a reliable experimental optical data for a highly Al concentrated $Al_xGa_{1-x}As$.

(ii) Surface roughness and non-uniformity thickness

Although, the features on the sample surface cannot be observed by an unaided eye, the existence of surface roughness layer can be inferred from the phenomena that light beam is scattered when it is reflected from the sample. According to Rode's analysis, terrace will formed on the surface of the LPE grown material. The surface terrace illustrated in Fig.7.15, is in fact a continuous tread layer formed on the substrate[65].

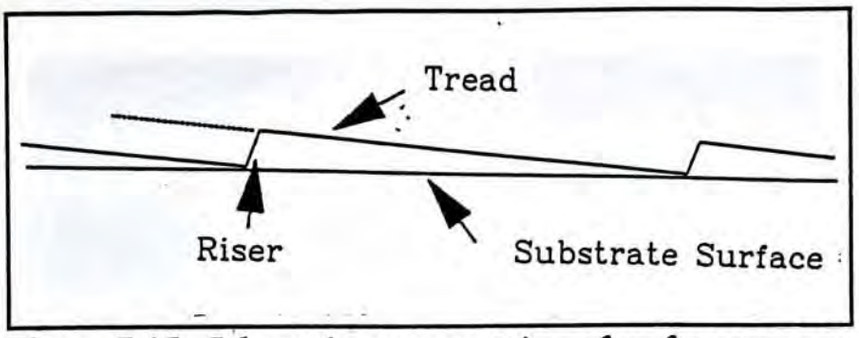

Figure 7.15. *Schematic representation of surface terrace.*

Based on the experimental result from Rode, the critical angle $\phi$ of a LPE growth $Al_xGa_{1-x}As$ was found to vary from about 0.8° to 0.1° when the growth temperature changed from 775°C to 850°C. The sample we measured was prepared at a growth temperature of about 780°C, thus we should expect that a larger critical angle of terrace will result. The formation of the terrace layer causes a layer thickness variation and therefore seriously affects the result of the optical measurement. Two specific features can be observed on the sample's surface. The Meniscus lines (Fig.7.16 and Fig.7.17) are a common feature appear on the surface of the LPE growth material. The Meniscus lines represent the contour of the trailing edge of the liquid as it moves across the substrate during the sliding procedure. The photomicrograph were taken by a Nomarski phase-contrast microscopy with amplification of 10x10. There also exist another kind of feature different from the Meniscus line formed by the terrace. Fig.7.18 and Fig.7.19 illustrate the second kind of feature. Both kinds of traits appear randomly on the sample surface but they are not independent. When we scan the sample surface with the help of microscopy, we found that the two kinds of features gradually change from one type to the other. However, the mechanism of the formation of these features is still not understood.

The optical properties of the material derived from the ellipsometric data are based on the assumption that the sample surface is flat and uniform. The existence of a rough surface layer will causing a large error in the determination of sample's characteristics.

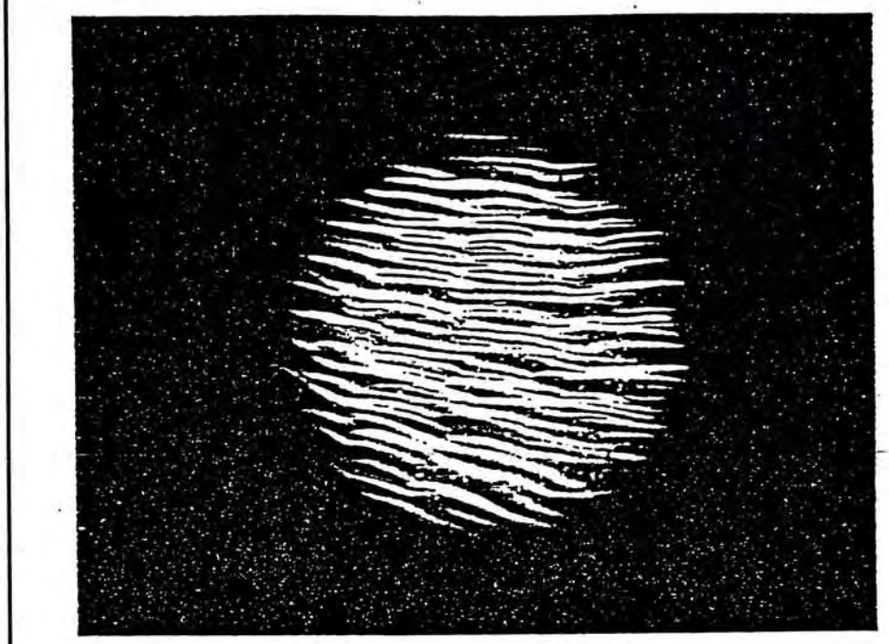

Figure 7.16. *Meniscus line feature on the LPE growth $Al_xGa_{1-x}As$ with a cooling rate of 0.2°C/min.*

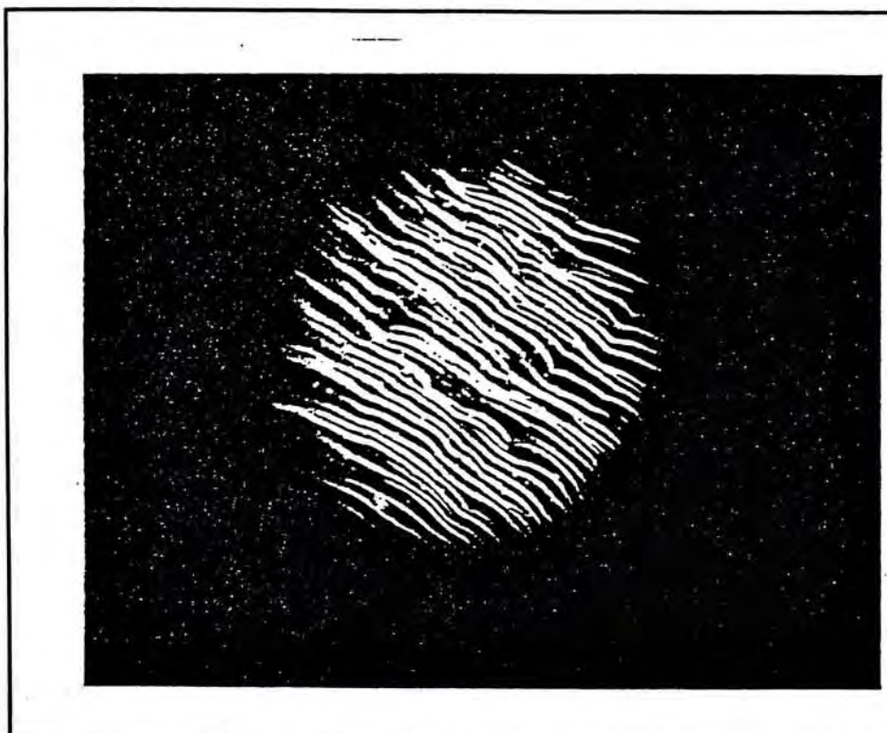

Figure 7.17. *Meniscus line feature of the LPE growth $Al_xGa_{1-x}As$ with a cooling rate of 0.4°C/min.*

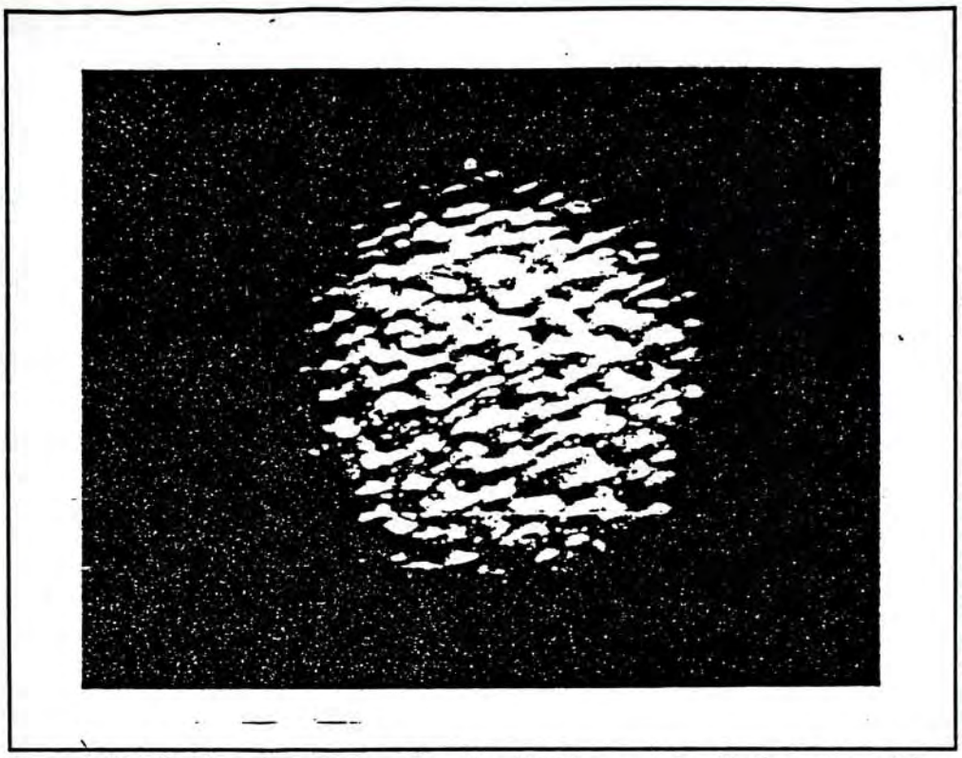

figure 7.18 *Roughness on the the LPE growth $Al_xGa_{1-x}As$ with a cooling rate of 0.4°C/min.*

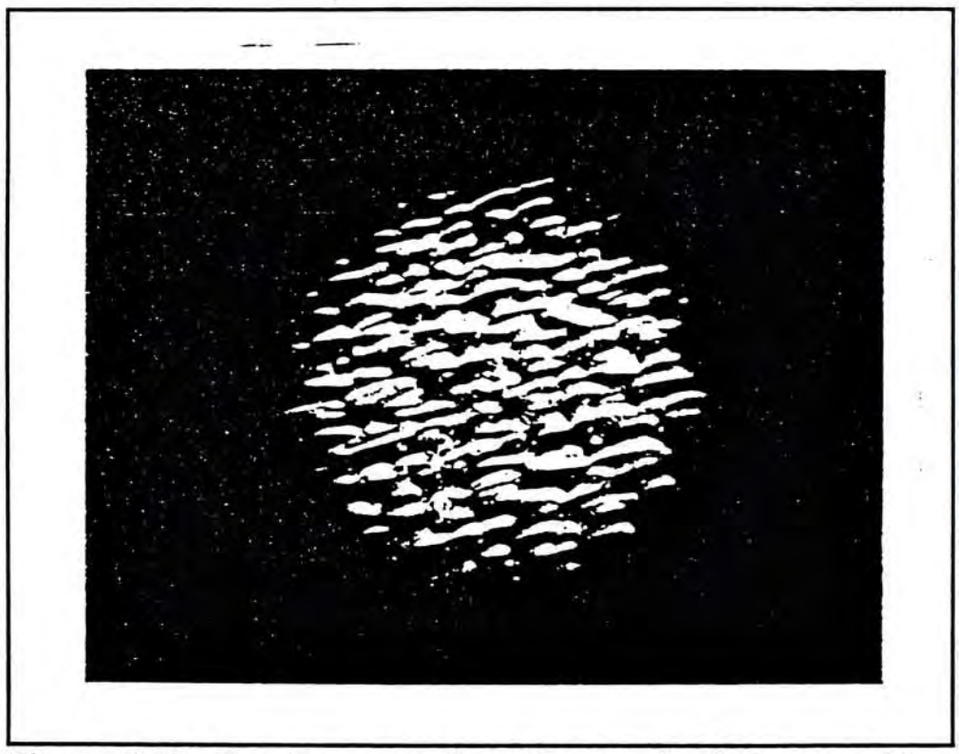

Figure 7.19. *Roughness on the LPE growth $Al_xGa_{1-x}As$ with a cooling rate of 0.5°C/min*

## Section 7.2 Comparison of ellipsometric spectra of SOI samples

In this section, the ellipsometric spectra of some buried nitride SOI (Silicon-on-insulator) samples prepared with different conditions will be compared with each other and discussed. The structures of these samples are much more complicated than those of the examples discussed in the previous section. In principle, the optical constants and the thicknesses of the different layers in these structures can be deduced by analyzing the ellipsometric spectra with appropriate models. However, such analysis will not be attempted in the present work and will be the topic of further investigation. In this section, we shall only present some qualitative discussion on the spectra obtained for these samples.

### Section 7.2.1 Difficulty in the analysis of multi-layer structures

The possibility to successfully analyses the ellipsometric spectra of a sample is dependent on our knowledge about the structure and composition of the sample. As we discussed before, the equations describing the polarization of the electromagnetic wave incident on and reflected from the sample are derived with the assumption that, the specimen is constructed with a parallel stratified planar structure. The optical properties are uniform within each layers and they change abruptly at the sharp interface between layers. When the properties of the sample change continuously within an inhomogeneous layer such as an ion implanted sample, we can approximate the inhomogeneous layer by a large number of sublayers. The simplest approach is to assume that each of these layers is homogenous.

Although multiple measurements on a sample at different wavelength should provide adequate information to analyses a sample with multi-layer structure, the equations involved in the calculation of the optical properties of the multi-layer structure are so complicated that, the unknown parameters have to be obtained from the spectroscopic ellipsometric data by fitting the experimental result with an appropriate model of the structure. Thus, the model

and the fitting approach we choose are of crucial importance for a successful analysis of the SE data.

The Marquart algorithm is a commonly used nonlinear regression method for the analysis of spectroscopic ellipsometric spectra. The convergence rate of the Marquart algorithm is faster than other approaches, provided the deviation of the initial guess from the solution is small enough. Otherwise, the fitting process may not be converged. In other words, we must have some idea on the structure and composition of the samples beforehand. It is unlikely that we can get to the correct solution if we start with an arbitrary set of the initial parameters.

As a first trial, a fitting program has been written using the Marquart algorithm to handle the SE data. When the structure of the sample is not complicated, the program is found to work well. In reality, since no sample is perfect, therefore the analysis of the ellipsometric parameters can be quite involved and not straightforward. Our program has been developed using the 2x2 scattering matrix approach, applicable to any multi-layer structures provided that each of the layer is uniform and isotropic.

Owing to the limitation of the fitting program for samples of complicated structures, we shall not attempt to fit the spectra which will be one of the objectives of future work. The spectroscopic ellipsometric spectra of the different SOI samples will only be compared to each other. From the comparison of the samples prepared under different conditions or with different treatments, we can still obtain useful information of the samples and obtain relationship between the treatments and the properties of the samples. The following section reports on the results we obtained for some silicon-on-insulator samples prepared by nitrogen implantation into silicon.

## Section 7.2.2 Silicon On Insulator (SOI)

High dose implantation of reactive ions such as oxygen and nitrogen provides an effective means to fabricate a silicon on insulator (SOI) structure for very large-scale integration (VLSI) applications. Device fabricated on a SOI structure has a higher response speed, since the parasitic capacitance of device is reduced. The microstructure of the SOI structure will directly affect the performance of the devices fabricated on it. These structures have been extensively studied by varies methods such as RBS, TEM , SIMS and AES. In recent years ellipsometry technique has also been widely applied to these structures for its ease of operation, its contactless and non-destructive characteristics.

The insulating buried layer of a SOI structure can be formed by the implantation of either oxygen or nitrogen ions. However, the SE analysis of the nitrogen implanted samples is more difficult when compared with the case of the oxygen implanted samples. It is because the microstructure of the buried silicon-nitride layer depends more strongly on the implantation dose[63]

In this section, SOI samples fabricated by $N^+$ implantation were measured by the spectroscopic ellipsometer. The IR absorption spectra and X-ray diffraction patterns of these samples have already been reported by Wong and Poon[62]. The ellipsometric spectra of different samples obtained were compared to analyses the condition required to produce a stoichiometric buried silicon nitride layer.

Samples to be investigated were fabricated by 150keV $N^+$ implant into a 50mm diameter <100> p-type silicon wafer. The implantation process was preformed using an Extrion 200-1000 implanter with a stationary beam. During implantation, the wafer is mechanically scan so that the substrate is suffering from the temperature cycling effect. There is also significant beam heating leading to in situ annealing of the samples. To study the

beam current effect, the beam current was varied from 50$\mu$A to 400$\mu$A and the maximum dose used was $1.2x10^{18}cm^{-2}$. The beam size is approximately 1x3 cm and the wafer was scanned horizontally so that the nitrogen ions were distributed over a strip of about 3x5cm in area and the middle region of implanted area was measured by the ellipsometer.

**Section 7.2.2.1 The beam current effect**

The spectroscopic ellipsometric spectra of samples implanted with 50uA,150uA, 200$\mu$A and 400$\mu$A before annealing are shown in Figure 7.20 to Figure 7.23. The parameters PSI($\psi$) and DEL($\Delta$) of different samples are plotted together in Figure 7.24 and Figure 7.25 respectively for comparison. When the beam current is small (50$\mu$A and 150$\mu$A), the SE spectra show no feature at all. We shall see that this featurelessness of the SE spectra is an indication that the buried silicon-nitride layer is not in crystalline form. When compared with the IR transmission spectra reported by Wong and Poon[62], we notice that the samples prepared with low beam current show broad band absorption. This indicates that the buried silicon-nitride layer is in the amorphous phase. However, as shown in Figure 7.26 to Figure 7.29 for the samples annealed in nitrogen at 1200°C for two hours, the spectra shows wavy features. It is also observed that the amplitude of the variation in the spectra against wavelength is larger for the samples prepared with larger beam current. It also clearly indicates that the optical properties of the samples after annealing have changed and the SE spectra become closer to the form of an ideal SOI sample with three layer structures as depicted in (Figure 7.32).

For the samples implanted with larger beam current (200$\mu$A and 400$\mu$A) , the spectra are completely different. Features are observable for the "as implanted" samples especially when the beam current is large (400$\mu$A). The substrate temperature of the sample

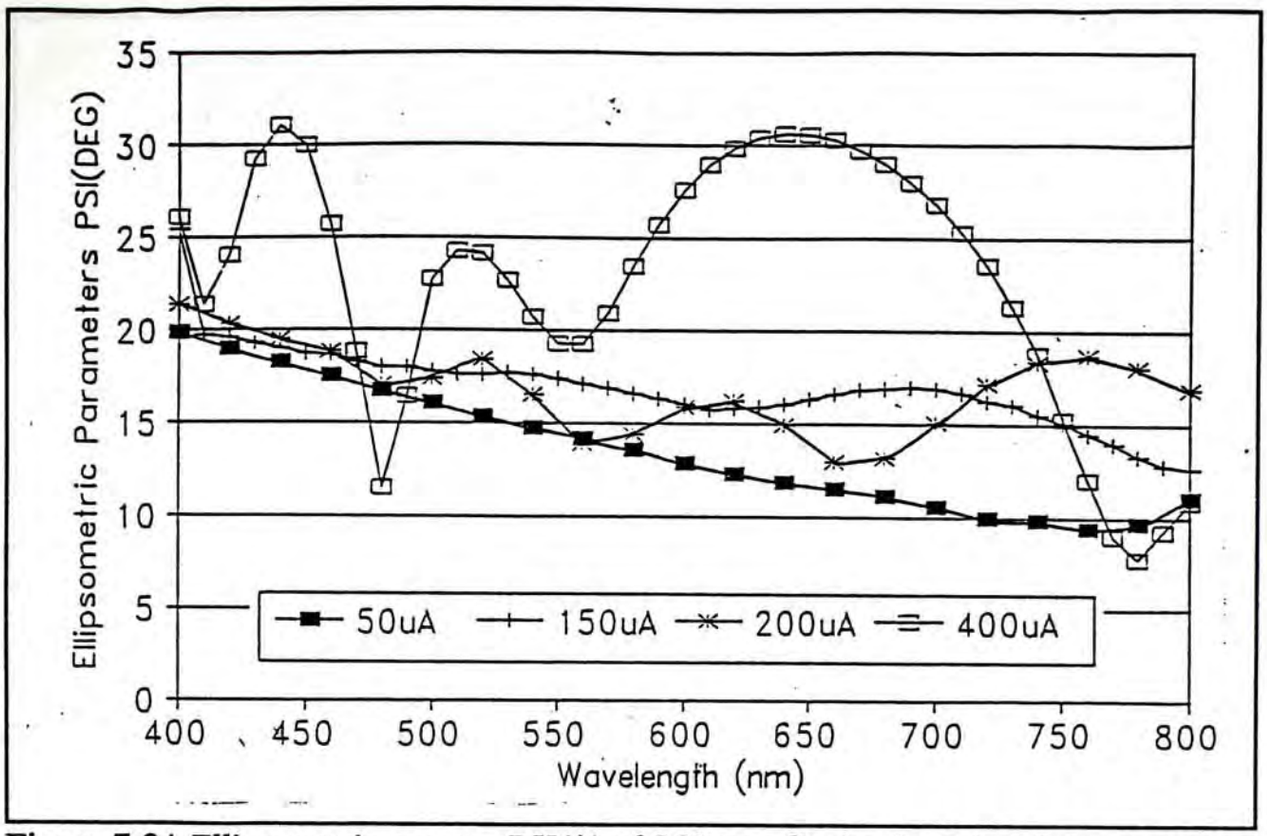


Figure 7.24 *Ellipsometric spectra PSI(ψ) of SOI samples implanted with beam current 50μA, 150μA, 200μA and 400μA. The curve feature increase with beam current.*

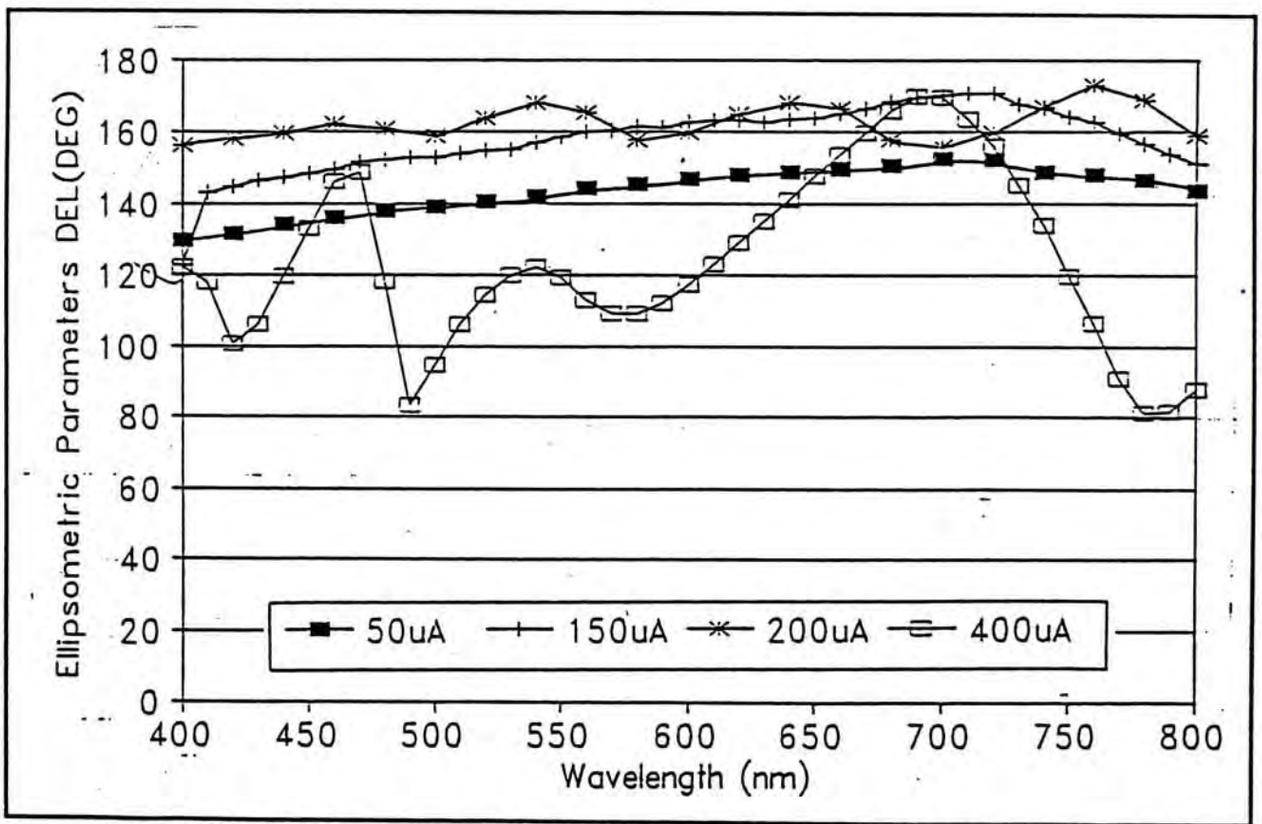


Figure 7.25 *Ellipsometric spectra DEl(Δ) of samples implanted with beam current 50μA, 150μA, 200μA and 400μA. The curve feature increase with beam current.*

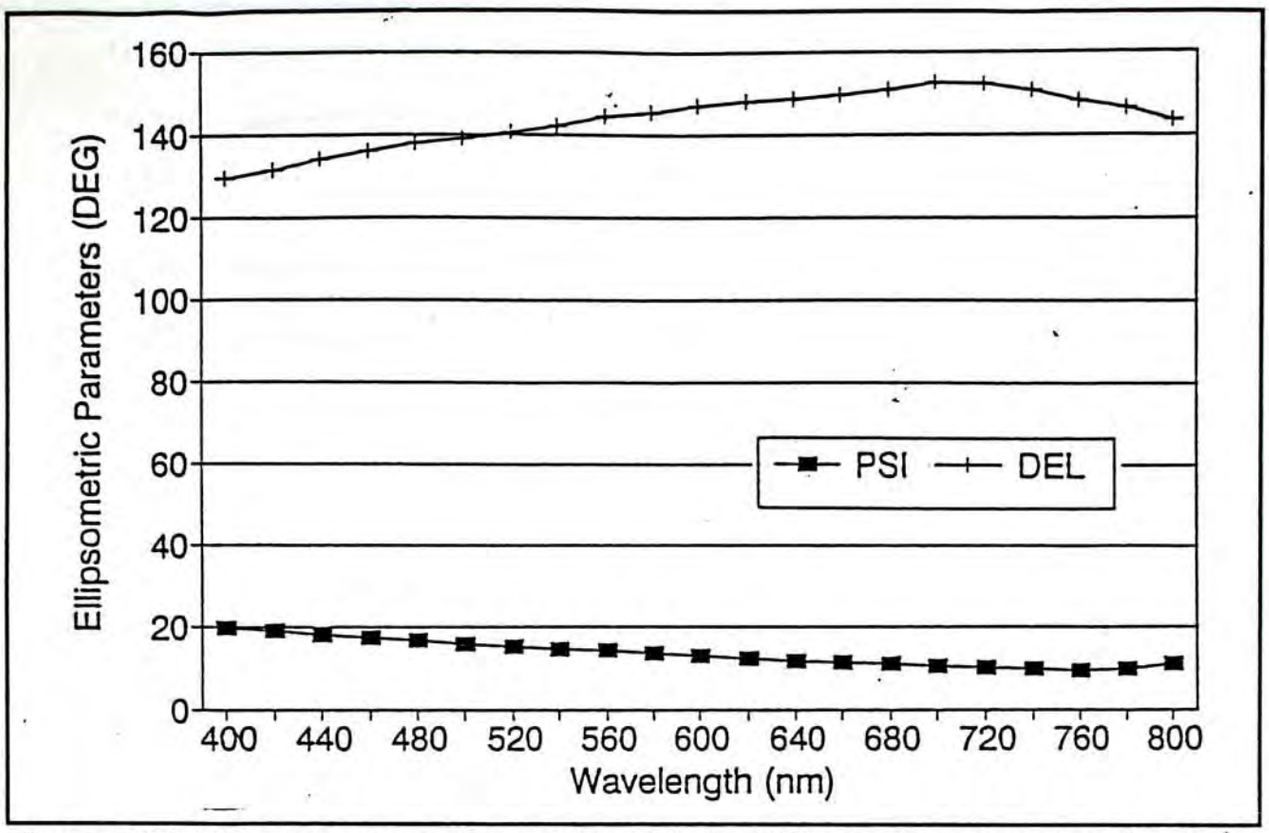


Figure 7.20 *Ellipsometric spectrum $\psi(\lambda),\Delta(\lambda)$of a SOI sample prepared with a beam current of 50μA.*

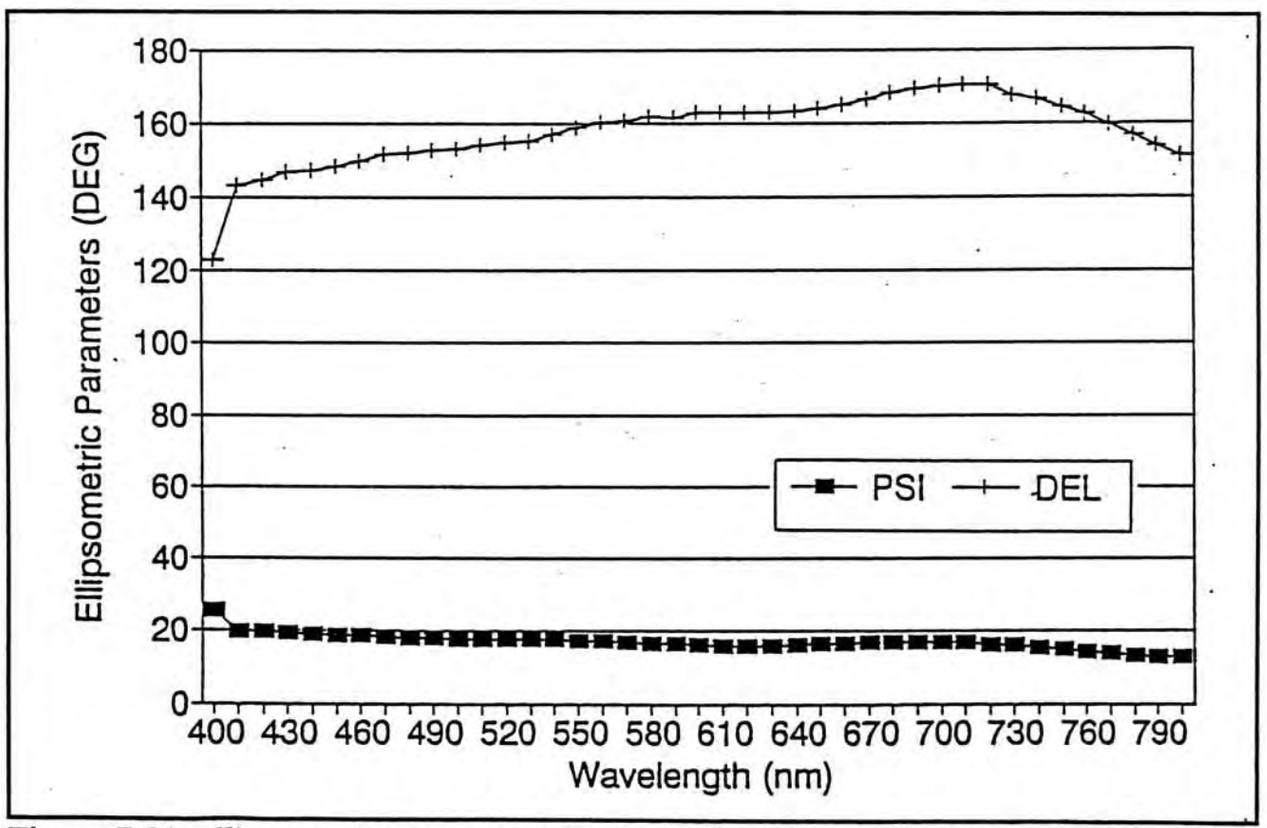


Figure 7.21 *Ellipsometric spectrum $\psi(\lambda),\Delta(\lambda)$ of a SOI sample prepared with a beam current of 150μA*

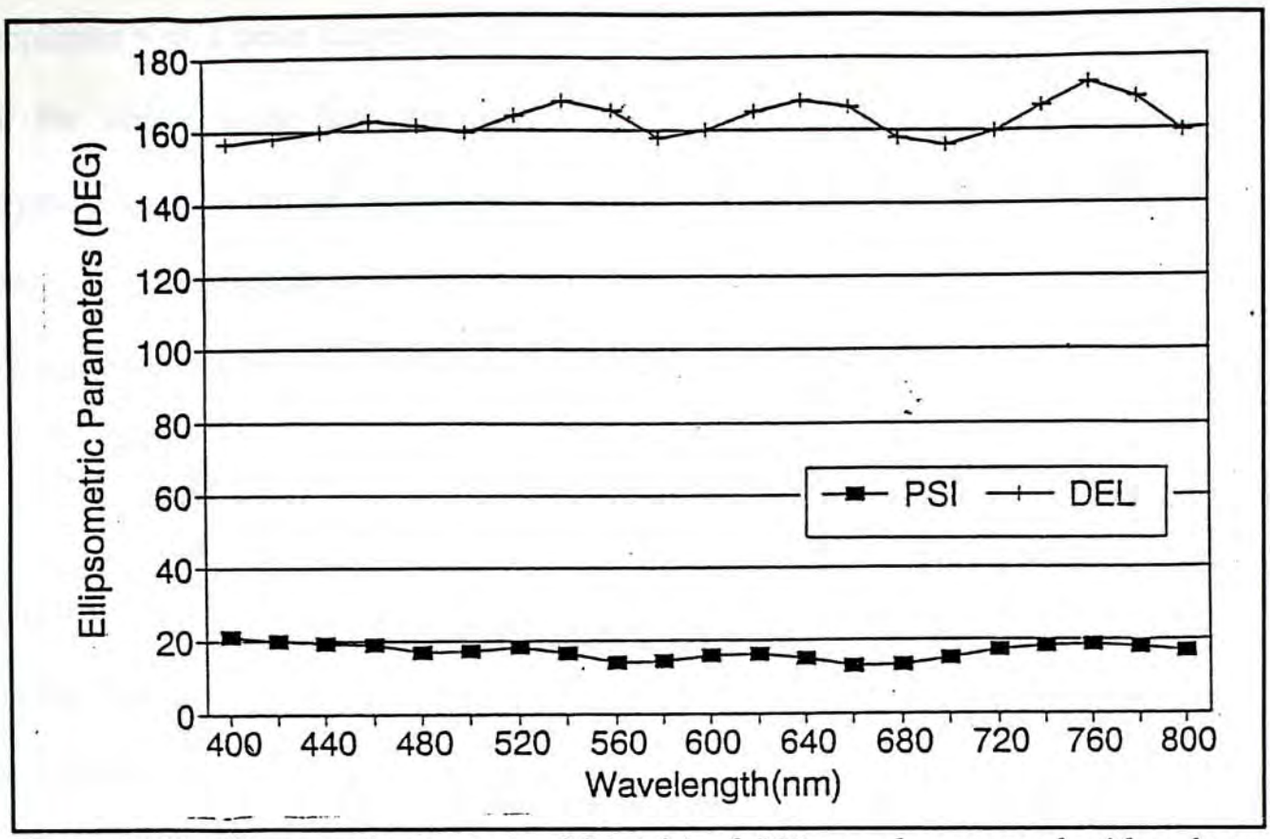


Figure 7.22 *Ellipsometric spectrum $\psi(\lambda),\Delta(\lambda)$ of SOI sample prepared with a beam current of 200μA.*

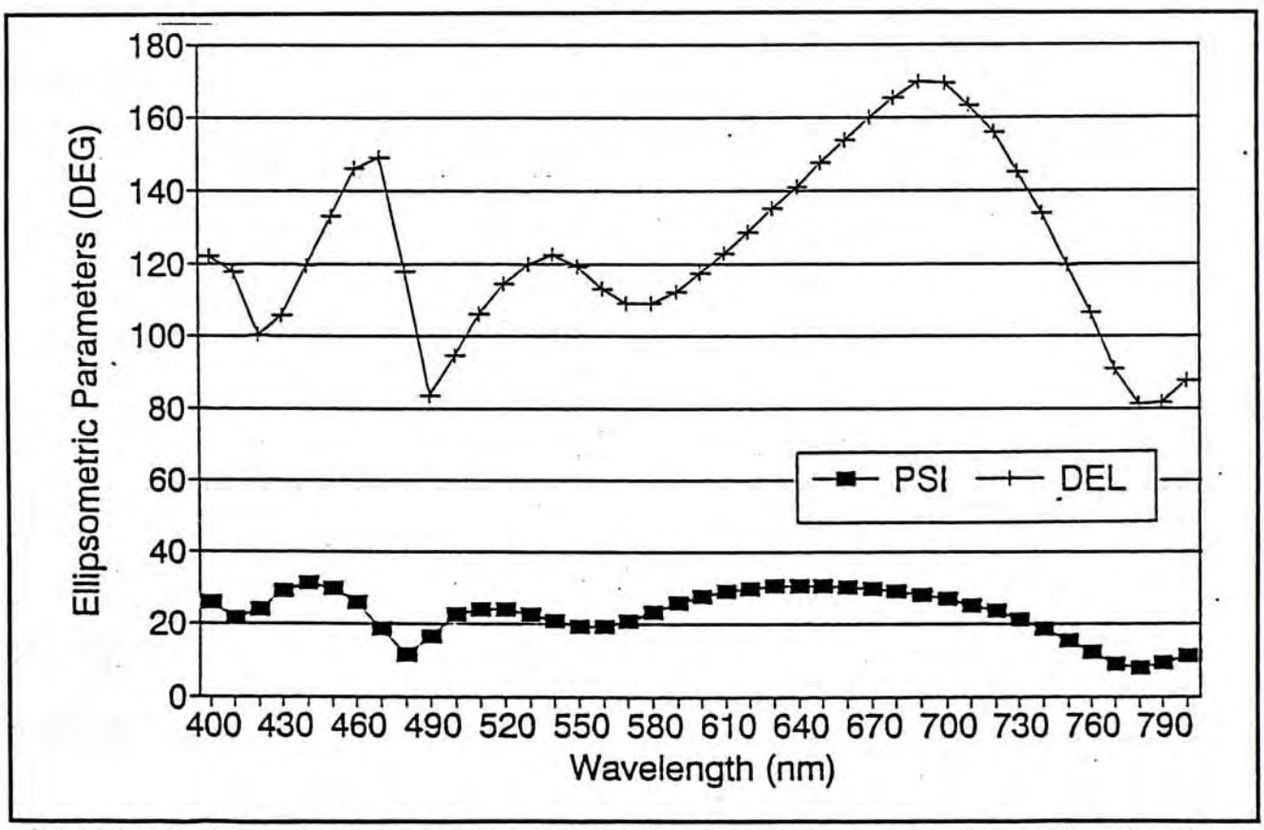


Figure 7.23 *Ellipsometric spectrum $\psi(\lambda),\Delta(\lambda)$ of a SOI sample prepared with a beam current of 400μA.*

implanted with a beam current of 200$\mu$A was found to be about 800°C and therefore portion of the silicon-nitride layer has already transformed from the amorphous phase to the crystalline phase during implantation. In the case of 400$\mu$A beam current, the substrate temperature was found to be higher than 1200°C. The sample is in fact already crystallized during implantation without the need of any post-implantation.

**Section 7.2.2.2 Annealing after implantation**

After implantation, samples are subject to isothermal annealing at 1200°C for two hours. The spectroscopic ellipsometry spectra of the annealed samples are illustrated in Figure 7.26 to Figure 7.29. Moreover Figure 7.30 and Figure 7.31 respectively show the ellipsometric parameter $\psi$ and $\Delta$ of the different annealed samples plotted together for comparison. As we mentioned previously, the buried nitride layer in the SOI sample implanted with an intermediate beam current (50uA and 150uA) becomes recrystallized after annealing. However, there is only a little variation in the curve feature for the sample implanted with a beam current of 50uA. On the other hand, samples prepared with middle amount beam current (150$\mu$A and 200$\mu$A) show clearly a change in the spectra curve feature after annealing. These differences in the features of the SE spectra indicate that the structures of these samples are different from each other even after annealing. This is consistent with the findings of reference 64 which directly shows from the X-ray diffraction pattern that the buried nitride layers can be of $\alpha$-phase or $\beta$-phase, or a mixture of the two. The top silicon layer can also be single crystalline (for beam current $>$ 150$\mu$A) or poly-crystalline (for beam current $=$ 50$\mu$A).

The typical thickness of the top Si layer and the buried silicon nitride layer are reported to be about 220nm and 330nm respectively[62]. A pair of ellipsometry spectra for an ideal three layer SOI structure with a buried silicon-nitride layer sandwiched between the

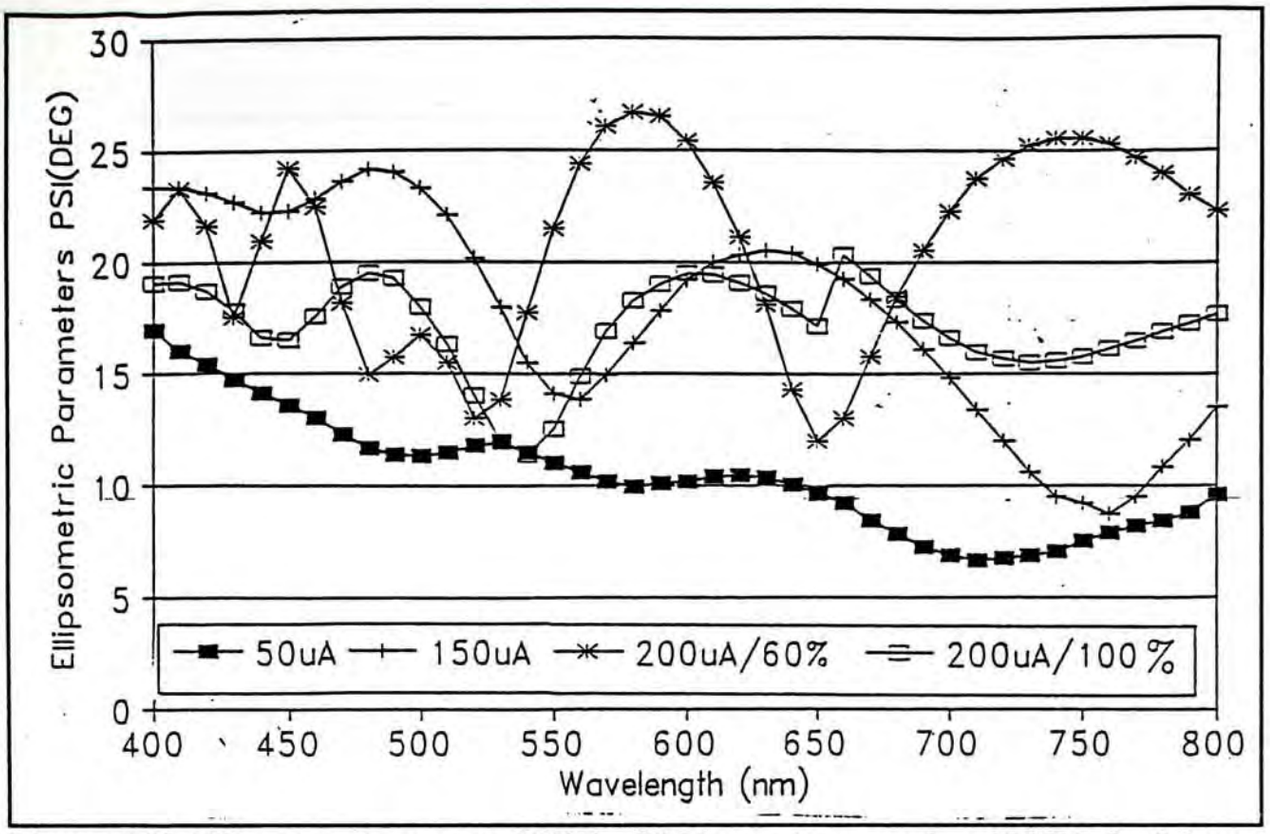


Figure 7.30 *Ellipsometric spectra PSI(ψ) of SOI samples anneal at 1200°C for 2 hours after implanted with different beam current.*

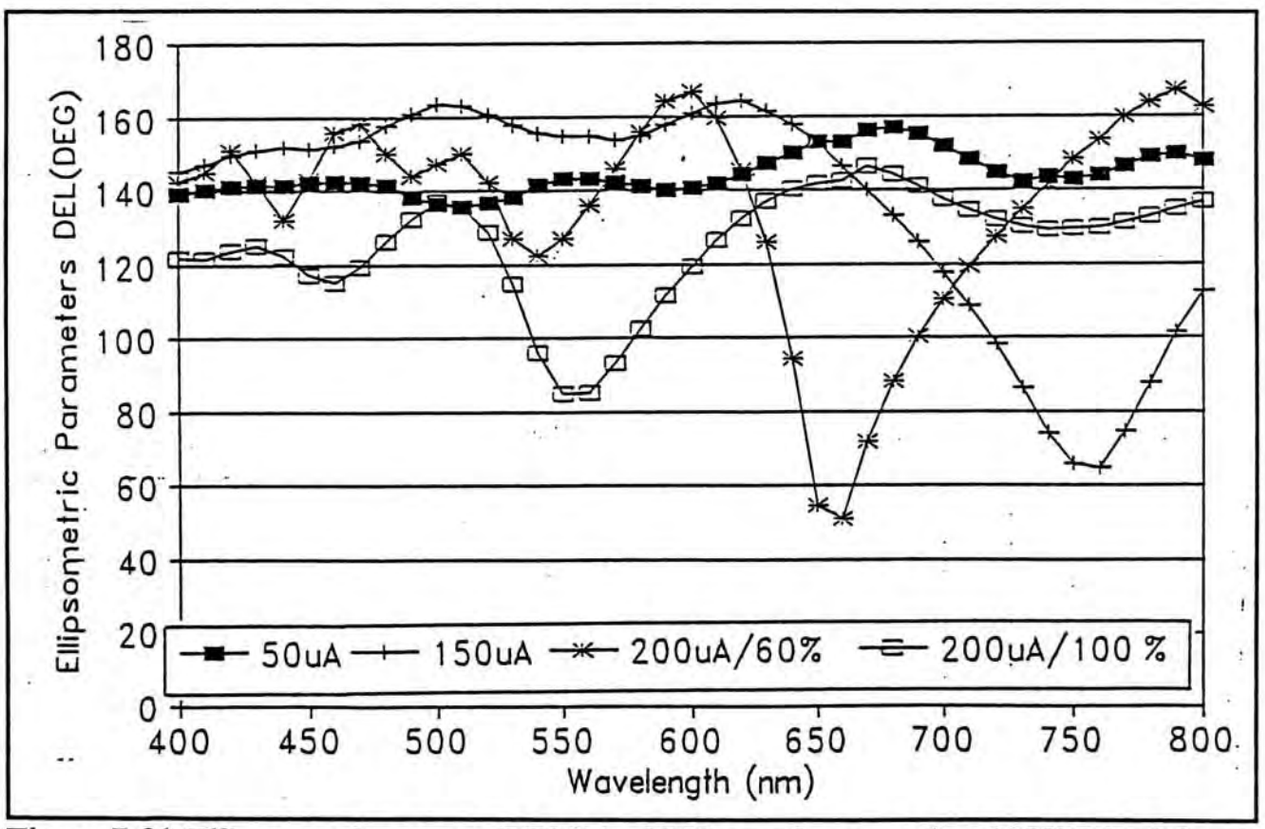


Figure 7.31 *Ellipsometric spectra DEL(Δ) of SOI samples anneal at 1200°C for 2 hours after implanted with different beam current.*

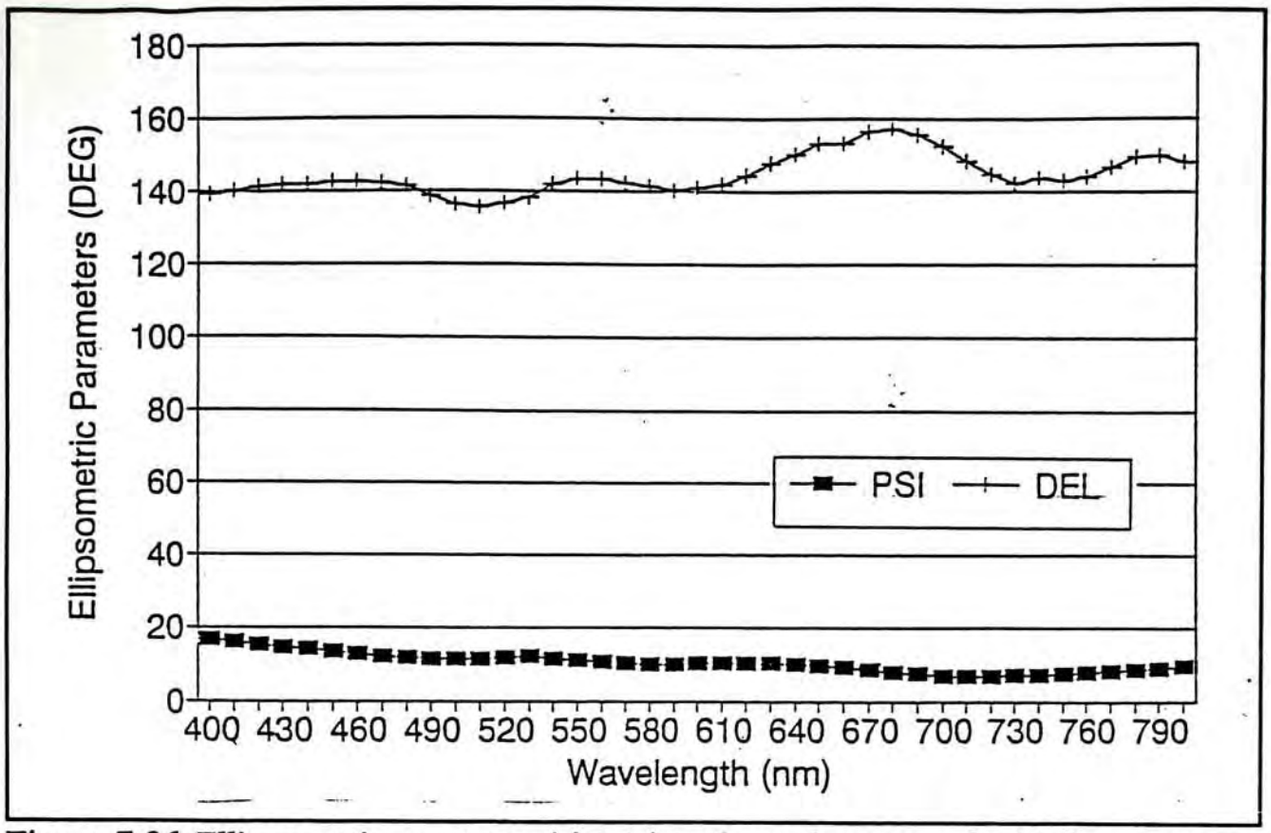


Figure 7.26 *Ellipsometric spectrum $\psi(\lambda)$,$\Delta(\lambda)$ of sample prepared with beam current 50μA and then anneal at 1200° for 2 hours*

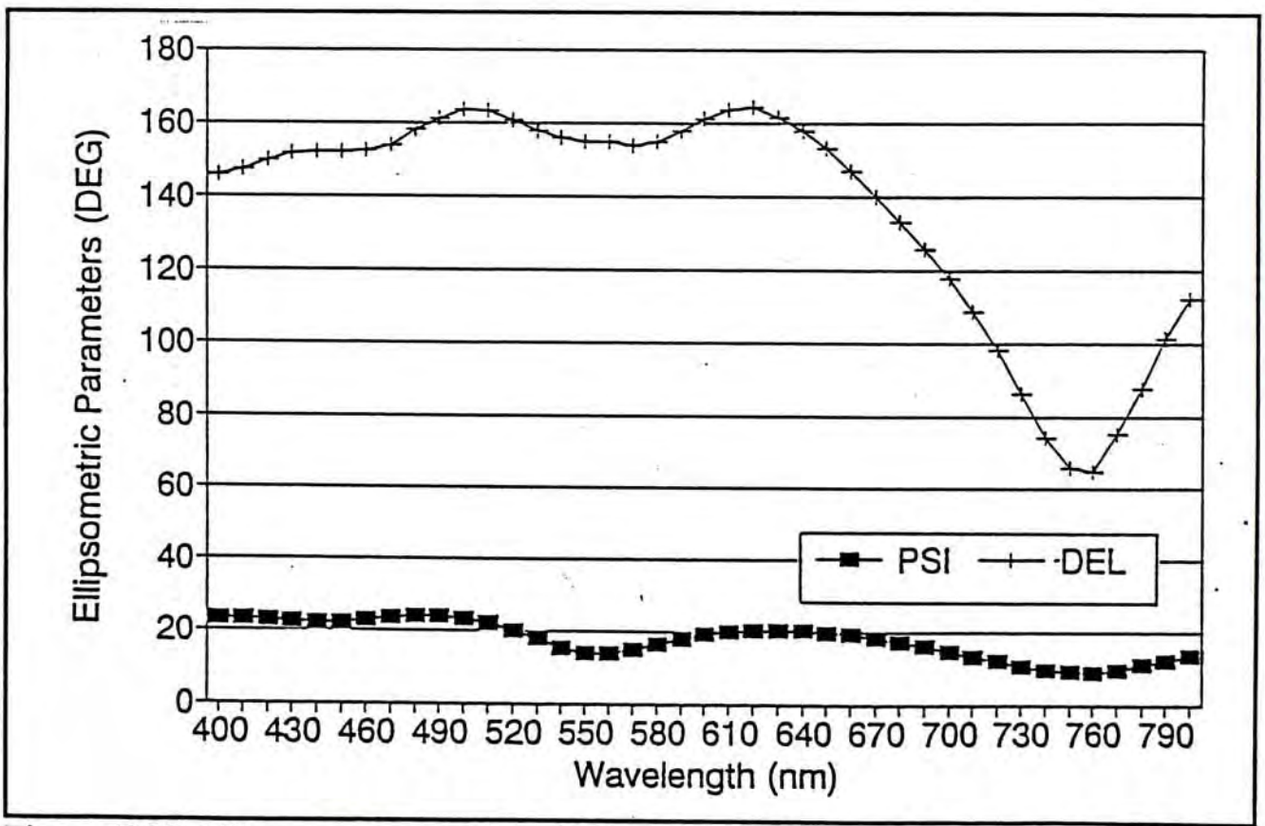


Figure 7.27 *Ellipsometric spectrum $\psi(\lambda)$, $\Delta(\lambda)$ of SOI sample prepared with beam current 150μA and then anneal at 1200°C for 2 hours.*

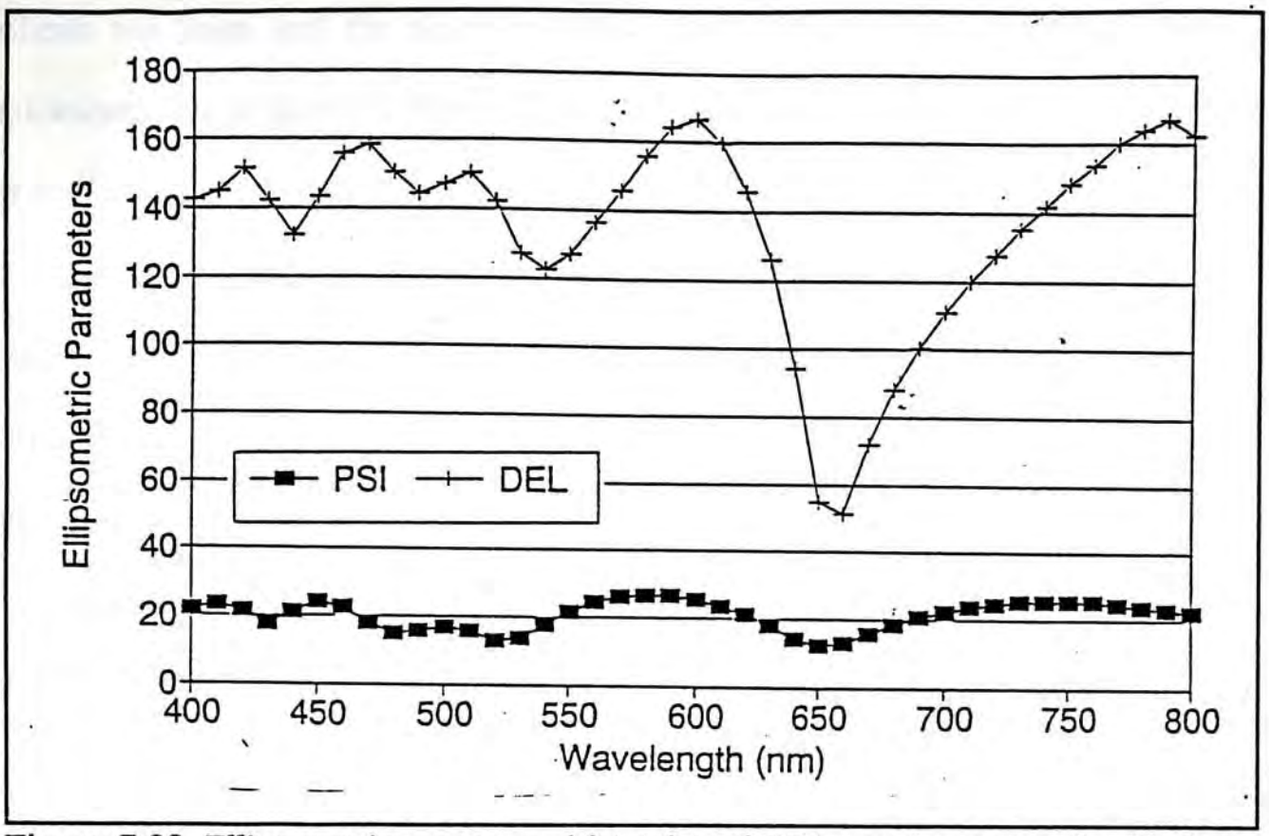


Figure 7.28 *Ellipsometric spectrum $\psi(\lambda)$,$\Delta(\lambda)$ of SOI sample prepared with beam current 200μA and then anneal. The dose is about $7.2x10^{17}cm^{-2}$.*

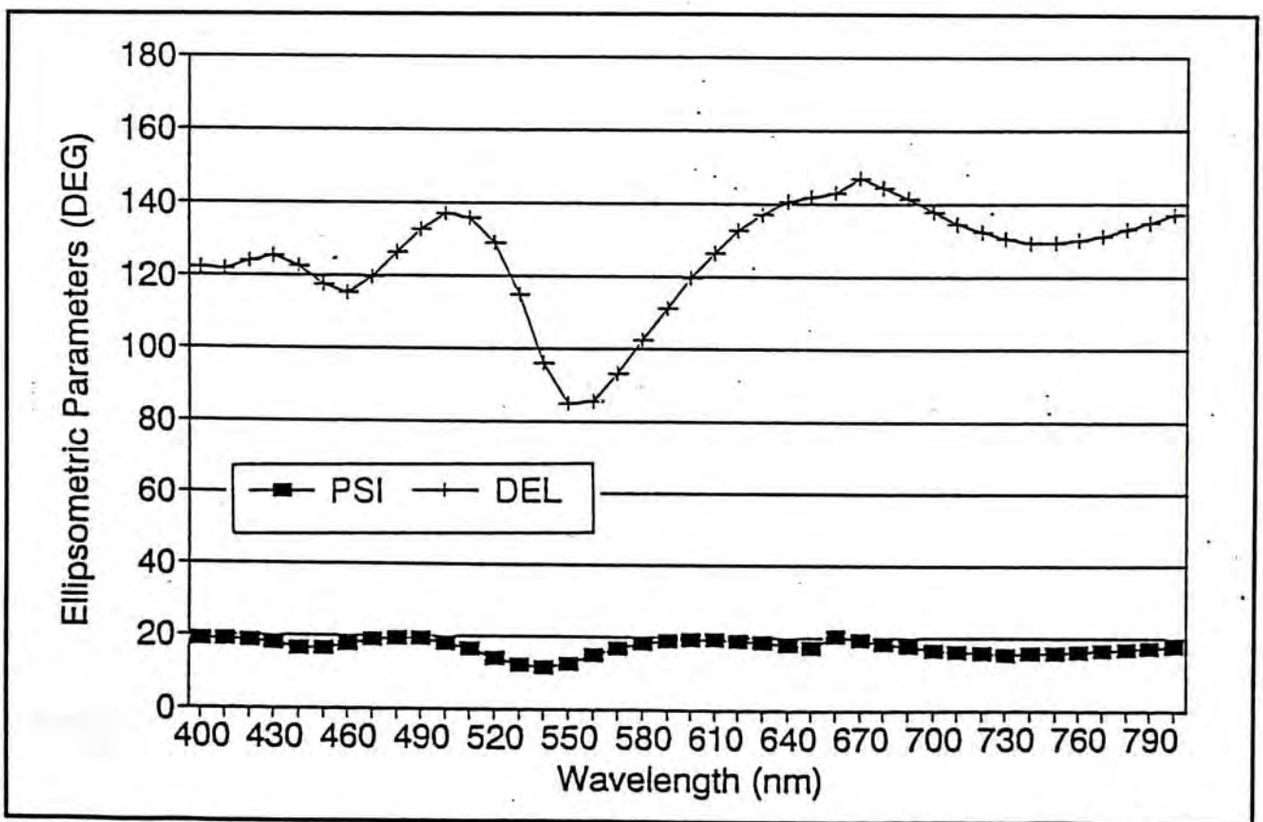


Figure 7.29 *Ellipsometric spectrum $\psi(\lambda)$, $\Delta(\lambda)$ of SOI sample prepared with beam current 200μA and then anneal. The dose is about $1.2x10^{18}$ $cm^{-2}$.*

silicon top layer and the silicon substrate has been generated using the above layer thicknesses and is shown in Figure 7.32 for comparison. A native dioxide overlayer of 20Å is assumed to be formed on the surface of the top silicon. From figure 7.32, we notice that the ellipsometry response of a buried nitride shows a markedly different from that of a bare silicon. The variation in PSI($\psi$) and DEL($\Delta$) is a reflection of the variation of the phase difference and the amplitude ratio between the orthogonal components of the elliptically polarized light. These features are result from the interference effects caused by the layered structure of the samples.

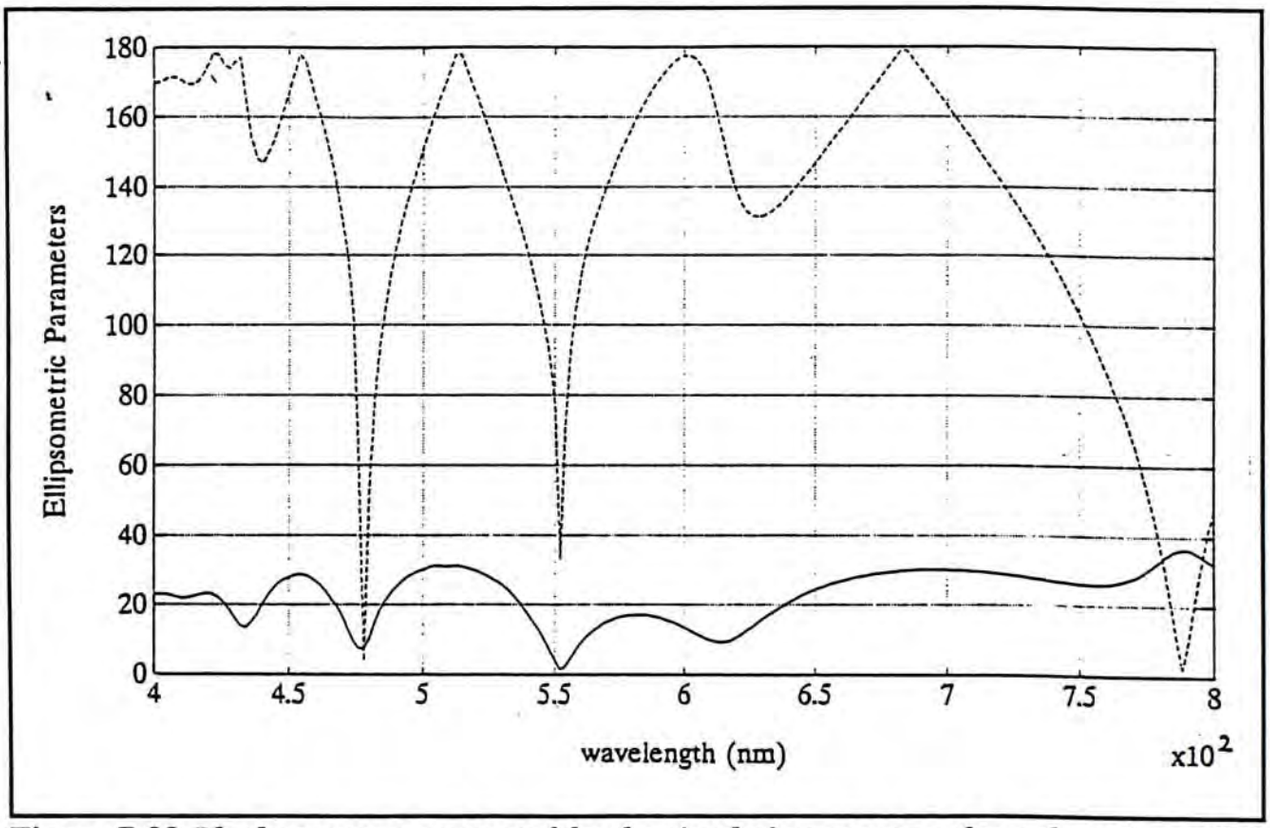


Figure 7.32 *Ideal spectrum generated by the simulation program for a three layer SOI structure (2nm $SiO_2$, 220nm c-Si, 330nm $Si_3N_4$ and Si substrate)*

Therefore, the appearance of the wavy features in the SE spectra should indicate the formation of silicon nitride layer. However, for a real buried nitride SOI sample formed by nitrogen ion implantation, the interface layer may not be abrupt and the optical constant is therefore varying continuously with depth. This is probably one of the reasons why the measured spectra are different from the generated spectra. On the other hand, in generating

the spectra shown in Figure 7.32, we have taken the values of the refractive index of the silicon nitride layer from reference 21 which are of non-crystalline silicon nitride. The refractive indices of $\alpha$-phase and $\beta$-phase $Si_3N_4$ have not been available in the literature. Moreover, the actual layer thickness of the buried nitride samples are also found to be different from sample to sample and so much more modelling work is necessary to obtain a quantitative fit of the SE spectra for these samples and will be the objectives of future work.

From the ellipsometric spectra of SOI samples, we know that the thermal history has significant effects on the optical properties of the samples. The variations of the curve features before and after annealing illustrate that the buried silicon-nitride layer can be crystallised in-situ during implantation with high current or by annealing in high temperature after implantation. Further analysis of the SE spectra can certainly provide more information about the SOI structures and be supplement to the results from other characterization techniques.

# CHAPTER 8 CONCLUSION

## Section 8.1 Summary of the results

A personal computer controlled automated rotating-analyzer type spectroscopic ellipsometer has been constructed. It has been used to measure the properties of bulk materials and thin films. The dielectric function can be measured as a function of wavelength cover the spectral range from 1.5eV to 3eV. The system has been verified by measuring the standard samples and the results were compared with those obtained from a commercial monochromatic null-ellipsometer. Beside the hardware construction and development of a control program for the system, an analysis program has also been developed to study the experimental results. An ellipsometric spectrum generator based on the 2x2 scattering matrix algorithm was written to generate the ideal spectra for samples with isotropic and homogenous stratified planar structure. The model parameters of the samples are analyzed by a fitting program which can modify the initial guess of the unknowns with the help of the Marquart Algorithm. It was found that the goodness of fit and the rate of convergence depend on the appropriateness of the model and the initial parameters selected, the number of variables involved in the calculation and the error function used. As examples of application, the system was applied to measure the properties of a few semiconductor systems. These include low temperature MBE grown GaAs on GaAs, amorphous carbon thin films on silicon, LPE $Al_xGa_{1-x}As$ films on GaAs and buried nitride silicon on insulator structure by nitrogen implantation into silicon. The refractive index of MBE growth GaAs on a low-temperature GaAs substrate was found to be similar to that of a crystalline GaAs but the extinction coefficient is much larger. The high absorption property of the low-temperature grown GaAs is believed to be the result of off-stoichiometric effect and is due to the point defects introduced. From the measured results of the amorphous carbon thin

films it was demonstrated that single wavelength measurement cannot determine the optical properties of absorption thin films even when the thin thickness is known. It is because the complex relation between the ellipsometric parameters and the complex optical function may not provide an unique solution. However, a spectroscopic measurement can help to solve this problem.

Measurements have also been make to study the optical properties of some LPE grown aluminium content $Al_xGa_{1-x}As$ films by spectroscopic ellipsometry. The refractive indices of these samples obtained from our measurements are compared with the results of other researchers. The existence of "terrace" and meniscus line features on the surface of the LPE grown $Al_xGa_{1-x}As$ samples has been shown and it is thought to be a major factor affecting the value of the absorption coefficient. The cooling rate during the growth of the epitaxial layers has been shown to have no significant influence on the optical properties of the samples.

Lastly, the ellipsometric spectra of SOI samples prepared using nitrogen implantation into silicon with different beam current were compared. It was found that there is an in-situ annealing effect due to the beam heating during implantation. When the beam current is large enough, portion of the amorphous $Si_3N_4$ has been transformed to crystalline form. The variation tendency matches well with the IR absorption results. Moreover, the crystalline $Si_3N_4$ layer can also be formed by annealing the sample after implantation. These results confirm the formation of a buried silicon nitride layer by implantation with a stationary beam and are consistent with the results obtained by other methods reported[62].

## Section 8.2 Suggestion for future work

Ellipsometry is a powerful technique for the non-destructive investigation of materials. This technique has been applied to various fields and the scope of its application is still expanding. An ellipsometer using a monochromatic light source at a single wavelength can applies to investigation of bulk materials and non-absorption thin films on absorbing substrate. For samples with more complicated structure structures spectroscopic ellipsometry has to be used. In recent years the ellipsometric measurements has been extended to infra-red region and ultra-violent region. In principle, spectroscopic measurements can provide more data for the analysis of samples with complicated structures. However, if the frequency range covered is not wide enough, the properties of the sample may not have significant change within a narrow frequency range and the information obtained will be limited. Therefore, it is desirable if measurements can performed at broader frequency range so that valuable information of the sample can be obtained. Moreover, the UV measurement can assist the investigation of multi-layer samples. In contrast, the measurements at longer wavelength contain more information on the buried layer. Since the penetration depth of ultra-violent light is short for most kind of material, if the samples are measured at shorter wavelength, the top layer of the multi-layer samples can be regraded as a semi-infinite material and so its optical parameters can be determined directly from the ellipsometric parameters. By replacing the light source, grating and some optical components, the frequency range of our system can easily be expanded.

The program written for the data analysis is limited to multi-layer structures system with homogenous and uniform isotropic medium in each layer. For simplicity, the refractive index of the sample has also been assumed constant within the visible range. However, when the variation of the optical properties of the samples against wavelength cannot be neglected,

frequency dependence has to be included in the program. In order to determine the refractive index n(λ) of the materials against the wavelength λ. A simple dispersion relationship for the films can be introduced. The asymptotic behaviour of n,k can be described by a dispersive equations[34].

$$n(\lambda) = n_0 + n_2\left(\frac{1}{\lambda^2}\right) + n_4\left(\frac{1}{\lambda^4}\right)$$
$$k(\lambda) = k_0 + k_1\left(\frac{1}{\lambda}\right) + k_3\left(\frac{1}{\lambda^3}\right) \qquad 8.1$$

The above equations describe the asymptotic behaviour of n,k when far from any specific absorption singularity. The constants $n_0, n_2, n_4$ and $k_0, k_1, k_3$ can be obtained from either from published experimental data or be regraded as a fitting parameters. When considering a sample with multi-layer structure with L layers, including the thickness $d_i$ totally 7xL parameters have to be deduced from the SE data. For samples with an arbitrary in-depth profile such as in the case of ion implantation, multi-layer optical model has to be used. Since optical properties of such samples vary continuously, transition layers should be added to represent the interface region. It has been found that, more the number of layers we divided the sample, a better fitting result of the experimental data will be obtained[63].

It is obvious that not all parameters are varied at the same time during the fitting process. If the measured frequency is broad enough, the surface layer of the sample can be investigate first by fitting the short wavelength region. After then, the parameters can keep fixed and fit the remaining parameters using the whole wavelength range[35,63].

The two orthogonal components of the incident waves will partially transmit and partially be reflected at the interface between two layers. A 2x2 scattering matrix formulation is good enough to describe the problem for isotropic stratified planar structures. However, if the sample is anisotropic, a new approach has to be used. In fact, a 4x4 matrix method has

been developed by Billard[13] to study the reflection and transmission of obliquely incident polarized light by stratified anisotropic planar structure. The method is a generalization of the 2x2 matric method and it involves the curl equations of the Maxwell's equations. The application of the 4x4 matrix method has been discussed by Berreman and Cohn but it has not yet been successfully put into practical use. Therefore, this will also be another direction for the future investigations.

**REFERENCE**


[1] D.Drude Annalen der Physik and Chemie, vol.14,July,452 (1888).

[2] R.M.A. Azzam, Selected papers on ellipsometry, SPIE Milestone series, (1989).

[3] B.D. Cahan, R.F. Spanier, Surface Sci, Vol. 16, 166 (1969).

[4] J.L.Ord and B.L. Wills, Appl. Opt.,6,1673 (1967).

[5] S.N. Jasperson and S.E. Schnatterly, Rev. Sci. Instrum., 40. 761 (1969).

[6] R. Greef, Rev. Sci. Instrum., 41,532 (1970).

[7] J.C. Suits, Rev. Sci. Instrum., 42,19 (1971).

[8] D.J. Scholtens, J.F. Kleibeuker and J.Kommandeur, Rev. Sci. Instrum., 44,153 (1973).

[9] H.J. Mathieu, D.E. McClure and R.H.Muller, Rev. Sci Instrum., 45,798 (1974).

[10] R.W.Stobie, B. Rao and M.J. Dignam, Appl. Opt. 14,999 (1975).

[11] P.S. Hauge and F.H. Dill, IBM J. Res. Rev., 17,473 (1973).

[12] D.E.Aspnes, Opt. Commun. 8,222 (1973).

[13] R.M.A. Azzam and N.M. Bashara, Ellipsometry and Polarized light, North-Holland, Amsterdam, (1977).

[14] Karl Rieling, Ellipsometry for Industrial applications, Springer-Verlag Wien, New York, (1987).

[15] D.E. Aspnes, S.M. Kelso, R.A. Logan and R.Bhat, J.Appl. Phys.,60,754 (1986).

[16] D.E. Aspnes, A.A. Studna and E.Kinsbron, Phys.Rev. B29,768 (1984).

[17] K.Vedam,P.J. McMarr and J. Narayan, Appl. Phys. Lett.,47,339 (1985).

[18] J.Narayan,S,Y.Kim,K.Vedam and R. Manukonda, Appl. Phys Lett. 51,343 (1987).

[19] J.A. Wollam, P.G. Snyder,AS.W. McCormick,A.K.Rai,P.Ingram and P.P.Pronko, J.Appl.Phys., 62, 4867 (1987).

[20] M.Erman, C.Alibert, J.B. Theeten, P. Fijlink and B. Cattles, J.Appl. Phys., 63,465 (1988).

[21] Edward D.Palik, Handbook of optical constants of solid I, Academic press, Inc., (1991).

[22] L. Ward, The optical constants of bulk materials and film, IOP publishing Ltd, (1988).

[23] M. Born and E. Wolf, Principle of optics, Pergamon, New York, (1970).

[24] Y.J. van der Meulen and N.C. Mien, J. Opt, Soc. Am., 64, 804 (1974).

[25] H.Takasaki, J. Opt. Soc. Am., 51, 463 (1961).

[26] D.E. Aspnes and A.A Studna, Appl. Opt., 14, 220 (1975).

[27] S.N. Jasperson and S.E. Schnatterly, Rev. Sci, Instrum., 40, 761 (1969).

[28] V.M. Bemudez and V.H. Ritz, Appl. Opt. 17,542 (1978).

[29] B. Drevillon, J. Penin, R. Marbot. A. Violet and J.L. Dalloy, Rev. Sci. Instrum., 53, 969 (1982).

[30] D.E. Aspnes, Appl. Opt., 14, 1131 (1975).

[31] H.F. Hazebrock and A.A. Holscher, Rev. Sci. Instrum., 6, 822 (1973).

[32] G.E. Jellison, Optics Lett., 12, 766 (1987).

[33] R.M.A. Azzam, I.M. Elminyawi and F.G. Grosz, Rev. Sci. Instrum., 59, 84 (1988).

[34] F.Ferrieu and J.H. Lecat, J. Electrochem. Soc., Vol.137, No.7, 2203, July (1990).

[35] Leo M. Asinovsky, Materials resarch society fall meeting, Simposium G, Amorphous Insulating Thin films, Dec (1992).

[36] M. Grasserbauer and H.W. Werner, Analysis of microelectronic material and devices, wiley, (1991).

[37] Drevillon, B. Perin, J. Marlot, R.violet, A Dally, Rev. Sci, Instrum., 53, 969 (1982).

[38] R.M.A. Azzam and Kurt A. Giardina, Ali G. L:opez, SPIE- The International Society for Optical Eng., Polarimetry: Radar, Infrared, Visible, Ultraviolet and X-Ray, Vol. 1317, 295 (1990).

[39] D. E. Aspnes amd A.A. Studna, Appl. Opt., 10, 1024 (1971).

[40] J.R. Zeidler, R.B. Kohles and N.M. Bashara, Appl. Opt., 13, 1115 (1974).

[41] Y. Hayashi, A. Itoh, Appl. Opt., 28, 703 (1989).

[42] D.E. Aspnes, A.A Studna, Rev. Sci. Instrum, 49, 291 (1978).

[43] R.W. Collins, Rev. Sci. Instrum., 61, 8 Aug (1990).

[44] David C. Nick, R.M.A Azzam, Rev, Sci. Instrum., 60, 12 Dec (1989).

[45] Mo Dang, S.G. Chen, ACTA Physica Sinica, Vol. 29, No.5, may (1980).

[46] C.A. Fenstermaker, F.L. Mc Crackin, Sur. Sci., vol. 16, 85 (1969).

[47] D.E. Aspnes,J.B. Theeten, F. Hottier, Physical Review B, Vol. 20, 8, 15 Oct (1979).

[48] R.J. Archer, J. Opt. Sco. Am. vol. 52,9 Sept (1962).

[49] F. Meyer, G.A. Bootsma, Sur Sci., Vol 16, 221 (1969).

[50] Chen Shuguang, Ye Yianging, Mo Dang, Chinese journal of semiconductor, Vol 3 , No.1, Jan., (1982).

[51] Samuel A. Alterovitz, John A. Woollam, Paul G. Snyder, Solid State Technology, March, (1988).

[52] G.E. Jellison, Jr., Appl. Opt., Vol. 30, No.23, 10 Aug (1991).

[53] J. Vanhellemont and H.E. Maes, Solid State phenomena, Vols 6&7, (1989).

[54] F.W. Smith, A.R. Calawa, C.L. Chen, M.J. Manfra and L.J. Mahoney, IEEE Trans. Electron Devices ED-9, (1988).

[55] R.A. Puechner, D.A. Johnson, K.T. Shiralagi, D.S. Gerber, R. Droopad and G.N. Maracas, Journal of Crystal Growth, 111,43-49 (1991).

[56] K.Xie, Z.C. Huang and C.R. Wie, Journal of Electronic Materials, Vol.20,No.7, 553-558 (1991).

[57] D.E.Aspnes, S.M. Kelso, R.A. Logan,R.Bhat, J. Appl. Phys. 60(2), 15 July (1986).

[58] Sado Adachi, J.Appl. Phys, 58(3), 1 Aug (1985).

[59] Huade Yao, Paul G. Snyder, John A. Woollam, J. Appl. Phys., 70(6), 15 Sept, (1991).

[60] Jia Gang, Chinese Journal of semiconductor, Vol.5, No.1, Jan., (1984).

[61] G.E.Jellison, Jr. B.B Sales, Appl. Opt., Vol 30, No.30, 20 Oct (1991).

[62] S.P. Wong, M.C.Poon, H.L.Kwok and Y.W.Lam, Nuclear, Instrum. and Materials in Phys. Res.,B17,24 april, 513-519 (1986).

[63] M.Fried, T.Lohner, J.M.M.deNijs, A.Van.Silifhout, L.J.Hanekamp, Z.Laczik,N.Q.Khanh and J.Gyulai, J.Appl. Phys,66(10), 15 Nov. (1989).

[64] S.P.Wong, M.C.Poon, Nuclear, Instrum and Methods in Phys. Res.,B22,22 sept, 122-126 (1986).

[65] H.C. Casey, Jr.,M.B.Panish, Heterstructure lasers, part A, Academic Poress Inc., 123-132 (1978).

## APPENDIX

## (A) MARQUART ALGORITHM

Error function mentioned in section 6.2.3 is in the format of sum of series of square terms (ie. $F(x) = \sum f_i^2(x)$)

The value of F is determined by the values of $\psi_i^c$ and $\Delta_i^c$. If the initial values of those parameters are equal to $\psi_i^m$ and $\Delta_i^m$, then the structure of sample we measured is equivalent to the model we assumed. However, there must be some deviation of initial guess from the measured values.

Gauss-Newton method is one way to modify the initial parameters so that the output should be more closely to the measured values. Consider the partial differentiation of f(x), we have

$$J_{i,j} = \frac{\partial F_i(x)}{\partial X_j} \qquad \text{(A.1)}$$

where $X_j$ represent the unknown optical parameters.

Let $X^k$ be a vector which contains all the parameters close to the solution . According to the Gauss-Newton formula, next set of data is given by

$$X^{k+1} = X^k - \{ [(J^k)^T J^k]^{-1} [(J^k)^T f(X^k)] \} \qquad \text{(A.2)}$$

The matrix J contain the partial differentiation of $f_i(x)$ with respect to different variables.

$$J^k = \begin{bmatrix} J_{11}^k & J_{12}^k & \cdots & J_{1n}^k \\ J_{21}^k & J_{22}^k & \cdots & J_{2n}^k \\ \cdot & \cdot & & \cdot \\ \cdot & \cdot & & \cdot \\ J_{m1}^k & J_{m2}^k & \cdots & J_{mn}^k \end{bmatrix} \qquad \text{(A.3)}$$

In fact, the method of Gauss-Newton is equivalent to solve the linear equation A.4

$$(J^k)^T J^k P^k = -(J^k)^T f(X^k) \qquad \text{(A.4)}$$

$$\textit{where} \qquad P_k = -[\,(J^k)^T J^k\,]^{-1}\,[(J^k)^T f(X^k)]$$

When $\mid X^{k+1} - X^k \mid \leq \varepsilon$, error function F is minimized, or in other words, the optical parameters are equal to $X^{k+1}$.

The disadvantage of Gauss-Newton method is that we may sometime found difficulty in getting $(J^TJ)^{-1}$. In a worse case, we cannot get the solution. Moreover, the rate of convergence of Gauss-Newton algorithm is too slow.

A modified method suggested by Marquart can solve the above problems. Marquart algorithm is basically the combination of the Newton and gradient method. Formula of $P_k$ is modified as equation A.5

$$P_k = -\left[\,(J^k)^T J^k + \alpha_k)^{-1}\,\right]\left[\,(J^k)^T f(X^k)\,\right] \qquad \text{(A.5)}$$

where I is a unit matrix

When $\alpha_k$ is near or equivalent to zero, the Marquart method will degenerate into Newton method. On the other hand, when $\alpha_k$ is large enough, it will become a gradient method.

Marquart Algorithm is summarised as a flow chart shown in Fig.A.1. Let $\alpha_0=0.01$ and $\gamma=10$. Subscript k represent $k^{th}$ operation of regression. When $F(X^{k+1}) < F(X^k)$, the result of error function has become smaller. It the rate of change of X has become steady such that $J^Tf \leq \varepsilon$, then the output is equal to $X^{k+1}$. Otherwise, the value of $\alpha$ is reduce a factor of $\gamma$ and do the regression again. In other case, $F(X^{k+1} \geq F(X^k)$. That means the solution has a tendency to be diverge or $F(X^k)$ has already reached the minimum location. .If the rate of change of X ($J^Tf \leq \varepsilon$) then the answer is equal to $X^k$. When $J^Tf > \varepsilon$, the set of data may only reached a local minimum. In order to jump over it, the step increment is increased by

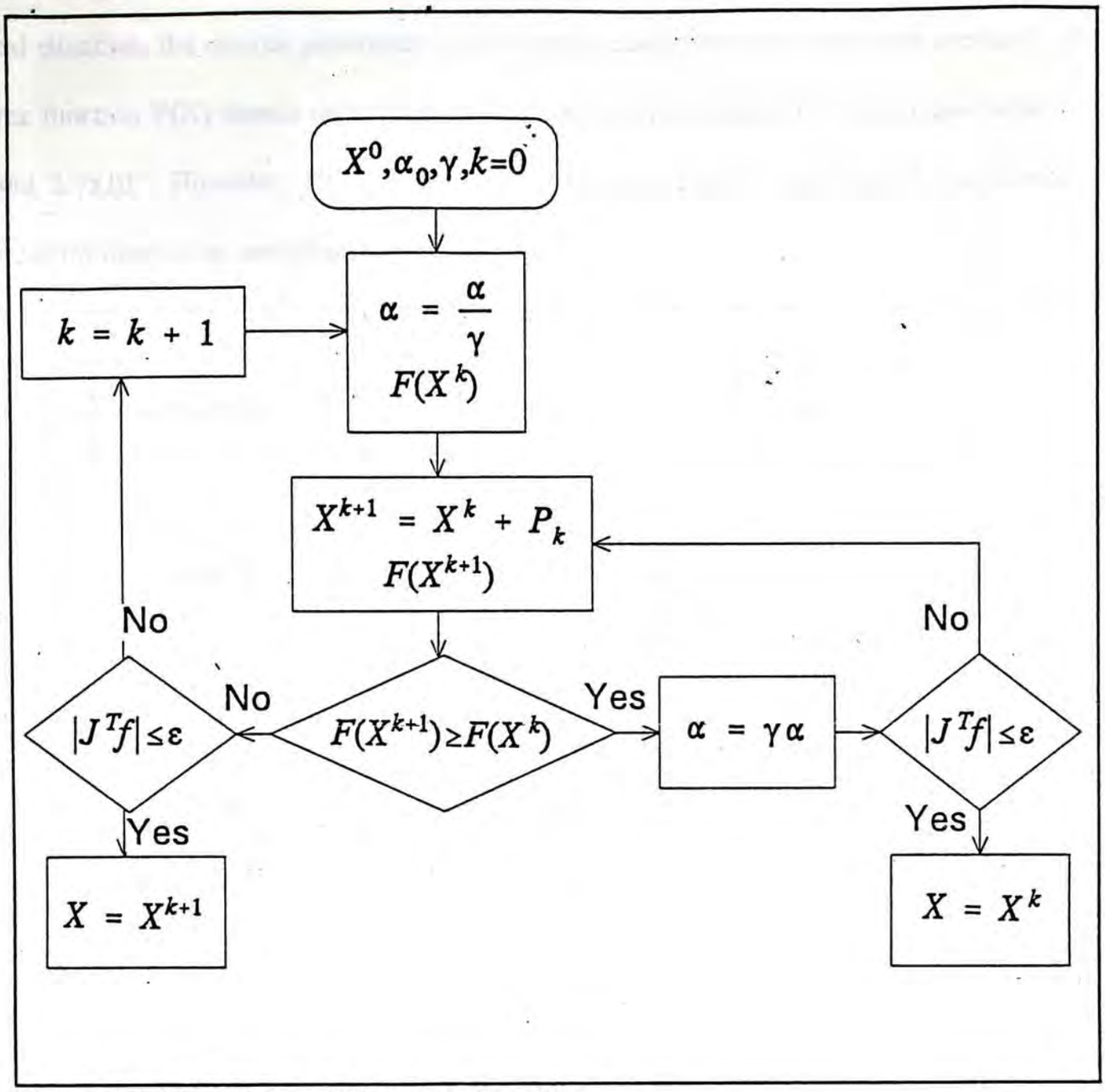


Figure A.1 *Flow chart of Marquart Algorithm*

multiple $\alpha$ to the factor $\gamma$ and then do the regression.

In fact, the value of $J^T f$ is a termination factor of the Marquart regression. When $J^T f \leq \varepsilon$, we believe that the change of output has become neglectable. However the value of $\varepsilon$ is different at different situation and it is hard to choose a fix value for it.

As an example, the optical properties of a layer of thin film on substrate is investigated. The matrix J include partial differentiation of f with respect to n,k,d. Since the system is very sensitive to the change of thickness, $|\partial f/\partial d|$ will be a value much more greater than the others. When we calculate $|J^T f|$. $\partial f/\partial d$ will be a dominate effect. For a

ideal situation, the optical parameters which match exactly the measured data are used, the error function F(X) should only show the truncation error caused by computation which is about $2.7\times10^{-2}$. However, $J^Tf$ in this case is as large as $1\times10^{4}$. Therefore, the termination procedure need to be modified.

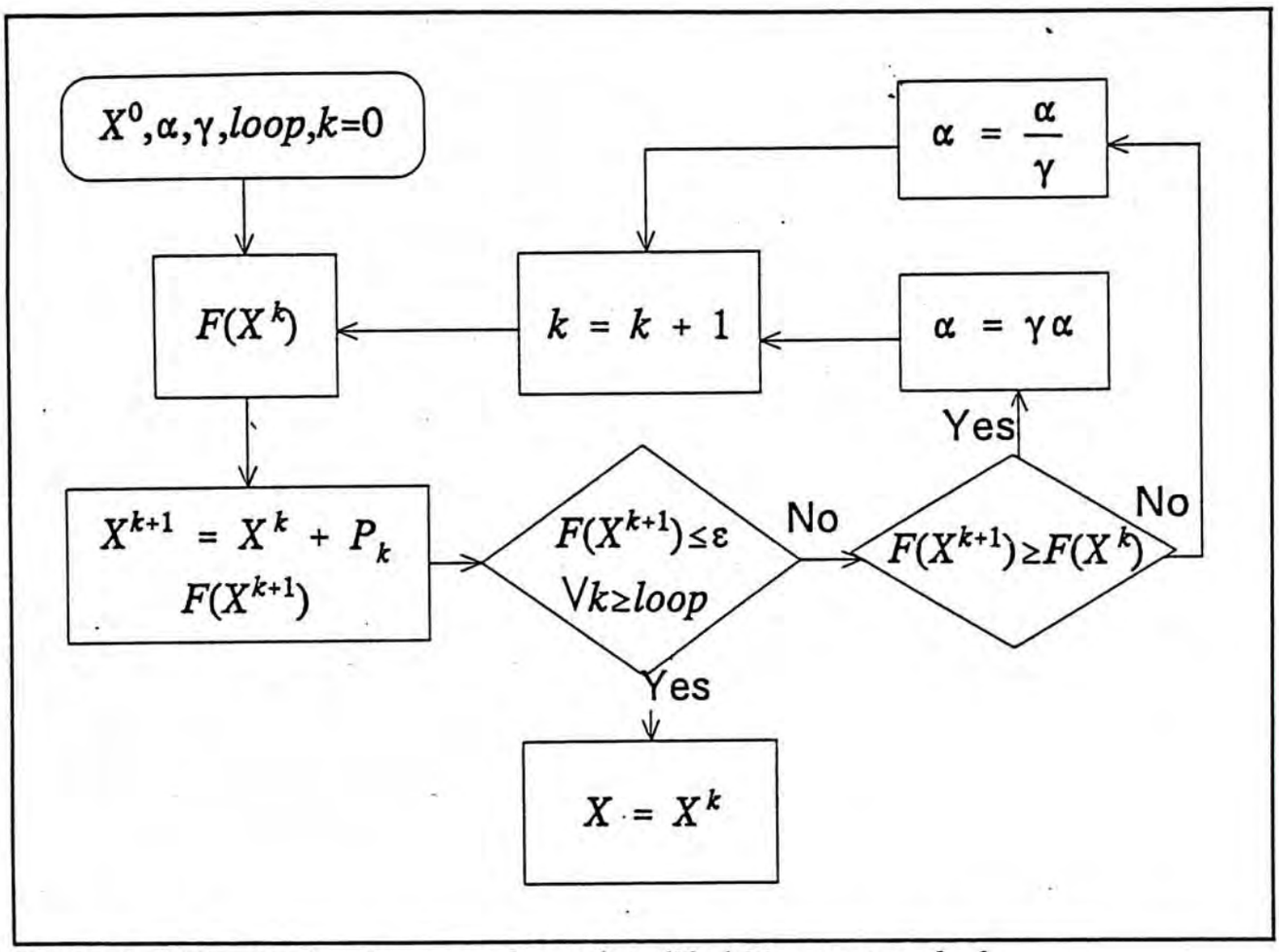


Figure A.2 *The termination procedure of modified Marquart method*

The simplest way to solve the problem is to neglect the effect of $J^Tf$. What we really concern about is the deviation of calculated data from the measured data. If F(X) is small enough, regression will stop. When more parameters are involved, larger value of F(X) will result. According to experience, the fitting result will converge within 50 successive looping. Expect the case of divergence, looping more than 50 times seldom change the output values anymore. In order to avoid the infinite looping during fitting a complex system, number of regression operation can be limited by users.

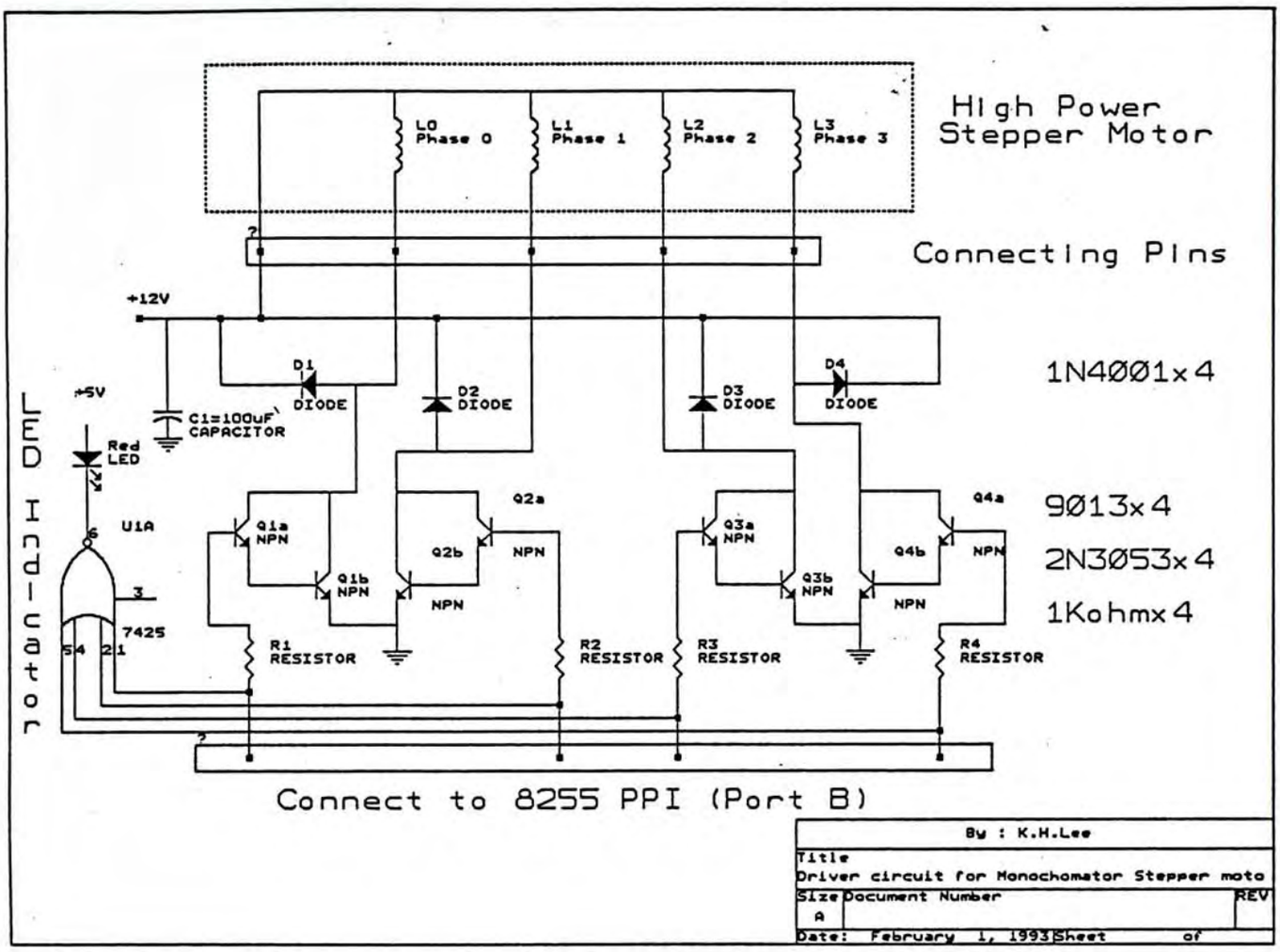
High Power
Stepper Motor
L0
Phase 0
L1
Phase 1
L2
Phase 2
L3
Phase 3
Connecting Pins
+12V
D1
DIODE
D2
DIODE
D3
DIODE
D4
DIODE
1N4001x4
+5V
C1=100uF
CAPACITOR
Red
LED
LED Indicator
U1A
7425
Q1a
NPN
Q1b
NPN
Q2a
Q2b
NPN
NPN
Q3a
NPN
Q3b
NPN
Q4a
Q4b
NPN
NPN
9013x4
2N3053x4
1Kohmx4
R1
RESISTOR
R2
RESISTOR
R3
RESISTOR
R4
RESISTOR
Connect to 8255 PPI (Port B)
By : K.H.Lee
Title
Driver circuit for Monochomator Stepper moto
Size
A
Document Number
REV
Date: February 1, 1993
Sheet
of

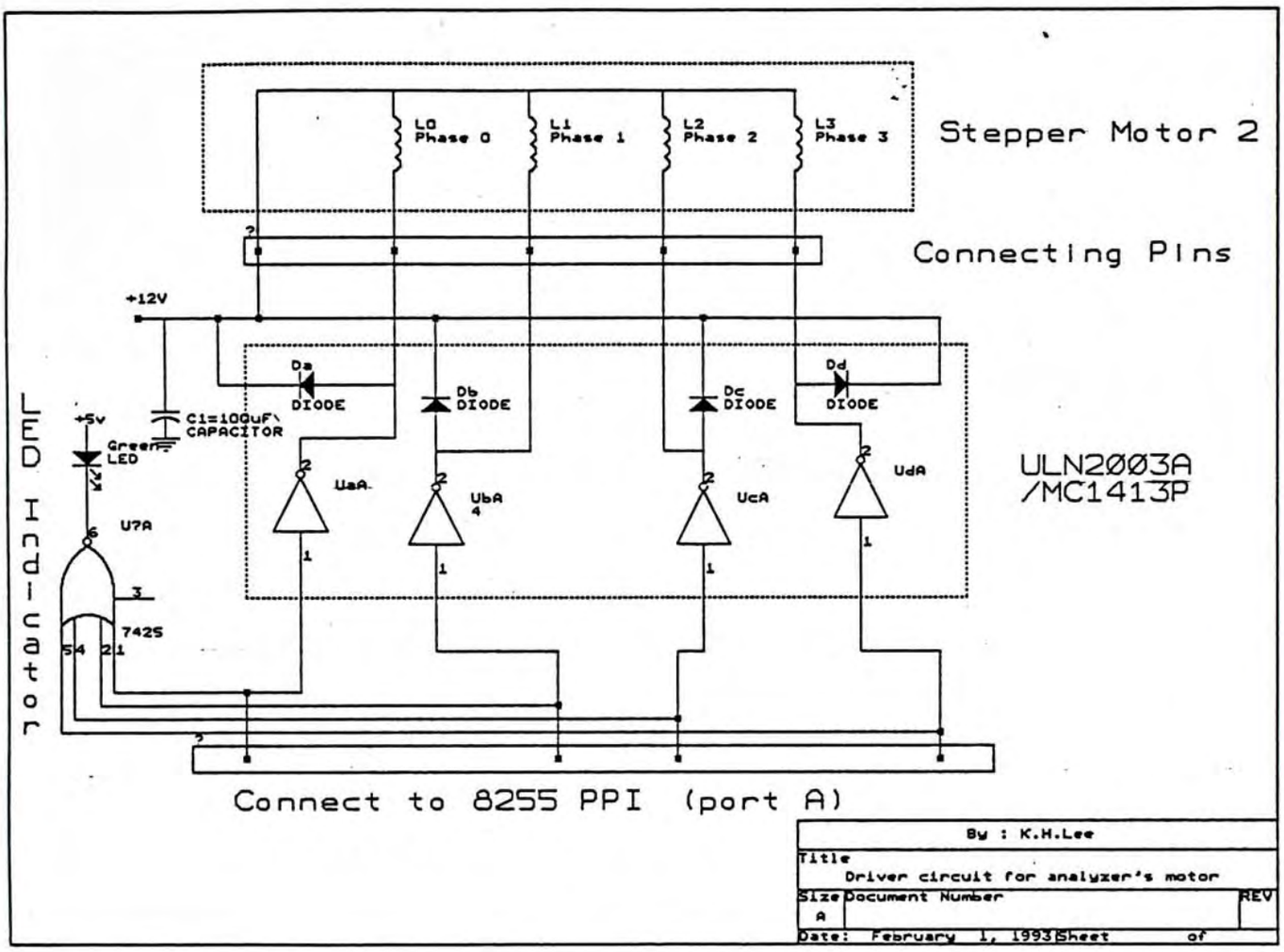
L0 Phase 0
L1 Phase 1
L2 Phase 2
L3 Phase 3
Stepper Motor 2
Connecting Pins
+12V
Da DIODE
Db DIODE
Dc DIODE
Dd DIODE
+5v
C1=100uF\ CAPACITOR
Green LED
U7A
7425
UaA
UbA
UcA
UdA
ULN2003A /MC1413P
LED Indicator
Connect to 8255 PPI (port A)
By : K.H.Lee
Title
Driver circuit for analyzer's motor
Size A
Document Number
REV
Date: February 1, 1993 Sheet of

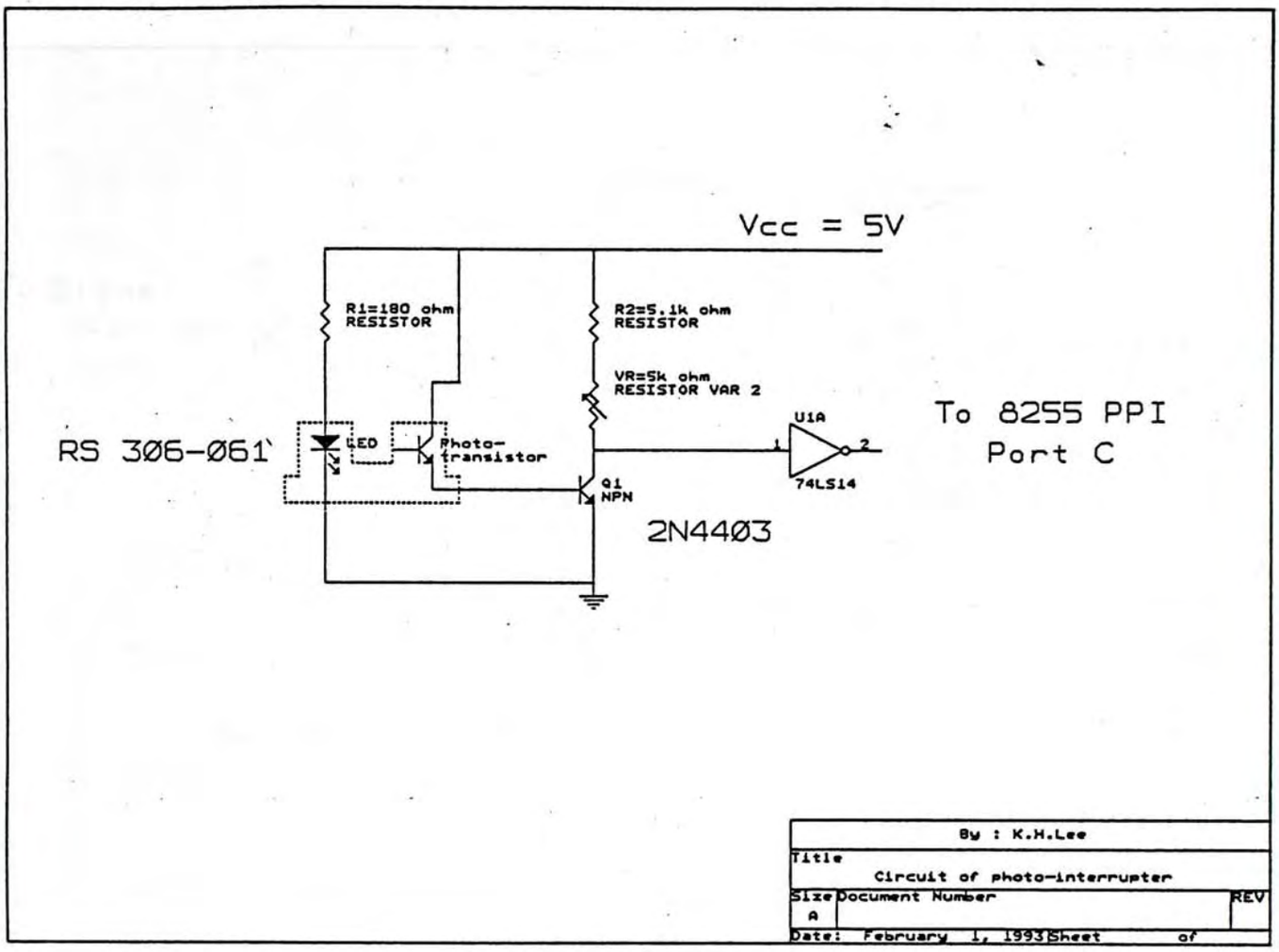
Vcc = 5V
R1=180 ohm
RESISTOR
R2=5.1k ohm
RESISTOR
VR=5k ohm
RESISTOR VAR 2
RS 306-061
LED
Photo-
transistor
Q1
NPN
2N4403
U1A
74LS14
To 8255 PPI
Port C
By : K.H.Lee
Title
Circuit of photo-interrupter
Size
A
Document Number
REV
Date: February 1, 1993 Sheet of

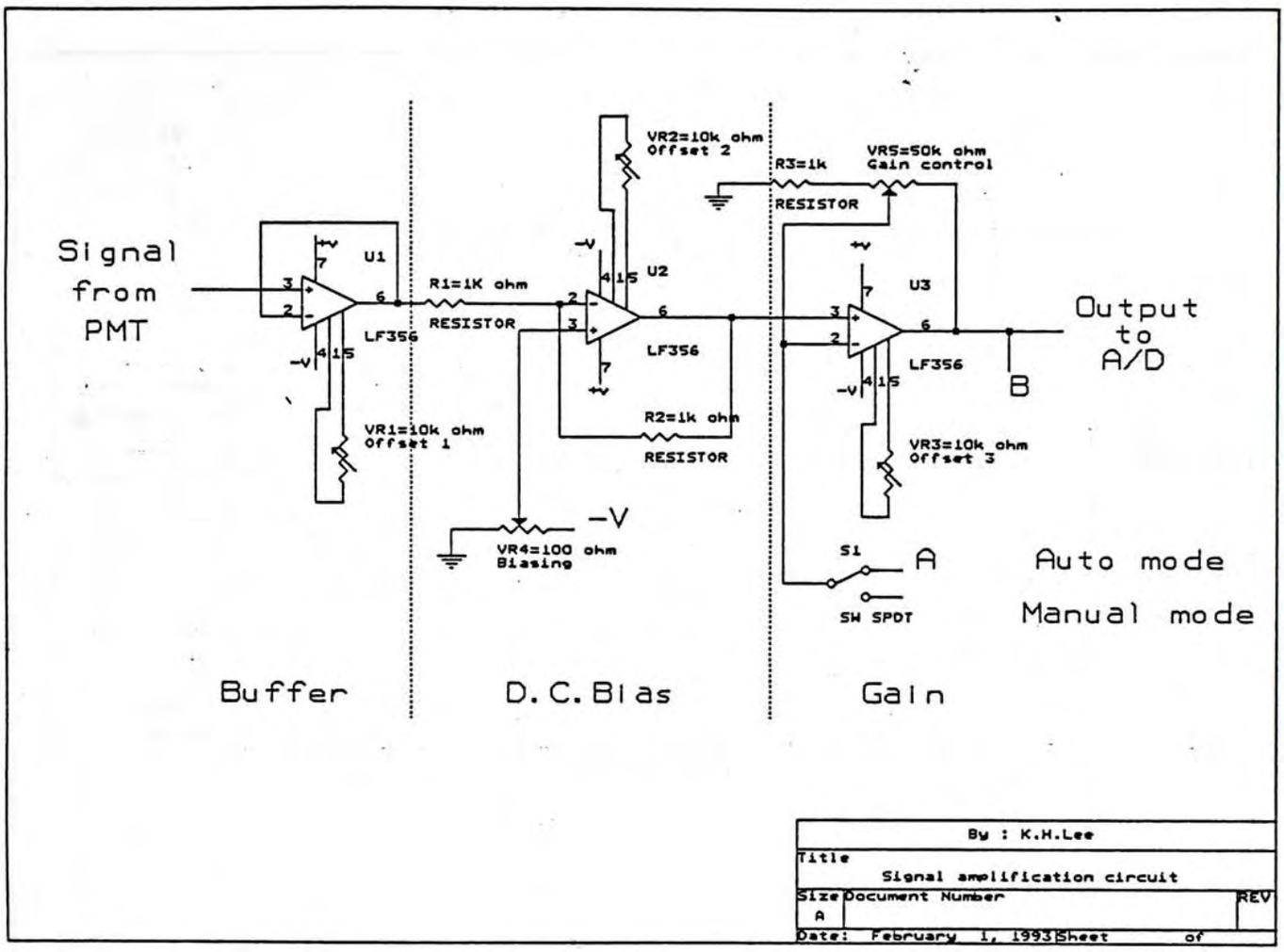
Signal from PMT
U1
LF356
R1=1K ohm
RESISTOR
VR1=10k ohm Offset 1
VR2=10k ohm Offset 2
U2
LF356
R2=1k ohm
RESISTOR
VR4=100 ohm Biasing
-V
R3=1k
RESISTOR
VR5=50k ohm Gain control
U3
LF356
VR3=10k ohm Offset 3
Output to A/D
B
S1
A
SW SPDT
Auto mode
Manual mode
Buffer
D.C.Bias
Gain
By : K.H.Lee
Title
Signal amplification circuit
Size A
Document Number
REV
Date: February 1, 1993 Sheet of

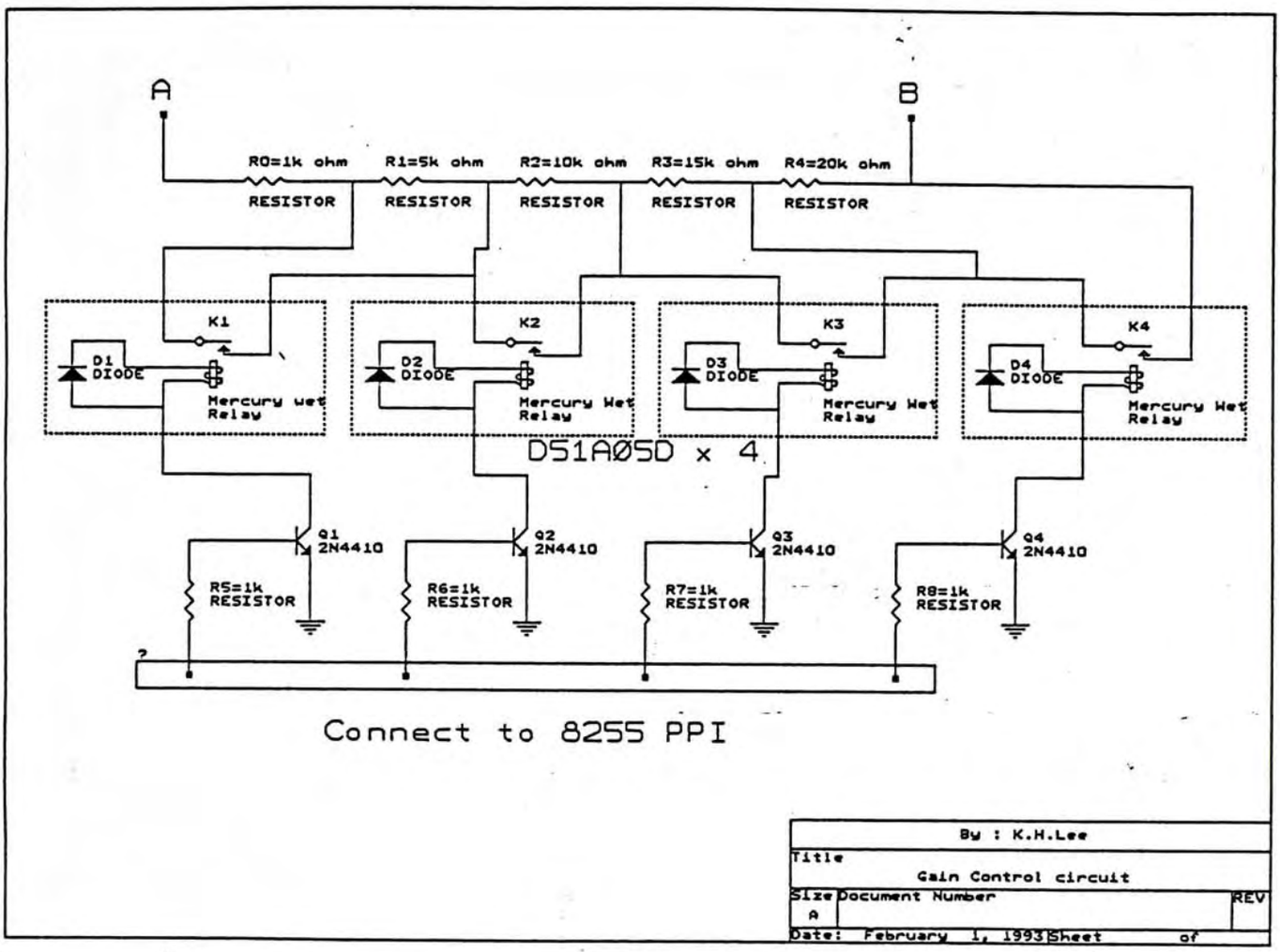
A
B
R0=1k ohm
R1=5k ohm
R2=10k ohm
R3=15k ohm
R4=20k ohm
RESISTOR
K1
K2
K3
K4
D1 DIODE
D2 DIODE
D3 DIODE
D4 DIODE
Mercury Wet Relay
D51A05D x 4
Q1 2N4410
Q2 2N4410
Q3 2N4410
Q4 2N4410
R5=1k RESISTOR
R6=1k RESISTOR
R7=1k RESISTOR
R8=1k RESISTOR
Connect to 8255 PPI
By : K.H.Lee
Title
Gain Control circuit
Size A
Document Number
REV
Date: February 1, 1993 Sheet of